Petroleum 10 (2024) 373–398

Contents lists available at ScienceDirect

Petroleum

journal homepage: www.keaipublishing.com/en/journals/petlm

Review Article

Approach for C_1 to C_2 products commencing from carbon dioxide: A brief review

G.R. Dey [a, b, *]

[a] Radiation and Photochemistry Division, Bhabha Atomic Research Centre, Trombay, Mumbai 400085, India
[b] Homi Bhabha National Institute, Anushaktinagar, Mumbai 400094, India

ARTICLE INFO

Article history:
Received 22 February 2023
Received in revised form
5 July 2023
Accepted 8 July 2023

Keywords:
Photocatalysis
Electrocatalysis
Plasmolysis
Thermolysis
Carbon dioxide
Chemical reduction

ABSTRACT

The carbon dioxide (CO_2) conversion to useable compounds remains a great contest to scientists, engineers, and environmentalists with regard to the reverse of the oxidative degradation of organics. This conversion is essential for the development of complementary fuels and raw materials for various industries, which in turn will help in avoiding the drastic increase in tropospheric temperature due to greenhouse effect leading to global warming. The solar energy is the earth's essential power source along with the other various forms of energy for example fossil fuels, hydropower, wind, and biomaterials, etc. The final goal is to establish the artificial photosynthesis, which can be replicated thru various chemical reduction techniques of CO_2 by employing appropriate photo-, thermal- and electro-catalysts in order to produce different one carbon atom (C_1) and higher carbon atoms containing products. Besides, the utilization of clean and sustainable CO_2 towards high-value products is of great interest today due to the recognized environmental worries and subsequent lessening of the fossil fuels utilization load to meet the energy demand of mankind. This way, solar energy can directly and/or indirectly be altered and stored in chemical energy form for industrial as well as societal applications. In this article our endeavor is to summarize the advances in CO_2 chemical reduction research area till date especially in free radical-based methods such as electrochemical, photochemical and plasma chemical for the development of carbon species up to two carbon (C_2) atoms containing products perceived in the chemical reduction of CO_2. The author hopes that this piece of work will be helpful to researchers and readers who are focused on the field of CO_2.

1. Introduction

The Paris agreement highlights that the global CO_2 emissions require to be halved by 2030 and total nil by 2050 [1]. Existing capture and utilization technologies of CO_2 along with forthcoming new technologies can help to achieve these goals. We have systematically gathered related information and summarized it to bring insight on capture and utilization of CO_2, thereby controlling the rise in global temperature. As CO_2 is the key leading subject of this article, at the onset we need to discuss some of its fundamentals. CO_2 is a colorless, odorless, and non-toxic gas which is generated through oxidation of organics and decomposition and/or acid reaction of inorganic carbonates. However, 1% of CO_2 makes people drowsy and at ~ 5% by volume, it is toxic [2]. Inhaling causes dizziness, visual and hearing abnormality/dysfunction due to binding with hemoglobin. Moreover, at ~ 10% by volume, it causes danger of asphyxiation [3] leading to death of human and animals. On the other hand, CO_2 is used as refrigerant, foaming rubber and plastics, for inflating life rafts and life jackets, in fire extinguishers, carbonated beverages, etc. Most importantly, it is a caretaker of blood pH, and hence is essential for survival.

CO_2 consists of one carbon atom and two oxygen atoms in a linearly arranged molecule. The UV–Vis absorption spectrum of CO_2 reveals a constant increase in absorption < 175 nm wavelength with a diffused peak having maximum absorbance ~ 135 nm with a very low absorption coefficient [4,5]. CO_2 is infrared (IR) sensitive due to some of its active vibrations, which produce an oscillating dipole. Two different types of IR active vibrations (stretching and bending modes) exist in CO_2 molecule. Each of these modes create 2 types of vibrations, producing a total of 4 (following $3n$-5 principle, where n is the total number of atoms present in the molecule) types of vibrations as shown in Fig. 1. The symmetrical stretching

* Corresponding author.
E-mail addresses: grdey@barc.gov.in, grdey62@gmail.com.
Peer review under responsibility of Southwest Petroleum University.

https://doi.org/10.1016/j.petlm.2023.07.002

vibration does not make any change in the dipole moment thus it is not active to IR spectroscopy, whereas the asymmetrical stretching vibration (Fig. 1) triggers activeness of the molecule resulting IR absorption in 2349 cm^{-1} region. The two bending vibrations of CO_2 (Fig. 1) with matching frequencies exist at the same region doubly degenerated at 667 cm^{-1} [6–8].

In natural atmosphere, currently CO_2 is available at ~ 0.04% [9] and the solubility of CO_2 is about 76 cm^3 in 100 mL water at 25°C, which alters the solution pH to 3.76–3.9, close to the pK_{a1} of H_2CO_3 [10]. Moreover, the CO_2 solubility changes with the change in temperature and pressure. With increase in temperature CO_2 solubility decreases whereas with increase in pressure the CO_2 solubility in water increases till the pressure reaches to a steady value (above 700 atm) of CO_2 pressure [11,12]. Furthermore, CO_2 solubility depends on the nature of solvents (non-aqueous/organic) [13]. The oxygen-rich organic solvents such as acetone, 1,4-dioxane, methyl acetate, and 2-methoxyethyl acetate, interact favorably with CO_2 via Lewis acid (which accepts a pair of electrons and forms a covalent bond) or Lewis base (which donates a pair of electrons and forms a covalent bond) resulting in their diverse solubility [14].

In aqueous solutions, CO_2 exists as $CO_2(aq)$, $H_2CO_3(aq)$, $HCO_3^-(aq)$ and $CO_3^{2-}(aq)$, which are generated through the below-mentioned reactions [15–18].

$$CO_{2(gas)} \rightarrow CO_{2(aq)} \quad (1)$$

Solution of CO_2 in water behaves as a weak acid having pH ~3.9.

$$CO_{2(gas)} + H_2O_{(liq)} \rightarrow H_2CO_{3(aq)} \quad (2)$$

Subsequently, it is equilibrated between the dissolved CO_2 and the carbonic acid (H_2CO_3), a weak acid, where only ~ 1% of H_2CO_3 dissociates to HCO_3^- and CO_3^{2-} following two different reaction steps.

$$H_2CO_{3(aq)} \rightleftarrows H^+_{(aq)} + HCO_{3(aq)}^- \quad (3)$$

$$HCO_{3(aq)}^- \rightleftarrows H^+_{(aq)} + CO_3^{2-}(aq) \quad (4)$$

Furthermore, it is understood that on CO_2 dissolution, pH of solution changes depending on the quantity of CO_2 dissolved. The weakness of the acid is a reason why the solutions of carbonates are often alkaline [17], which is because of the release of OH^- (see reaction 5).

$$CO_3^{2-}{}_{(aq)} + H_2O_{(liq)} \rightarrow HCO_{3(aq)}^- + OH^-_{(aq)} \quad (5)$$

The carbonate also gives HCO_3^- when it reacts with H_2CO_3,

$$CO_3^{2-}{}_{(aq)} + H_2CO_{3(aq)} \rightleftarrows 2HCO_{3(aq)}^- \quad (6)$$

The solubility of CO_2 also depends on pH of solution. It increases in the pH range between 6 and 11 because of the increase in HCO_3^- concentration [11]. The CO_2 solubility in water is also enhanced upon addition of additives such as NaOH, Na_2CO_3 or $NaHCO_3$ because of their alkaline nature. Moreover, the chemical reductions of carbonates and bicarbonates are difficult.

In nature, plants play a significant role in CO_2 preservation in Earth's atmosphere through a natural CO_2 cyclic process [19,20]. In brief, terrestrial CO_2 is consumed by plants to produce their own food (carbohydrate) through photosynthesis. The living animals present worldwide, including human beings use plants and plant materials as food and on their decay, CO_2 returns back to atmosphere. The CO_2 cycle is presented in Fig. 2.

Historically, the CO_2 concentration in the atmosphere has varied significantly with respect to time. As believed, the early atmosphere of Earth was predominantly comprised of CO_2 [21,22] and around 14,000 years ago (end of the last ice age), the CO_2 level in air increased to about 50%. Following this global climatic transition, the CO_2 concentration in the atmosphere remained almost steady (~ 280 ppm) until the end of 18th century [3,18,23]. As human civilization progressed, based on the higher energy requirement/consumption versus lesser energy generation, the emission of CO_2 from different anthropogenic activities for example deforestation, fossil fuels burning, cement manufacturing, and waste incineration in total have disturbed the balance between CO_2 sinks and natural sources. CO_2 emission has been escalating continuously in the atmosphere since 1900 through the aforesaid activities and has hence disturbed the natural CO_2 conservation cycle (Fig. 2). Other sources of CO_2 emission such as living beings' respiration, the decay of dead plants and animals matters, volcanic eruptions and evaporation from oceans add up more CO_2 to the atmosphere. At present, the CO_2 concentration has reached ~ 405 ppm (0.04%), which grew with a rate of about 2–3 ppm annually since 2009 [24] and is currently reaching a total global anthropogenic CO_2 emissions amount ca. 35.5 Gt per year [25]. Again, CO_2 is plentifully present in ocean water than in air with an estimated net growth of 2 Gt dissolved CO_2 in seawater per annum [26–29].

On a daily basis we notice concerning CO_2 emissions contributing to global temperature rise through various news agencies. Human activities releasing CO_2 and the burning of fossil fuels together contribute nearly 80% of total emission into the air [30].

CO_2 is the major contributor to the enhanced greenhouse effect accounting for a total of around 60% of the increase in heat trapping

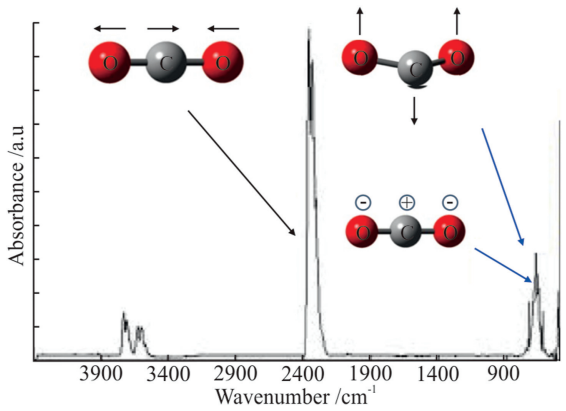

Fig. 1. IR spectra of CO_2, adopted from Ref. [8].

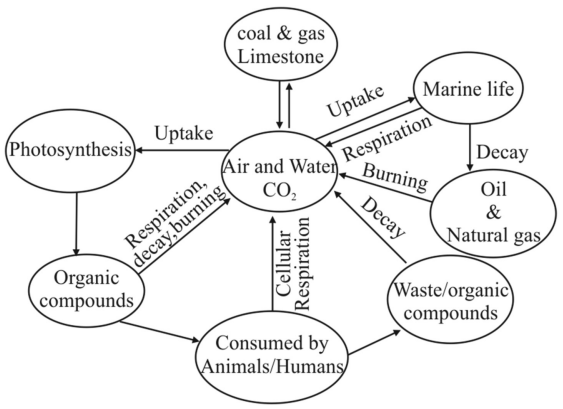

Fig. 2. CO_2 conservation cycle.

[21,31,32] over the geological time as estimated using GEOCARB modelling. The scientists and the meteorologists are with an agreement that the most probable cause of these changes is the man-made emission of "greenhouse gases" (GHGs), which trap the heat in the Earth's atmosphere. High CO_2 concentration in the environment consequently increases the input of radiative energy to the Earth. And the increase in CO_2 concentration in atmosphere is connected to the observable climatic changes, which has been tested using modern methods of time-series analysis. Furthermore, the rise in global temperature due to CO_2 insights the significant role of CO_2; as estimated, the average global temperature increases with a rate of 0.0055 ± 0.00096°C per year [33–38]. It is also apparent that the rise in abnormal weather events, for example summer droughts, flooding, etc., is someway related to the changes in global climate.

2. Materials and methods

For this article, the available literature on CO_2 chemical reduction was analyzed carefully, which especially deals with the generation of products up to C_2 containing compounds. Three different fields such as electrochemical, photochemical and plasma chemical were shortlisted due to their high impact on green chemistry when compared to thermal chemical reactions where the left-over chemicals load extra care for their cleaning/purifications. As compared to C_1 containing products derived from CO_2, C_2 containing products are very few but their inclusion is crucial for the further development in this field. In this article, we summarize the advancements in the field of CO_2 chemical reduction listed in the literature to date, which are discussed in the following sections.

Due to the rise in CO_2 amount in atmosphere, the interest in its chemical reduction is growing with time because of its prospective use as carbon source, and the efforts to mimic the photosynthetic carbon incorporation [39–44]. The transformation of CO_2 using different energy inputs in various methods such as photolysis [44–56], radiolysis [57–62], electrolysis [63–77], sonolysis [78,79], plasmolysis [80–94], and thermal/thermolysis [95–103] have been investigated by researchers/scientists around the world during last few decades. We have aimed to review the applications of various methods (electro, photo, and plasma) for chemical reduction of CO_2 into a variety carbon (up to 2 carbon atoms) containing products through this article. In the subsequent sections, we present the fundamental aspects of electro-, photo-, and plasma chemical methods in brief.

2.1. Electrochemical processes

Before we implement the electrochemical method for CO_2 reduction, it will be beneficial to include the thermodynamical data such as heat of formation of CO_2 = 336 kcal·mol^{-1} [104] and electron affinity = −0.6 ± 0.2 eV [105] for realizing the stepwise reduction processes as given below:

$$CO_2(aq) + 2e^- + 2H^+ \rightarrow HCOOH \quad (7)$$

$$HCOOH + 2e^- + 2H^+ \rightarrow HCHO + H_2O \quad (8)$$

$$HCHO + 2e^- + 2H^+ \rightarrow CH_3OH \quad (9)$$

$$CH_3OH + 2e^- + 2H^+ \rightarrow CH_4 + H_2O \quad (10)$$

According to reactions (7)–(10) to transform CO_2 to HCOOH, HCHO, CH_3OH and CH_4, 2, 4, 6 and 8 electrons are needed respectively [106].

Electrochemistry discusses the transformation of electrical energy into chemical energy and vis-à-vis. Oxidation or reduction of materials/compounds at well-controlled electrode potentials by withdrawing or adding electrons in electrochemistry proposes several prospects in environment related engineering. Normally, an electrochemical cell [107] operates redox reactions, which in general comprises of three (counter, working, and reference (one each)) electrodes, an electrolyte (conducting medium), cell boundaries, and optional facilities such as cooling/heating of the entire cell for desire experimental temperature control and stirring of electrolyte to get uniform reactants/products distribution. Similarly, gas inlet and outlet along with pressure control facility are attached to get desired experimental pressure. To prevent metal leaching or corrosion associated contamination because of structural material, the inner part of the autoclave cell is either made up of quartz/glass or Teflon coated to make the surface inert. The quantitative information of an electrochemical cell is generally achieved considering the potential difference between the working and counter electrodes as monitored with respect to the reference electrode. Normally, standard calomel electrode (SCE) or normal hydrogen electrode (NHE) or standard hydrogen electrode (SHE) or reversible hydrogen electrode (RHE) is used as reference electrode.

The yields of products in electrochemistry are expressed in faradaic efficiency (FE) and energy efficiency (EE). The faradaic efficiency (η_F) is defined as [108]:

$$\eta_F = \frac{Coulombs\ obtained}{(Total\ molecules\ consumed) \times nF} \quad (E1)$$

where F is Faraday constant (96,500 coulombs/mol), and n is number of electrons.

The electrochemical reduction of CO_2 generates several products such as HCOOH, HCHO, CO, CH_4, etc. The energy efficiency ($\in$), for a product for instance HCOOH formation [109] is expressed as:

$$\in = \frac{\Delta H \times (percent\ faradaic\ efficiency)}{nF\ (E_{rev} + \eta_c + \eta_a + \eta_{IR})} \quad (E2)$$

where ΔH = 64.4 kcal/mol; E_{rev} = 1.43 V, for $CO_{2(g)} + H_2O_{(l)} = HCOOH_{(aq)} + O_{2(g)}$ reaction and η_c, η_a and η_{IR} represent the concentration, the activation and the ohmic over potentials respectively.

As mentioned above, CO_2 is believed to be a feasible energy storage medium [66]. The transformation of CO_2 to useful products is a capable long-term goal for generation of raw materials for industries and/or for fuels. It will be noteworthy to include at this juncture the knowledge about the redox potentials of CO_2 and its different product couples (see reactions 11–15).

$$CO_2 + 2e^- + 2H^+ \rightarrow HCOOH\ (E^{o\prime} = -0.61\ V) \quad (11)$$

$$CO_2 + 2e^- + 2H^+ \rightarrow CO + H_2O\ (E^{o\prime} = -0.52\ V) \quad (12)$$

$$CO_2 + 4e^- + 4H^+ \rightarrow HCHO + H_2O\ (E^{o\prime} = -0.48\ V) \quad (13)$$

$$CO_2 + 6e^- + 6H^+ \rightarrow CH_3OH + H_2O\ (E^{o\prime} = -0.38\ V) \quad (14)$$

$$CO_2 + 8e^- + 8H^+ \rightarrow CH_4 + 2H_2O\ (E^{o\prime} = -0.24\ V) \quad (15)$$

Although, the $CO_2/CO_2^{\bullet-}$ redox potential value is −2.21 V vs SCE [109–111], but $E^{o\prime}$ (standard electrode potential) turns into less and less negative when employs more and more electrons in the reduction reactions.

In this process, the products for instance CO, HCOOH, CH_4, C_2H_4, $C_2O_4^{2-}$, CH_3OH, C_2H_5OH, $(CH_3)_2CO$, etc. observed by reduction differ with reaction conditions, electrolyte, electrode material, etc. The extensive research on CO_2 electrochemical reduction have been reported in recent past for generation of different products, which are summarized in this review.

2.2. Photochemical processes

The utilization of photochemical means to destroy harmful organics due to oxidation and alternatively to transform them to beneficial and/or less harm products during the chemical reduction is the finest approach to take on the environmental pollution related issues [112–119]. In addition, the utilization of CO_2, the final oxidized product of organics, through its conversion to suitable and value-added products realizes an interesting awareness of the high value of CO_2. The use of solar light for such conversion at enhanced rate using photocatalyst such as titanium dioxide (TiO_2), zirconium dioxide (ZrO_2), iron(III) oxide (Fe_2O_3), cadmium sulphide (CdS), tungsten oxide (WO_2), tin oxide (SnO_2), etc. is an attractive alternative. Amongst these, TiO_2 (a model semiconductor chosen to discuss general properties) is considered as an economical, and easily available non-toxic photo catalyst, which can work under solar light. The band gap energy (E_{bg}) between valence and conduction bands of TiO_2 is ~ 3 eV (E_{bg} for anatase (one form) is 3.2 eV and for rutile (another form) is 3 eV) [113,114]. On light exposure (when the incident light energy ($E_{h\nu}$) > (E_{bg}), TiO_2 generates electron (e^-) -hole (h^+) (charge carrier) pair. The primary step in TiO_2 photo catalytic oxidation due to the formation of both $^\bullet OH$ ($E^o = 2.72$ V) [120,121], an oxidant and $O_2^{\bullet-}$ ($E^o = -0.33$ V) [121,122], a reductant occurs during the reactions of photo-generated charge carrier with air/O_2 available in aqueous system through reactions 16–20.

$$TiO_2 \xrightarrow{h\upsilon} e^- + TiO_2^+ \quad (16)$$

$$TiO_2^+ + H_2O \rightarrow {}^\bullet OH + H^+ + TiO_2 \quad (17)$$

$$e^- + H^+ \rightarrow H \quad (18)$$

$$H + H \rightarrow H_2 \quad (19)$$

In presence of O_2 (in air or oxygen containing systems),

$$e^- + O_2 \rightarrow O_2^{\bullet-} \quad (20)$$

The photo-generated e^- having $E^o = -2.8$ V [120,121] reduces the available solute(s) present in the system. Furthermore, the generation of $^\bullet OH$ in TiO_2 photolysis has been understood with the generation of hydroxy products of aromatic compounds [123,124]. The EPR and absorption spectrum studies confirmed the existence of $^\bullet OH$ [116] and the trapped electron [113,114,125,126] in light exposed TiO_2 systems. All the processes together along with photolytic charge carrier generation within the conduction and valence bands and the redox reactions proceeding on semiconductor surface are explained in Fig. 3. In the presence of $^\bullet OH/h^+$ scavenger (normally alcohol), the TiO_2-based system is converted to reducing condition, and on addition of an electron scavenger (N_2O or O_2), the absolute oxidation favoring environment can be made.

Conversely, TiO_2 is inherently acting as an n-type (donor levels) semiconductor but with doping of pentavalent cations such as: Nb, Ta, etc. it is modified/changed to p-type (acceptor levels) semiconductivity for diverse applications. It belongs to transparent semiconducting oxides (TSOs) category materials (which are

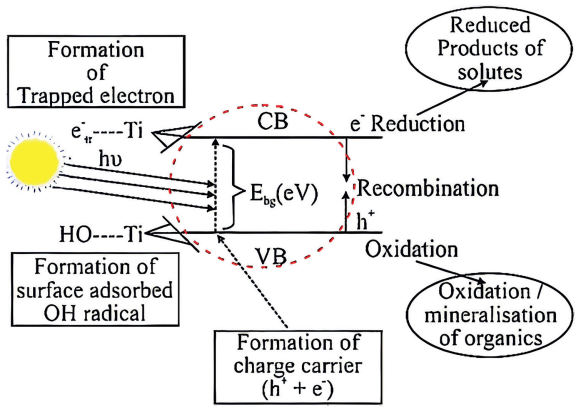

Fig. 3. Primary steps along with their redox reactions in TiO_2 photolysis.

simultaneous optically transparent and electrically conductive and offer important opening to formulate all-transparent homojunction devices for energy storage and light harvesting) [127–129]. Furthermore, the particle size and the quantity of semiconductor play important roles in photo catalytic activity [116,130]. Laboratory synthesized and commercially available TiO_2 in various forms are employed for CO_2 chemical reduction [116,131–138] to generate various products, which depend on experimental conditions as discussed in the following sections.

2.3. Plasma chemical processes

Many thermal reactions utilize catalysts, which are often costly, prone to poisoning, and necessitate periodic standard regeneration/replacement. To improve these issues, plasma-based technologies can possibly offer a different alternative to produce high-value products. These technologies are faster and relatively cheaper as compared to conventional methods.

The word 'Plasma' was first introduced by Irving Langmuir while discussing a low-pressure discharge [139], which was generated when a carrier gas gets in contact with electric field. In this process, the neutral carrier gas is energized until an inter-atomic collision becomes sufficiently violent and detaches electrons [140] ensuing in the formation of reactive species, which is composed of charged particles, free radicals, excited species, and various radiations (photons) [141–143]. Plasma possesses net zero charge due to the formation of equal quantity of negative and positive charged species. Plasma is of two types: thermal and non-thermal. The generation of thermal plasma requires high pressure and high temperature with high energy electrons. Non-thermal plasma describes a non-equilibrium condition at ambient pressure and temperature, in which the electron temperature ~ 1 eV–10 eV remains much higher than medium temperature. Non-thermal plasma is a weak ionized gas, viable for weak bonds breaking, which is conducive for free radical chemistry.

Generally, a very low (10^4 mL^{-1}–10^5 mL^{-1}) amount of free electrons and the counter cations are present in gaseous medium due to natural radioactivity or cosmic ray background. In absence of any dielectric (insulator) barrier, when the potential '*V*' volt is applied between the two parallel electrodes separated by a distance '*d*' mm, the background electron and counter ions contribute to insignificant current flow. As potential/applied voltage increases, the electrons and counter ions gain energy and start accelerating in opposite direction towards the relevant electrode. The applied electric field '*V/d*' causes the electron and counter ion to gain energy by increasing the collision rate. Electrons undergo elastic collision with different gas molecules while travelling towards the

anode. During the process, electron transfers its partial energy to target gas molecule and ionizes, thereby reducing its own energy. In the influence of electric field, constellates of electrons are formed before reaching anode. At the same time the cathode ions move slowly towards the cathode and neutralize. With the passage of time this vast number of electrons (electron avalanche) increases the current above the background level, which is known as *dark* or *Townsend discharge*. When the localized developed electron avalanche between charged electrodes increases the space charge field and reaches equal to applied electric field, then the Townsend discharge converts into streamer discharge due to the breakdown of medium (gas), and noticeable due to heating of the medium and the light emanation. At favorable unrestricted current, a weak spark grows, the ion bombardment increases the temperature of electrode, and it starts to heat up and melts resulting in high ampere arc; the operation of high-pressure xenon arc lamp is typical example. Breakdown voltage is the minimum applied voltage at which a portion of an insulator becomes conductive, which depends on ionization step, electronegativity of gas component(s), the electrode surface, and mean free path of electron in gas medium. There is a significant difference between spark and filamentary/micro-discharge. In spark, temperature of gas medium becomes equal to the temperature of electrons i.e., 10^6K. Also, it draws high current (~ 100 A), high power (~ 100 W) and turns out to be uncontrollable. Spark is a non-uniform discharge. If the electrode surface becomes conducting then they allow high current to flow, which normally damages electrodes. Alternatively, if one or more electrode(s) is(are) covered with dielectric or a dielectric barrier is placed in between electrodes, the applied potential helps in polarizing dielectric layer(s)/surface(s), preventing free flow of charge and restricts the system current. In discharge, the dielectric surface charge gets neutralized because of current flow, hence its density becomes restricted and discharge process remains nanosecond pulsed event. This phenomenon causes minimal heating of the medium; it draws less current (μA to mA) hence uses less power (mW). The dielectric layers control the discharge characteristics, and the process is known as dielectric barrier discharge (DBD) or *cold plasma* or non-thermal plasma or 'silent discharge' [144]. This system is familiarly used in ozone generation [145]. The dielectric, being an insulator, cannot pass direct current (DC); hence DC is not used for dielectric barrier discharge. In DBD the thickness and the dielectric constant, in combination with time derivative of the applied voltage, *dU/dt* determines the quantity of displacement current, which passes through dielectric(s). In the discharge gap, the electric field must be high enough to cause the gas breakdown [145,146]. Typically, chemically inactive materials such as quartz, glass (Pyrex), mica, alumina, etc. Are used as dielectric.

The micro-discharge generation within the plasma due to the absorption of energy by carrier gas consists of photons, excited species, free radicals, ionized species, small ionic clusters, etc. Each of these constituents initiates physicochemical changes and chemical reactions. Thus, either by selecting appropriate reactant(s) within the gas stream, or by suitably coating of electrode surface(s) or even by using different reactant mixture for instance gas-solid or gas-liquids as packed bed, homogeneous and heterogeneous reaction conditions can be achieved. The charge transferred amount in micro-discharge depends on gas properties, discharge gap and nature of dielectric [147,148]. DBD plasma has wide applications in medical and societal welfare [149,150].

In plasma chemistry, energy conversion and the conversion efficiency are normally used for quantitative measurements. For typical CO formation from CO_2, these quantitative parameters are defined as:

$$Conversion\ of\ CO_2\ (\%) = \frac{[CO]_{Outlet}}{[CO_2]_{Inlet}} \times 100 \tag{E3}$$

where $[CO_2]_{Inlet}$ is the $[CO_2]$ before the discharge operation and $[CO]_{Outlet}$ is $[CO]$ measured during plasma discharge in CO_2 to CO conversion. The percentage of CO_2 conversion is evaluated with the difference in $[CO_2]$ in discharge operation.

Likewise, the energy efficiency is calculated from CO_2 decomposition by following E4 expression:

$$Energy\ Efficiency\ (\%) = \frac{[\Delta H_{298}](kJ/mol)}{Energy\ consumed\ (kJ)/moles\ of\ converted\ CO_2(mol)} \times 100 \tag{E4}$$

(CO_2═CO + ½O_2; ΔH_{298} = 283 kJ/mol) [151].

The possible one carbon (C_1) atom containing stable chemical products generated from CO_2 include CO, HCOOH, HCHO, CH_3OH and CH_4. This kind of CO_2 conversion does not need C—C formation. The other intermediate and/or stable products/species containing only C atom(s) such as coal, graphene, etc. Are also produced from CO_2 under diverse conditions other than $\geq C_1$ containing compounds. The details of their formations are discussed below.

At the onset we will discuss the formation of compounds containing only C atom(s) and subsequently the discussion will be focused on C_1 and C_2 compounds.

3. Discussion

3.1. Carbon based compounds

3.1.1. C radical and C compounds

In CO_2 approximately 73% oxygen (O_2) and 27% carbon (C) are available in the molecule. O_2 is a major product obtained efficiently from CO_2 in human metabolism during respiration. An ideal method which can convert CO_2 to C and O_2 under moderate conditions is greatly attractive; however, because of the extremely adverse thermodynamics, direct CO_2 transformation requires extreme conditions. A direct methodology is required to minimize the oxygen supply, which is in high demand in deep space exploration missions of man. For this an electro-thermochemical hybrid looping (ETHL) has been developed to convert CO_2 to C and O_2 at mild conditions with theoretically 100% oxygen recovery efficiency [152]. In ETHL process, the electrochemical step generates CO initially from CO_2 reduction. This combines in a thermochemical step, and further converts CO to C in a catalytic bed reactor following the Boudouard reaction as mentioned below:

$$2CO_2 \rightarrow 2CO + O_2 \tag{21}$$

$$2CO \rightarrow C + CO_2 \tag{22}$$

In another research, the oxygen-deficient magnetite prepared from magnetite powder and H_2 reaction, decomposes CO_2

efficiently into C at 300°C. The formation mechanism emphasizes that the adsorbed CO_2 on oxygen-deficient magnetite surface undergoes decomposition into elemental C and oxygen ions. Later, the C converted to CH_4 after reaction with H_2 at 150°C–300°C [153] as shown in Fig. 4. Moreover, elemental C can be extracted prior to its reduction with H_2.

Furthermore, many catalytic methods that work above 600°C necessitate high energy to meet heat requirement, which makes these methods financially expensive. During the process the catalysts gum up speedily, limiting catalyst's ability to continue the reaction progress [154–156]. A new catalyst (active palladium combined with liquid gallium) has been developed by Esrafilzadeh et al. [157] in which the liquid allows palladium to convert alkanes into alkenes without gumming up. This concept has been implemented in CO_2 conversion by using a prepared room temperature electrical conducting liquid alloy of gallium, indium, and tin. This silvery mixture later spiked with catalytically active cerium. This catalyst helps CO_2 reduction electrochemically to a layered solid carbonaceous species, at low potential (−310 mV). In this process, a part of cerium at liquid surface reacts with O_2 from the surrounding air forming ultrathin layer of cerium oxide, and the high fraction of cerium remains protected by the liquid metal. CO_2 was dissolved in dimethylformamide (DMF)-based liquid electrolyte containing less quantity of liquid metal. The metal later is charged with an electrical current; as a result, the surface CO_2 slowly gets transformed into solid carbon flakes [158–160], which was later detached naturally from metal surface. The mechanism proposed with multiple steps reactions is shown below:

$$4Ce_{(Galinstan)} + 3O_2(air) \rightarrow 2Ce_2O_3 \quad (23)$$

$$Ce_2O_3 + 3H_2O + 6e^- \rightarrow 2Ce^{(0)} + 6OH^- \quad (24)$$

$$Ce^{(0)} + CO_2 \rightarrow CeO_2 + C \quad (25)$$

$$CeO_2 + 2H_2O + 4e^- \rightarrow Ce + 4OH^- \quad (26)$$

$$4OH^- \rightarrow O_2 + 2H_2O + 4e^- \quad (27)$$

During the process, CeO_2 was constantly reduced to elemental Ce through reaction 26 with applied reductive potential, which led to the catalytic process, and correlated with the incipient hydrous oxide adatom mediator (IHOAM) [161] principle. The reactions (23)–(26) occur at working electrode whereas O_2 evaluation (reaction 27) occurs at counter electrode.

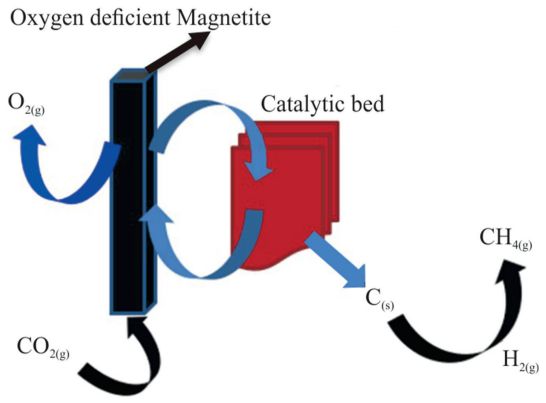

Fig. 4. Generation of elemental C and CH_4, concept adopted from Ref. [153].

3.1.2. Graphene

Graphene, the strongest (> 40 and > 300 times stronger than diamond and A36 structural steel respectively) carbon allotrope, consists of a single layer of C atoms arranged in a 2D honeycomb lattice type nanostructure [162]. It is used in paints, anti-corrosion coatings, sensors, efficient electronics, flexible displays, efficient solar panels, DNA sequencing, drug delivery, etc. Molina-Jirjn et al. [163], have reported an extraordinary CO_2 utilization for graphene production. In their work, a simple single-step process has been developed where CO_2 is converted to a multi-layer graphene by atmospheric pressure chemical vapor deposition (APCVD) directly. Cu and Pd bi-metallic alloy film has been employed both as heterogeneous catalyst as well as substrate. High Cu amount is essential for CO_2 conversion. This discovery serves as a groundwork for further development of alloy materials for CO_2 reduction to graphene.

Furthermore, many catalytic reactions require high temperature to synthesize high quality graphene [164]. A graphene synthesis method using different carbon sources such as C_2H_2, CO_2 and CO have been developed using copper foil, which in turn inspires the role of electronic promoters in catalysis sciences at room temperature. The promoters are the substances which increase the catalytic activity, but actually they are not catalysts. Under the study, Hajian et al. [165] have applied charges to modify the electronic effects of piezoelectric materials.

Additionally, the generation of graphene through CO_2 reduction electrochemically is high challenge; this requires good control over the reaction kinetics, solubility of various gases, diffusivities of multiple ions, and growth/nucleation of carbon on desired surface. Graphene has been generated successfully from CO_2 using $CaCl_2$–NaCl–CaO molten salts [166]. In this case CO_2 is effectively fixed by oxygen ions in molten salt to form carbonate ions, and later it splits into graphene electrochemically at stainless steel cathode, while O_2 is released at RuO_2–TiO_2 anode. This finding leads to a new generation procedure for high-valued graphene synthesis from CO_2, contributing also to establishing a low-carbon and sustainable world.

The utilization of graphene has slowed down due to its high cost. A low carbon footprint and low-cost graphene synthesis from CO_2 has been introduced to overcome these issues. This technique is initiated by direct molten carbonate electrolytic CO_2 splitting to a nano-thin carbon nanoplatelets of 25–125 graphene layers, which later transformed to graphene electrochemically. This worthwhile product (graphene) incentivizes the utilization of CO_2 [167]. Graphene has also been successfully synthesized by using Ni, Fe and Ce containing trimetallic novel catalyst [168]. In another work, a three-dimensional crape myrtle flower-like graphene of large surface area with high conductivity has been generated after the reaction of CO_2 and sodium metal [169]. Additionally, the burning of magnesium in dry ice generates few layers of nanosheets of graphene, which is an innovative way for the production of graphene, a most promising carbon nanostructures by capturing CO_2 [170].

Under plasma application, CO_2 and N_2 are used in a closed reaction container; with applied high-voltage electricity graphene has been generated [171]. In another work, the researchers have synthesized graphene-like vertical structures from CO_2 using plasma enhanced chemical vapor deposition [172].

The transformation of CO_2 to CO, $HCOO^-$/HCOOH, HCHO, CH_3OH, CH_4, etc. may perhaps be considered under artificial photosynthesis. The adsorption and the activation of CO_2 and/or the intermediate species at electrode and/or catalyst surface are crucial steps to improve the conversion kinetics and product efficiencies [173]. The electro-, photo- and plasma chemical efficiency could be

improved by the utilization of various materials, which is discussed in the following sections.

3.2. C_1 compounds

3.2.1. Carbon monoxide

The major advantage of chemical reduction and/or utilization of CO_2 is the generation of C_1 products such as CO, HCOOH, HCHO, CH_3OH and CH_4. Although CO is a toxic gas, it possesses several applications in bulk chemicals manufacturing, and thus is recognized as an industrial gas [174].

The reaction of carbonaceous CO_2 feedstocks producing CO is endothermic in nature. This gasification reaction is thermodynamically favored at higher temperature (> 680°C) (CO_2 gasification) [95,96]. CO_2 gasification is available from biomass, coal, municipal solid wastes, sewage sludge, etc. to produce CO. The Boudouard reaction is well-known CO generating reaction, in which charcoal (solid carbon) reacts with CO_2 and produces CO.

$$CO_2(g) + C(s) \rightarrow 2CO(g) \quad (28)$$

This is an easy way for CO_2 mitigation through which CO_2 obtained from a variety of combustion outlets is converted to CO fuel gas.

3.2.1.1. Electrochemical. An economical bismuth-carbon monoxide evolving catalyst (Bi-CMEC) has been produced upon cathodic polarization of an inert glassy carbon electrode in acidic solutions containing Bi^{3+} [175]. This catalyst has been applied in combination with 1-ethyl-3-methylimidazolium tetrafluoroborate ([EMIM]BF4) ionic liquids to affect the CO_2 electrocatalytic conversion to CO with significant current density at < 0.2 V. Bi-CMEC is selective and operates with ~ 95% FE for CO generation.

Single-atom catalysts with interesting properties have been developed as an exciting example but unique from their nanocrystal counterparts. For example, Ni single atoms dispersed into graphene nanosheets have active sites for electrocatalytic CO_2 reduction reaction (CO_2RR) to CO [176] without the involvement of Ni nanoparticles. Normally, Ni catalyzes the hydrogen evolution reaction (HER) solely in CO_2RR conditions, whereas the available Ni single atom exhibits high selectivity for CO (95%) at 550 mV overpotential in water. The current density has been topped up to > 50 mA · cm^{-2} with CO formation turnover frequency of 2.1×10^5 h^{-1} with 97% CO selectivity. Furthermore, the HER is known since the 18th century, and is often studied in electrochemical processes [177,178] in water. Water electrolysis is not a very economic method for hydrogen production, but it supplies high purity H_2 without polluting the environment. The possible reactions taking place in HER are:

$$2H_2O(l) \rightarrow 2H_2(g) + O_2(g) \quad (29)$$

which includes a cathodic reaction,

$$2H_2O + 2e^- \rightarrow 2OH^- + H_2 \quad (30)$$

and an anodic reaction

$$4OH^- - 4e^- \rightarrow 2H_2O + O_2 \quad (31)$$

It is important to note that in aqueous systems or solvents containing significant quantities of water, the HER is constantly in competition with CO_2 reduction [179–181].

The highly conductive and porous 3D graphene structure in iron porphyrin-based graphene hydrogel (FePGH) electrocatalyst has shown effective CO production from CO_2. High FE ~ 96.2% of CO production has been achieved at low overpotential (280 mV) [182]. Moreover, in absence of porphyrin, this hydrogel system exhibited 100% H_2 efficiency but with modification of material (simply by adding porphyrin) the efficiency and product selectivity are changed significantly (see Fig. 5). In the presence of porphyrin, the graphene hydrogel showed as an efficient and strong catalytic activity for CO_2 reduction at low overpotential, and these changes varied with porphyrin loading amount. The high porphyrin loading FePGH showed substantially improved current densities which reduced the thermodynamically stable CO_2 to form $CO_2^{-\cdot}$.

The application of precious group metal (PGM) for example gold, palladium, platinum, rhodium, and silver catalysts on CO_2 reduction to CO under alkaline conditions via electro catalyzed is limited due to the high material price [183]. Nickel and nitrogen-doped porous carbon catalyst (Ni–N–C) [184] has been developed and suggested as an alternative of PGM catalyst based on the performance on pure CO formation from CO_2 under industrial electrolysis conditions. The developed PGM-free catalyst has been used as Gas Diffusion Electrodes (GDEs) to produce reactive three-phase interface which exhibited CO partial current densities above 200 mA · cm^2 and stable faradaic CO efficiencies (~ 85%).

Furthermore, the electrochemical reduction of CO_2 at cathode is always balancing with the oxygen evolution reaction (OER) at anode. The energy barrier and OER kinetics should be considered for overall efficiency of electrical energy to chemical fuel conversion. The OER in $KHCO_3$ electrolytes mostly depends on noble metal (Ir- and Ru-) based electrocatalysts present at anode. By anodizing a metallic Ni–Fe composite foam in low (0.1 M) $KHCO_3$ solution at 85°C under a high-current ~ 250 mA/cm^2, OER on NiFe foam is accompanied by anodic etching, and the surface layer evolves into a nickel–iron hydroxide carbonate (NiFe-HC) material. The resulting NiFe-HC electrode in CO_2-saturated 0.5 M $KHCO_3$ showed superior OER activity to IrO_2 with an overpotential of 450 and 590 mV to achieve 10 and 250 mA/cm^2, respectively. The paired NiFe-HC with a CO_2RR catalyst of cobalt phthalocyanine/carbon nanotube (CoPc/CNT) in a CO_2 electrolyzer has brought a selective CO_2 conversion to CO with >97% FE and concurrently anodic water oxidation to O_2 [185].

In a combined experimental and theoretical investigation on CO_2 electrochemical reduction, polycrystalline Sn surfaces [186] have been proved as capable catalysts for selective $HCOO^-$ production. Sn electrodes produce CO, $HCOO^-$ and H_2 across a range of potentials where $HCOO^-$ production becomes favored at below −0.8 V vs RHE with highest 70% FE at −0.9 V vs RHE. The scaling relations for Sn and other metals have also been analyzed with experimental current densities and theoretical (density functional theory (DFT)) binding energies. *COOH, a key intermediate has been reported for CO formation.

Generally, for catalyst design on transition metal-based materials, the role of morphology, size, surface modifications, grain boundary densities and metal support interaction are significant [187], Au catalyst is one of the excellent examples. Because of the low product formation rates (photocatalysis) and high capital

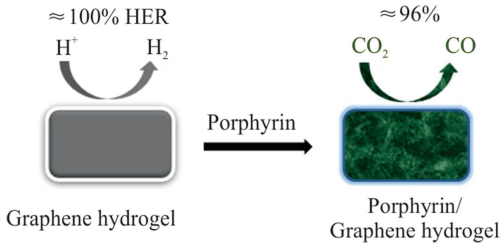

Fig. 5. Product selectivity changes from 100% HER to 96% CO_2 conversion to CO with the introduction of porphyrin in graphene hydrogel system [182].

investments (solar thermo-chemical cycles) in competing technologies, the reverse water-gas shift (rWGS) catalysis emerges as a leading technology to transform CO_2 to CO efficiently. It is noteworthy to describe at this point about the water-gas shift (WGS) reaction [188], which is the reaction between CO and H_2O vapor leads to CO_2 and H_2 products. This is an important reaction, which is normally used in manufacturing hydrogen along with ammonia, hydrocarbons and methanol syntheses.

$$CO + H_2O \rightarrow CO_2 + H_2 \quad (32)$$

The rWGS reaction with support of suitable catalyst is an efficient way to utilize CO_2 in CO production and subsequently to minimize its environmental impact as a greenhouse gas. For this purpose, active $CuFe/Al_2O_3$ catalyst is used in a solid oxide electrolysis cell [189]. The rWGS is followed by the modified Fischer–Tropsch (FT) reaction [190–192]. On hydrogenation, the generated CO is converted to liquid fuel (alcohols, diesel, and gasoline) [193]. Furthermore, the novel-Cs doped Fe–Cu–Cs/Al_2O_3 multicomponent catalyst has exhibited high level CO_2 conversions with absolute selectivity to CO [194]. On the other hand, the formate obtained from CO_2 and H_2 has been anticipated with CO intermediate formation. Nevertheless, the formate dissociation mechanism is the key reaction path for CO production where Cu(I) species are formed from Cu^0 oxidation [195]. Fe-based catalysts are highly active for CO_2 to CO conversion, and their activity and selectivity are enhanced upon addition of promoter (Cs) [194,196].

As mentioned above the modified Fischer–Tropsch is utilized for CO_2 conversion, it will be supportive if the actual FT process is explained in brief at this point. The FT process [197–199] is the chemical reaction that converts CO and H_2 (syngas) mixture into liquid hydrocarbons in presence of catalysts at one to several tens of atmospheres pressures and temperatures of 150°C–300°C. This process has three main elements: catalyst, gas loop and reactor, which works in three steps. The first step includes the conversion of a carbon source, such as natural gas, biomass, coal, or organic waste, into syngas. Syngas is the feed material for FT process, which is the second step in the indirect liquefaction process. FT synthesis is the catalytic polymerization and hydrogenation of CO, and finally produces a synthetic crude oil (syncrude, a multiphase mixture of hydrocarbons, oxygenates and water). The third step includes the refining of syncrude to products.

Interestingly, electrochemical reduction of CO_2 at an extremely low temperature (−30°C) has also been investigated with Cu electrode in methanol electrolyte. CH_4, CO and ethylene (C_2H_4) are found as CO_2 reduction products. Under ideal experimental conditions, the FE of CH_4 reported is > 42%. At this temperature, the efficiency of HER is decreased to < 8% because of the competition reaction [200].

The metal complex $[(tpy)(Mebim\text{-}py)Ru(II)(S)]^{2+}$ (tpy = 2,2′:6′,2″- terpyridine; Mebim-py = 3-methyl-1-pyridylbenzimidazol-2-ylidene; S = solvent) is reported as a strong reactive electrocatalyst for CO_2 reduction to CO. In this case, an electrocatalyst in two-compartment electrochemical cell has been explained for CO_2 splitting [$CO_2 \rightarrow CO + 1/2\ O_2$] [201]. In presence of $[(tpy)(Mebim\text{-}py)Ru(II)(NCCH_3)]^{2+}$, CO_2 experiences further reduction at ligands to produce CO and CO_3^{2-} as end products through metallocarboxylate intermediate formation [202–215].

$$2CO_2 + 2e^- \rightarrow CO + CO_3^{2-} \quad (33)$$

3.2.1.2. Photochemical. The anatase and the rutile forms of TiO_2 signify that the former is superior catalyst for CO supply, while the latter (rutile) is more efficient in hydrogenation of the adsorbed CO [216]. The pure or doped photocatalysts as composites or as solid solutions are generally presented along with their corresponding preparative methods and catalytic performances. A monolith photoreactor has been evaluated with a cell type reactor for photocatalytic reduction of CO_2 in presence of H_2. The monolith (monolith is a geological feature comprising of a single massive stone or rock) channels have been dip-coated with TiO_2 nanoparticles and its performance on CO_2 photoreduction has been reported higher in presence of H_2 than H_2O with 200 CPSI cell density. The higher CO evolution has been observed at 1.5 CO_2:H_2 molar ratio [217].

In another work, Cu^{II} quaterpyridine complex $[Cu(qpy)]^{2+}$ catalyst has been designed to transform CO_2, and found highly efficient and high selective for visible light driven CO_2 reduction in acetonitrile (CH_3CN) containing $[Ru(bpy)_3]^{2+}$ (bpy: bipyridine) as photosensitizer and BIH/TEOA (1,3 dimethyl 2 phenyl 2,3 dihydro 1*H* benzo [*d*]imidazole/triethanolamine) as sacrificial reducing agent. The photocatalytic reaction enhances significantly in presence of H_2O (1%–4% *V/V*), with a turnover number (TONco) of > 12,400 and 97% selectivity for CO production [218].

Furthermore, three different kinds of photocatalytic systems for CO_2 reduction have been utilized. First, two component systems with different rhenium(I) complexes have redox photosensitizer and catalyst characteristics used in the reaction solution. The ring-shaped rhenium(I) trinuclear complex and fac-[Re(bpy)(CO)3(MeCN)]$^+$ mixed system displays as most capable photocatalytic system with quantum efficiency (Φ_{CO}) 0.82 at 436 nm. The second, supramolecular photocatalysts, possesses different uses such as a catalyst, redox photosensitizer, and bridging ligand in one molecule which brings $\Phi_{CO} = 0.45$, turnover number (TON_{CO}) = 3029, and turnover frequency (TOF_{CO}) = 35.7 min^{-1}. The third is artificial Z-Scheme photocatalyst in which the photocatalysis is shown by stepwise excitation of both semiconductor and supramolecular photocatalyst [219]. In supramolecular photocatalysts, the photosensitizer and catalyst, linked to each other are more efficient and durable photo catalyzer as compared to their corresponding mixtures and hold strong oxidation and reduction powers. Similar observation has also been observed in hybrid photocatalyst with a semiconductor system. This is an example of photocatalyst for CO_2 reduction using visible-light via Z-Scheme mechanism, where the semiconductor and the photosensitizer unit of supramolecular photocatalyst are excited stepwise to transfer electron from semiconductor to catalyst unit. In the next steps the photocatalytic reduction of CO_2 includes the addition of various functions to the photocatalytic systems, for example CO_2 collection for using low CO_2 concentration, water oxidation, and light-harvesting [219]. As mentioned, the artificial Z-scheme photocatalyst comprises of two connected semiconductor photocatalysts: oxidation photocatalyst and reduction photocatalyst one each. The electron cascade steps of vectorial charge flow profile in this two-step photoexcitation system [220,221] resembles with Z alphabet, thus naming as Z-scheme system (shown in Fig. 6). Its mechanism confers an efficient charge

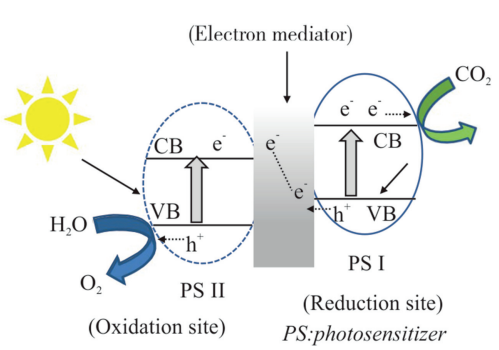

Fig. 6. Schematic presentation of Z-scheme.

separation and shows strong oxidation and reduction abilities within the system.

More interestingly, the N, S co-doped aminated coal-based carbon nanoparticles (NH_2-CNPs) are synthesized by thionyl chloride chlorination followed by passivation with ethylenediamine. The NH_2-CNPs vesicle-type spherical particles containing mesoporous structure are capable of adsorbing CO_2. The defect NH_2-CNPs structure due to N and S doping has a capability to produce electrons under visible-light irradiation along with efficient photogenerated carriers' separation. This leads to the production of CO along with CH_3OH, C_2H_5OH, H_2 and CH_4 as photocatalytic CO_2 reduction products with 76.6% CO_2 conversion relating to CH_3OH selectivity [222].

Another photocatalyst has been prepared by a combination of commercial TiO_2 P25 with a mesopore structure and carbon spheres with a microporous structure for superior CO_2 adsorption capacity. The combined TiO_2-carbon spheres/silica cloth photocatalysts exhibited better efficiency in CO_2 reduction to CO than CH_4 formation. The 0.5 g graphitic carbon spheres combined with 1 g of TiO_2 P25 has resulted in ~ 100% CO selectivity, eliminating CO separation process from CH_4 and H_2 gas mixture after reaction completion [223].

Furthermore, the formation of S-scheme heterojunction is well recognized as a favorable approach for the improvement of efficient photocatalytic system. $CsPbBr_3$ nanocrystals/CoAl layered double hydroxide (LDH) nanosheets S-scheme heterojunction has been fabricated and employed in photocatalytic CO_2 conversion to CO and CH_4. The composite containing 60 wt% $CsPbBr_3$ has exhibited the best performance under visible light, which was enhanced by 2.6 and 9.9 times as compared to $CsPbBr_3$ and CoAl-LDH, respectively. The S-scheme heterojunction promotes the electron-hole separation and also provides a higher redox potential of the composite material, resulting in an outstanding CO_2 photocatalytic reduction performance [224].

3.2.1.3. Plasma chemical. A successful demonstration on DBD cold plasma for the conversion of CO_2 to CO has been presented [91,92,225–227]. Using low (50 Hz) and high frequencies (11, 15, 19 and 25 kHz) the instant production of CO has been reported. Various central electrodes, for example Pyrex and bare metal (aluminium, copper, and stainless steel) along with outer Pyrex tube combinations respectively in double dielectric (DD) and single dielectric (SD) coaxial reactors have been utilized separately. The copper central electrode containing SD reactor system produced the highest CO translating 13% CO_2 conversion efficiency in neat CO_2 systems. The gas residence time, applied electric voltage, and discharge gas gap are significant parameters to control over the CO production [91]. The 353 nm band in optical emission spectrum in CO_2 DBD cold plasma signifies the CO formation follows one route through CO_2^+ species [91,225,226]. The activated species such as CO, CO_2^+ and $^{\bullet}OH$ in CO_2 plasma are also detected [228]. Moreover, the extent of Ar control over the CO_2 conversion efficiency and brings the highest ~ 26% CO_2 conversion in 90% Ar mixing CO_2 system [92,229].

CO generation takes place in Ar mixed CO_2 plasma systems through plasma derived Ar-species, few selective reactions of which are listed below:

$$Ar \rightarrow Ar_m^*(m = 1–3) + Ar_n^+ (n = 1, 2) + e^- \quad (34)$$

$$Ar^*/Ar_n^+ + CO_2 \rightarrow CO_2^*/CO_2^+ + nAr \quad (35)$$

$$Ar^* + CO_2 \rightarrow CO + O + Ar \quad (36)$$

$$CO_2 \rightarrow CO_2^* \rightarrow CO + O \quad (37)$$

$$CO_2^+ + e^- + Ar \rightarrow CO + O + Ar \quad (38)$$

$$O + O \rightarrow O_2 \quad (39)$$

$$CO_2 + e^- \rightarrow C + 2O + e^- \quad (40)$$

$$CO + e^- \rightarrow C + O^- (O + e^-) \quad (41)$$

$$CO_2^+ + e^- \rightarrow CO_2^* \rightarrow CO + O \quad (42)$$

In another experiment, the researchers have suggested that the frequency and dielectric material have no effect on CO_2 conversion and energy efficiency; however, the discharge gap causes a considerable effect on CO_2 transformation. Furthermore, the specific energy input results in a significant effect on energy efficiency and CO_2 conversion. The plasma chemistry model for CO_2 splitting has revealed the rational agreement with experimental CO_2 conversion and the energy efficiency [230,231].

Similarly, CO_2 decomposition has also been investigated in helium and nitrogen diluents systems [232–234]. Zeng et al. [235] have employed Ar diluents for CO_2 decomposition using packed (Ni/Al_2O_3) bed plasma systems and achieved 56% CO_2 conversion showing the importance of suitable packing for enhancing conversion efficiency. Furthermore, the plasma decomposition of CO_2 diluted (2.5%) in He has been performed in presence of metal (Au, Pd, Pt, Rh and Cu) catalysts. The 30.5% CO_2 conversions are obtained with 80% selectivity for CO [234]. Also, the DBD reactor packed with hydrotalcite (magnesium-aluminium hydroxycarbonate) as solid sorbent, plasma has shown capable of desorbing CO_2 from the hydrotalcite surface, and this desorption starts instantaneously after plasma ignition indicating the possibility for immediate control over the process [236]. More packed-bed DBD coaxial reactors have been developed to split CO_2 into industrial fuel CO [228,237,238]. The foam Fe, Al, and Ti packing materials are placed into the discharge gap of the DBD reactor and investigated for CO_2 conversion. The foam Ti has shown the best CO_2 decomposition rate (46.61%) amongst these foam metals. The density functional theory indicates that CO_2 adsorption possesses a lower activation energy barrier on foam Ti surface.

CO_2 can also be converted to CO and O by non-thermal plasmas (NTPs) even in the presence of substantial amount of O_2. CO_2 conversion is reported as 15%–21% in presence of 0–20% O_2, but the conversion declined with 50% O_2. This conversion in conventional thermal chemistry requires a few thousand K temperature in absence of catalyst. But in the NTP reactor, with $BaTiO_3$ packing CO_2 conversion to CO is achieved at ambient pressure and temperature below 373K. In this case other than CO generation, it brings an opportunity to use CO_2 as an oxidant, i.e., a source of O radical [239].

3.2.2. Formic acid

Formic acid (FA) (HCOOH), a beneficial chemical holds wide applications in agriculture, food, pharmaceutics, textiles, and laboratory because of its reducing and strong acidic properties. It is a potential hydrogen storage component through its decomposition to H_2 and CO_2 and works as a material for chemical energy storage [240]. The HCOOH synthesis methods are mainly based on fossil fuels utilization, which are classified into various processes such as methyl formate hydrolysis, formamide hydrolysis and oxidation of hydrocarbons. Among these, the methyl formate-based method is presently dominant and in 2014, the HCOOH production capacity through this method has been estimated to be 770 kton·year^{-1} comprising ~ 90% of total worldwide installed capacity [241].

3.2.2.1. Electrochemical. The electrocatalytic CO_2 reduction to HCOOH in alkaline aqueous solution with differently synthesized

tin-oxide (SnO_2) particles on multi-walled carbon nanotubes (MWCNT) using $SnCl_2$ or $SnCl_4$ precursors has been reported. The highest Faradaic and energy efficiencies 64% and 27% respectively have been reported at −1.40 V vs. SCE with SnO_2 obtained using $SnCl_2$. The $SnCl_2$ and $SnCl_4$ precursors exhibit different retention of Sn(II) valence state in a surface of tin oxyhydroxide [$Sn_6O_4(OH)_4$]. The particle morphologies control over the activity and product selectivity [242]. Furthermore, a high-pressure semicontinuous batch electrolyzer has been employed for CO_2 conversion to $HCOOH/HCOO^-$ on a tin-based cathode employing different membranes such as bipolar membranes (BPM) and cation exchange membranes (CEM). The effects of CO_2 pressure, flow rate, cell potential, electrolyte concentration, and membrane type on FE and current density (CD) for FA formation have been investigated. The increasing CO_2 pressure causes high FE up to 90% and CD ~ 30 mA/cm^2 at 3.5 V, but FE value decreases significantly at higher potentials. Although BPMs are expensive but these have several advantages over monopolar ion (cation or anion) exchange membranes, (i) BPMs permit the use of two different electrolyte solutions to sustain a constant pH gradient over the membrane, (ii) low product crossover, and (iii) performs basification and acidification without addition of bases and acids [243–246]. Even though the working principles of BPM and CEM are different, both exhibit analogous performances for CO_2 electrolysis with respect to FE and CD.

The grain boundaries (GBs) are modified to manipulate the binding energies of reaction intermediates and thus step up the CO_2RR with < 10 nm size nanostructured materials. Around 2 nm SnO_2 quantum wires (QWs) composed of individual quantum dots (QDs) and various GBs on the surface are synthesized and explored for CO_2RR. The ultrathin SnO_2QWs with exposed GBs have shown greater current density and enhanced FE over 80% for HCOOH and ca. 90% for C_1 products as compared to SnO_2 nanoparticle with larger electrochemically active surface area 60% [247], showing the importance of quantum wires in product formation.

The electrochemical CO_2RR to liquid products suggests a direction for the energy-dense storage of alternating renewable electricity. The superior Si photocathodes decorated with Sn porous nanowire (having high density of grain boundaries) catalyst offered photovoltage-assisted conversion of CO_2 to liquid HCOOH under visible light [248]. The FE ~ 60% for HCOOH formation has been achieved at −0.4 V vs. RHE under visible light leading 11.0% efficiency for HCOOH formation. The high-selectivity electrochemical CO_2RR to HCOOH using conductive single-crystal Ga_2O_3 has also been reported. The single-crystalline Sn- and Si- doped Ga_2O_3 are produced adopting an edge-defined film fed growth method [249]. Both Sn- and Si-doped Ga_2O_3 cathodes produced HCOOH with about 80% FE. The DFT calculation revealed that the adsorbed CO_2 reacts with protons and electrons to form H−CO_2 on Ga_2O_3 surface, as shown in reaction (43). The weakly bind adsorbed formate confirmed with Raman scattering analysis [250], which quickly desorbs by reacting with another proton and electron:

$$CO_2{-}Ga_2O_3 + H^+ + e^- \rightarrow HCOO{-}Ga_2O_3 \quad (43)$$

$$HCOO{-}Ga_2O_3 + H^+ + e^- \rightarrow HCOOH + Ga_2O_3 \quad (44)$$

As discussed above in the CO product section, a combined theoretical and experimental investigation on electrochemical CO_2RR to $HCOO^-$ selectively [186] using polycrystalline Sn electrode surface as catalyst has been reported. This electrode produces multiproduct such as $HCOO^-$, CO and H_2 across a wide range of potentials, wherein $HCOO^-$ formation favored at potentials more negative than −0.8 V vs RHE and achieving to an utmost FE of 70% at −0.9 V vs RHE. The *OCHO has been recommended intermediate theoretically for $HCOO^-$ formation where Sn's optimal *OCHO binding energy helps this selectivity. In another study, the electrochemical cell with a Dioxide Materials Sustainion™ anion exchange membrane along with a nanoparticle Sn GDE (Gas Diffusion Electrodes) cathode containing an imidazole ionomer has exhibited better performance on CO_2 electrochemical reduction to pure HCOOH [251]. Hg and Pb electrodes are also explored for CO_2 reduction. The observed high overvoltage in CO_2 reduction to $HCOO^-$ at Hg electrode with a neutral electrolyte reveals a low value for efficiency of electric energy utilization. HCOOH is further reduced to methanol in perchloric acid electrolyte (at Pb electrode) or in buffered HCOOH electrolyte (at Sn electrode). The potential dependency of HCOOH reduction to CH_3OH indicates that the HCOOH adsorption on electrode surface near pzc (point of zero charge) is the overall reaction rate controlling step [136]. Likewise, the $Bi_2O_2CO_3$-coated carbon fibre electrodes with higher selectivity and stability have also been designed for electrochemical CO_2RR to HCOOH [252]. These electrodes produced $HCOO^-$ in liquid phase selectively with maximum 69% FE.

In another report, using lead dioxide (PbO_2) electrode in ionic liquid (IL)-containing catholytes, the electrochemical reduction of CO_2 to HCOOH has been demonstrated. 1-benzyl-3-methylimidazolium tetrafluoroborate ([Bzmim]BF4) has been observed as the superior IL to improve the efficiency of PbO_2 electrode on HCOOH formation [253].

The role of oxygen vacancy in Co_3O_4 single unit cell layer exhibited significantly on CO_2 reduction in 0.1 M $KHCO_3$ electrolyte for specific formate generation. The FE is 87.6% with oxygen vacancy rich in contrast to 67.3% FE with poor oxygen vacancy Co_3O_4 at −0.87 V vs SCE. The oxygen vacancy herein serves as active sites for stabilizing the intermediate species by lessening activation energy barrier [254]. The electrochemical CO_2 reduction in methanol-based electrolyte has been reported with zinc particle-pressed electrodes. In this case, zinc particles mixed with CuO and Cu_2O powders are pressed and engineered to a disk plate electrode. In absence of copper oxide, only CO and HCOOH are produced [255]. Methanol is used as it has 4 times higher CO_2 solubility than water.

3.2.2.2. Photochemical. In photocatalytic sciences the researchers have insighted interesting findings on chemical reduction of CO_2. The synthesized ternary metal chalcogenides with molybdenum, bismuth, and cadmium (Mo–Bi–Cd) combination have been employed for CO_2RR [256]. The HCOOH formation rate is high 208 $\mu mol \cdot g^{-1} \cdot h^{-1}$ with 72% FE. Mele et al. [257] have prepared a low-cost stable composite material using TiO_2 powder with Cu(II), porphyrins and phthalocyanines, and applied it for CO_2 photoreduction [258].

Solar energy has been utilized to react CO_2 with water to generate HCOOH at an energy conversion efficiency of 0.15%. Under the investigation, AlGaN/GaN anode and indium (In) cathode are used. The high energy conversion efficiency has been achieved because of high quantum efficiency (28%) at 300 nm, which is attributed to effective electron-hole separation in heterostructure of the semiconductor [259]. This shows the alteration of solar energy conversion efficiency with material modifications.

The application of renewable energy, for example PV (photovoltaic) solar energy is one of the essential restraints for realizing HCOOH generation with more carbon footprint (CF) value than the standard HCOOH production. However, the impact of CF on electricity from PV is still shadowed by CF derived from the high requisite of steam in purification stage to achieve commercial purity [241]. The metal sulfide semiconductors (Zn-based sulphides for example Ni-doped ZnS) combined with various Ru-complex such as Ru(4,4′-diphosphonate-2,2′-bipyridine) $(CO)_2Cl_2$ catalysts have been synthesized and employed in visible light-driven CO_2

reduction. The highest CO_2 photoconversion activity with a turnover number > 100 has been achieved for HCOOH formation with this hybrid photocatalysts [260]. Furthermore, the possibility of continuous production of HCOOH in a two-step process has been studied by exploiting a thermodynamically stable methyl formate intermediate [261].

The photocatalytic performance of CdSe quantum dots (QDs) anchored onto the nanosized Pt or Pd metal decorated TiO_2 nanofibers (NFs) has been tested for activation as well as reduction of CO_2 using UV-B light separately. The UV-B light, a spectrum of ultraviolet light in 290 nm–320 nm wavelengths region causes Vit D production (advantage) and skin cancer (disadvantage). In this research, the generation of HCOOH, CH_3OH, and methyl formate are reported as primary products [262].

The metal-free, chemically stable, and visible light sensitive graphitic carbon nitride (g-C_3N_4) semiconductor has drawn much interest in CO_2 reduction research to get CH_3OH, HCOOH, and CH_4 products. This material is not suitable for water oxidation. The hybridization of g-C_3N_4 and tungsten (VI) oxide (WO_3) has been explored further to increase the oxidation potential of g-C_3N_4 for water oxidation. The g-C_3N_4 and WO_3 composite photocatalyst has shown maximum photocatalytic activity on CO_2 reduction [263] for HCOOH and other products. In another investigation, the cadmium-loaded ZnS microcrystals and ZnS–CdS solid solution microcrystals have been employed for CO_2 photoreduction to $HCOO^-$. The quantum efficiency of $HCOO^-$ production is 32.5%, which is two times higher than that observed with plain ZnS microcrystals [264].

The metal–organic frameworks (MOFs), a class of crystal-line micro-mesoporous hybrid materials with extended 3D network exhibit a variety of prospective applications [265–272]. For example, photoactive catalyst $Ti_8O_8(OH)_4(bdc\text{-}NH_2)_6(NH_2\text{-}MIL\text{-}125(Ti))$ (a MOF material) (bdc-NH_2 = 2-amino-benzene-1,4-dicarboxylate; ATA = 2-aminoterephthalate) reduces CO_2 to $HCOO^-$ effectively in acetonitrile on visible light irradiation. The reaction is quite similar to the formation of charge carriers over photoexcited metal oxide semiconductors. In this case Ti^{4+} is reduced to Ti^{3+} whereas triethanolamine, a sacrificial agent works as electron donor. The colour change (from bright yellow to green) insights the existence of Ti^{3+} in titanium oxo-clusters of NH_2-MIL-125(Ti) and later confirmed by ESR and UV-DR spectral measurements. The isotopic labelled $^{13}CO_2$ experiments confirmed the CO_2 reduction into $HCOO^-$ [272]. Similarly, synthesized carbon dots (CDots) based materials such as (CDots)-decorated, and CDots-embedded NH_2-UiO-66 particles (another MOF) are investigated for photocatalytic activity on CO_2 chemical reduction. The results indicate that the location of CDots can significantly affect the photocatalytic activity of NH_2-UiO-66 particles. The embedded CDots exhibit highly improved activity. The charge kinetic investigations suggest that the embedded CDots are more promising for charge separation and transfer. Besides acting as electron receptors, CDots also serve as photosensitizer [273].

The photocatalytic reduction of CO_2 in different solvents such as water, acetonitrile and CCl_4 has been studied with TiO_2 nanocrystals embedded in SiO_2 matrices (Q-TiO_2/SiO_2) photocatalyst. The total yields of reduction products ($HCOO^-$ and CO) increase with the increase in dissolved CO_2 concentration. Furthermore, the ratio of $HCOO^-$ to CO is influenced by solvent nature and increases with the dielectric constant of solvent (for example: CCl_4 has the lowest dielectric constant amongst these solvents hence yielded less products). The rate of CO_2 reduction is higher in Q-TiO_2/SiO_2 than that in bulk TiO_2, but the $HCOO^-$ to CO ratios in both systems remain identical. The solvent polarity plays a crucial role in products formation through initially generated CO_2^- and its adsorption performance within the photocatalyst [274–277].

CO_2 photoreduction is an interesting method that permits the synthesis of fuels and chemicals. One of the constraints of CO_2 photoreduction in the liquid phase is the low solubility of CO_2 in water. This has been focused on designing a fully innovative pressurized photoreactor (up to 20 bar pressure) to improve productivity. The photoreduction of CO_2 in liquid phase has been performed using commercial TiO_2 (Evonik P25), TiO_2 obtained by flame spray pyrolysis (FSP) and gold doped P25 (0.2 wt% Au–P25) in the presence of Na_2SO_3 as hole scavenger (HS) to produce HCOOH and HCHO. In basic environment (pH = 12 to 14), the CO_2 solubility is enhanced, and it forms carbonates (as discussed above) which is reduced to HCHO and HCOOH and consequently forms CO/CO_2 + H_2 in the gas phase through photo reforming. Furthermore, the deposition of 3 nm–5 nm Au nanoparticles onto TiO_2 influences the products distribution quantitatively and increases the selectivity to gas phase products [278].

Furthermore, there are reports on photochemical HCO_3^- conversion to formate/formic acid [279–284], however as we have concentrated mainly on CO_2 hence these are not explained elaborately.

3.2.2.3. Plasma chemical. A DC plasma electrochemical system has been explored for the conversion of dissolved CO_2 into some useful products such as HCOOH and $(COOH)_2$. Using the optical absorption technique, it has been noticed that a single plasma-injected solvated electron reduces a single CO_2(aq) to CO_2^-, which either combine to produce $C_2O_4^{2-}$ or disproportionate to give $HCOO^-$ [285].

3.2.3. Formaldehyde

Formaldehyde (HCHO) is a naturally occurring and pungent smell giving colourless gaseous organic compound. It polymerizes spontaneously into paraformaldehyde (8–100 units degree of polymerization), hence it is stored in aqueous solution. It is an important precursor to many chemical materials, which are used in synthesis of polyoxymethylene plastics, industrial resins, and important building chain to produce useful life commodities, etc. [286]. It has been a main reagent in chemical industries for several decades, and its overall demand reached 30 megatons annually. At present it is exclusively produced under methanol oxidation over a catalyst such as silver, a mixture of iron and molybdenum and vanadium [287,288]. More recently, the application of HCHO and its derivatives have been suggested as a disinfectant or as a synthetic reagent. The aqueous HCHO and paraformaldehyde function as a liquid organic hydrogen carrier (LOHC) molecule for hydrogen generation and proposed as to use for hydrogen fuel cells [289].

3.2.3.1. Electrochemical. CO_2 electrochemical reduction in seawater with a boron-doped diamond (BDD) electrode at ambient conditions has led to generate HCHO with FE 74% at −1.7 V vs. SCE. The low FE 15 and 1.1% respectively for HCOOH and H_2 have also been reported as electrochemical products at −1.7 V vs. SCE [290]. The activation of stable CO_2 through complexation with an activator N-heterocyclic polymers (e.g., poly(4-vinyl) pyridine, PVP) can control both the kinetics and thermodynamics of CO_2 photoelectrochemical reduction reaction. In this case a solar light driven photoelectrochemical process for producing HCHO and CH_3CHO selectively on multi-layered Cu/rGO/PVP/Nafion hybrid cathode has been presented where the reaction pathway-initiated with CO_2 activation followed by electron-coupled proton transfer across rGO layer [291].

3.2.3.2. Photochemical. Commercial and laboratory prepared TiO_2 samples have been used in CO_2 reduction photo catalytically. TiO_2 samples prepared in laboratory by using $TiCl_4$ and $Ti(OC_4H_9)_4$

precursors are labelled as sample A and sample B respectively, and later prepared Cu-loaded and SiO_2 supported TiO_2 samples. HCHO and CH_3CHO are major products obtained with sample A prepared from $TiCl_4$ whereas CH_4 is mainly produced in the presence of sample B synthesized from $Ti(OC_4H_9)_4$ in CO_2 reduction reaction. Furthermore, the formation of HCHO increased by an order of magnitude with bare or silica supported sample A in presence of 1 wt% Cu loading as compared to sample B with respect to photoreduction of CO_2 [138]. The reactions taking place for the formation of HCHO, CH_3CHO and CH_4 other than the charge carrier formation reaction (reaction 7) are listed below:

$$CO_2 + 2H^{\bullet} \rightarrow HCOOH \quad (45)$$

$$HCOOH + 2H^{\bullet} \rightarrow HCHO + H_2O \quad (46)$$

$$HCHO + 2H^{\bullet} \rightarrow CH_3OH \quad (47)$$

$$CH_3OH + H^{\bullet} \rightarrow {}^{\bullet}CH_3 + H_2O \quad (48)$$

$${}^{\bullet}CH_3 + H^{\bullet} \rightarrow {}^{\cdot}CH_4 \quad (49)$$

$${}^{\bullet}CH_3 + HCHO \rightarrow CH_3CHO + H^{\bullet} \quad (50)$$

A bifunctionalized TiO_2 film consisting of a catalysis zone and a dye-sensitized zone has been fabricated for visible-light utilization. HCOOH, HCHO and CH_3OH [292] are produced in CO_2 photocatalytic reduction efficiently following electrons transfer mechanism. CO_2 reduction and O_2 evolution take place simultaneously on different catalysts zones. The products' yields are enhanced with external electrical power.

CO_2 photoreduction has been performed with various photoactive materials of metal oxide systems supported on magnesium oxide (MgO), aluminium oxide (Al_2O_3) and silicon dioxide (SiO_2) using a batch reaction system. C_1–C_3 compounds are reported as CO_2 conversion products. Acidic oxide supported catalysts exhibited high selectivity towards C_1 compounds such as HCHO, etc. whereas basic oxide supported systems preferentially produce C_1–C_3 compounds. No change in the characteristics of photocatalytic materials was observed even after 6 h operation [293].

Ti-SBA-15 (Ti doped SBA-15) (SBA-15 is a mesoporous silica uniform hexagonal pores material with a narrow pore size distribution and tunable pore diameter to 5 and 15 nm) has been exposed to light in presence of different gas mixtures such as CO_2 and H_2O or CO_2 and H_2 separately. The CO_2 and H_2 mixture led to the lowest formation rate of CH_4, C_2H_4, and C_2H_6 products. H_2O is found to be more efficient than H_2 in CO_2 activation. HCHO is extremely reactive over the catalyst system, yielding a product distribution (C_1–C_2) of similar nature as observed with CO activation. The proposed mechanism indicates that the involvement of initially generated CO followed by the consecutive formation of HCHO converts later to hydrocarbons apparently by the reaction with photo-activated H_2O and its associated intermediates [294,295].

As discussed above, with pressurized photoreactor, CO_2 photoreduction in liquid phase has been investigated using commercial TiO_2 (Evonik P25), TiO_2 obtained by flame spray pyrolysis (FSP) and gold doped P25 (0.2 wt% Au–P25) containing hole scavenger (Na_2SO_3). HCHO has been reported as products in liquid phase along with HCOOH [278].

3.2.3.3. Plasma chemical. The selective reduction of CO_2 with Ar carrier in presence of organic compound either mixed in the gas-phase or present as a contact solid surface has been investigated under *DBD cold plasma* to yield HCHO. C_6 to C_{12} hydrocarbons and organic surfaces such as wax, plastics and polymers are employed separately as H-atom source. HCHO as a DBD product retains on solid surfaces and in gas phase are analyzed by pre-concentration using appropriate HCHO absorber solutions followed by colorimetric measurement. On leaching out the HCHO retains on surfaces into the absorber solution, HCHO production efficiency has been reported as ~ 5% of CO_2 [89]. The reactions taking place in addition to above mentioned plasma-based reactions (reactions 34–36,38) are listed below:

$$Ar^* \text{ (or } Ar_n^{\bullet+}) + >CH\text{-} \rightarrow >CH\text{-}^* \text{ (or } > CH^+\text{-} + e^-) + Ar \quad (51)$$

$$>CH\text{-} \rightarrow >CH\text{-}^* + >C^{\bullet}\text{-} + H^{\bullet} \quad (52)$$

$$>CH^+\text{-} + e^- \rightarrow >C^{\bullet}\text{-} + H^{\bullet} \quad (53)$$

$$>CH\text{-}^* \rightarrow >C^{\bullet}\text{-} + H^{\bullet} \quad (54)$$

$$CO + H^{\bullet} \rightarrow HC^{\bullet} = O \quad (55)$$

$$HC^{\bullet} = O + H^{\bullet} \rightarrow HCHO \quad (56)$$

$$>C^{\bullet}\text{-} + >C^{\bullet}\text{-} \rightarrow \text{Dimeric Product} \quad (57)$$

3.2.4. Methanol

Methanol (CH_3OH), the simplest alcohol, is a chemical building block for hundreds of daily use products, including plastics, paints, construction materials, etc. It is a light, colorless, volatile, and flammable liquid. Methanol, an energy carrier is generally used to fuel automobiles, ships, boilers, and cooking stoves as a clean energy resource [296]. It is a toxic alcohol, on exposure it is extremely dangerous, with significant illness and mortality if left untreated. Furthermore, cold methanol is also used as CO_2 absorbent industrially in Rectisol process [297], and as mentioned above it possesses higher CO_2 solubility than water. In earlier times, methanol was synthesized by the destructive distillation of wood. In industry either from pure CO_2 and pure H_2 mixture or from a mixture of CO, CO_2, and H_2, methanol is synthesized by using suitable catalyst [298].

3.2.4.1. Electrochemical. The selective conversion of CO_2 to methanol has been investigated with p-GaP semiconductor electrode containing a homogeneous pyridinium ion catalysts using Hg–Xe light as reaction initiator and obtained FEs ~ 100% at potentials (> 300 mV) below the standard potential (−0.52 V vs SCE) at pH 5.2. In absence of pyridinium ion no CH_3OH is produced indicating that CO_2 interacts directly at the electrode surface via a pyridinium-mediated process and generates CH_3OH possibly through hydride transfer mechanism from pyridinium ring to CO_2 [299]. The pyridinium and its derivatives are useful for CO_2 reduction to HCOOH, HCHO, and CH_3OH. Interestingly, high faradaic yields for CH_3OH have been reported in both photoelectrochemical and electrochemical systems at low overpotentials. At electrodes, HCOOH and

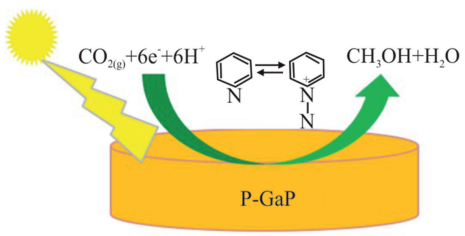

Fig. 7. Photo-electrochemical reduction of CO_2 on p-GaP catalysts, adopted from Ref. [300].

HCHO are reported as several intermediate products enroute to sequential $6e^-$ reduction product CH_3OH, where the pyridinium radical plays a crucial role (see Fig. 7). The mechanisms of the reduction process proceed through different coordinative interactions between the pyridinium radical and CO_2, HCHO, and other related species where the pyridinium radical [300] binds to intermediates and radical species covalently at various steps as shown in Fig. 7 and in reactions 58–65.

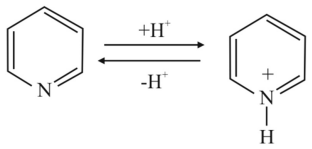

(58)

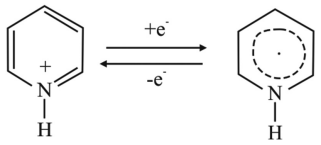

(59)

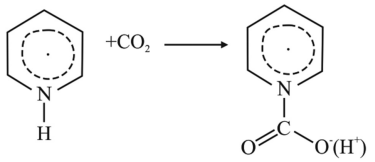

(60)

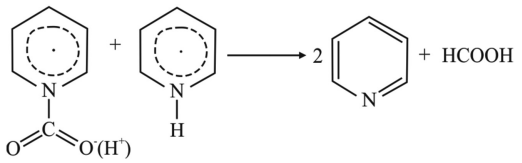

(61)

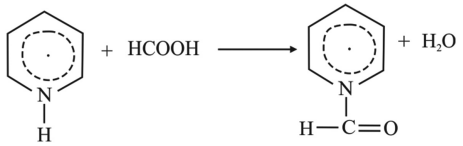

(62)

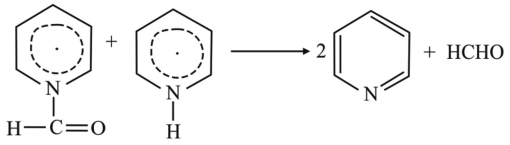

(63)

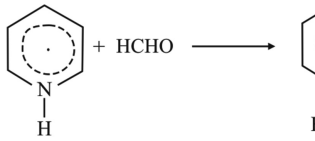

(64)

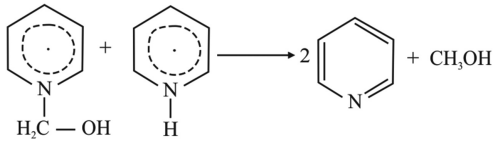

(65)

In this mechanism, the initially reduced pyridinium (pyH^+) to a surface hydride $pyH^\bullet$ at Pt electrode plays important role in methanol formation [301] via several covalently bonded intermediate species. Furthermore, the quantum chemical calculations elucidated the stage-wise mechanism for pyridine-catalyzed CO_2 reduction to CH_3OH. In first stage, the pyridine (Py) transforms into pyridinium (PyH^+) through a H^+ transfer (PT) (pH effect), later it followed by an e^- transfer (ET) to produce pyridinium radical ($PyH^\bullet$) in photoelectrochemical p-GaP system and photochemical [Ru(phen)3]2+/ascorbate system. $PyH^\bullet$ undergoes further PT–ET steps to form dearomatized 1,2-dihydropyridine (PyH_2) species, the key closed-shell. The second phase involves several reduction steps, and it is predicted that the PyH_2/Py redox couple is kinetically and thermodynamically capable in hydride and proton transfers catalytically to CO_2 and other succeeding intermediates (HCOOH and HCHO) to yield ultimately CH_3OH.

The gas-diffusion electrodes are fabricated using commercial Cu_2O and Cu_2O–ZnO mixtures deposited on carbon papers and assessed for continuous CO_2 electroreduction in a filter-press electrochemical cell [302]. In this system CH_3OH as major and small amounts of ethanol (C_2H_5OH) and *n*-propanol (C_3H_7OH) are produced. The highest CO_2 conversion efficiencies to liquid-phase products are 54.8% and 31.4% for Cu_2O and Cu_2O/ZnO-based electrodes respectively at −1.39 V and −1.16 V vs. Ag/AgCl.

The FE for methanol production is close to 100% at Sn electrode in a limited potential region related to a low current density. The potential dependence of HCOOH reduction to methanol proposes HCOOH adsorption on electrode near the point of zero charge (pzc) could be the rate-controlling step in overall reaction. Several transition metals for example Au, Ag, Zn, Cu, Ni, Pt, and Fe surfaces have been employed in electrocatalytic conversion of CO_2 to CH_3OH. The reaction rates for CH_3OH and CH_4 products selectivity in the framework of CO binding energies for these metals are described. The selectivity toward CH_4 or CH_3OH for most of these metals is low. In this study, deeper surface chemistry for transition metals with new insights to direct development of the advanced CO_2 conversion catalysts have been presented [303].

3.2.4.2. Photochemical. The synthesized TiO_2 species within the mesoporous zeolites (Ti-MCM-41 and Ti-MCM-48) framework by hydrothermal synthesis method has demonstrated unique photocatalytic reactivity for CO_2 reduction with H_2O to CH_4 and CH_3OH. TiO_2 dispersion within the zeolite framework along with the existence in tetrahedral coordination is realized with the *in-situ* photoluminescence, diffuse reflectance absorption, ESR and XAFS investigations. The excited state of highly dispersed TiO_2 species plays a significant role in this reduction exhibiting a high selectivity towards CH_3OH production [304].

The CO_2 has been photo-catalytically reduced to methanol in a steady-state optical fibre photoreactor containing ~ 120 Cu/TiO_2-coated fibres with 365 nm light from Hg lamp. Using 53 nm thick Cu/TiO_2 film [305] containing 14 nm sized spherical particles with 1.2 wt% material loading, the utmost CH_3OH rate (0.45 μmole/g cat hr) has been achieved. The Cu_2O clusters and active Cu species on TiO_2 surface play key role in CH_3OH formation. Moreover, > 1.2 wt% Cu loading brings a lower rate of CH_3OH yield due to its masking effect on TiO_2 surface. Similarly, the photocatalytic ability of rGO–CuO nanocomposites has been explored for CO_2 reduction under visible light irradiation. The neat CuO nanorods exhibit very low photocatalytic activity owing to fast recombination of charge carriers. But rGO–Cu_2O and rGO–CuO have shown significant photocatalytic activities with 5 and 7 times higher CH_3OH yield than pristine Cu oxides respectively. The better activity of CuO in

rGO–CuO nanocomposites has been ascribed to slow recombination of charge carriers and efficient photo-generated electrons transfer through rGO skeleton [306]. Furthermore, TiO_2-rGO nanocomposites has shown excellent photocatalytic activity on CO_2 reduction to CH_4 (2.10 μmol · g^{-1} · h^{-1}) and CH_3OH (2.20 μmol · g^{-1} · h^{-1}), showing the collective effect of TiO_2 and graphene [307].

The enzyme containing amorphous TiO_2 particles consists of interconnected 400–600 nm range sizes nanospheres. The encapsulated dehydrogenases such as formaldehyde dehydrogenase, formate dehydrogenase and alcohol dehydrogenase sequentially convert CO_2 to HCOOH, HCHO and CH_3OH using a terminal electron donor nicotinamide adenine dinucleotide (NADH) for catalyzed reduction [308].

The photocatalytic activity as well as visible light response of Bi_2S_3 are higher than CdS. Hence, the photocatalytic properties of Bi_2S_3, CdS and Bi_2S_3/CdS have been studied for CO_2 conversion to CH_3OH utilizing visible light source. The photocatalytic activity of Bi_2S_3/CdS hetero junction photocatalyst has been observed higher than those of plain CdS and Bi_2S_3 and yielded utmost methanol (613 μmol · g^{-1}) when the weight proportion of Bi_2S_3 to CdS used was 15% [309].

The developed synthetic approaches have been adopted to engineer nanostructured photocatalytic materials for effective light harnessing as well as charge separation and later applied on CO_2 photoreduction to CH_4, CH_3OH and some olefins [50,310,311]. As discussed above, in the absence of CdSe QDs, Pd-decorated TiO_2 nanofibers (NFs) have exhibited superior performance for CH_3OH along with HCOOH production. Moreover, the presence of CdSe, Pt-decorated TiO_2 NFs showed higher selectivity towards CH_3OH following CO_2 photoreduction mechanism pathway through hydrogenation [262].

3.2.4.3. Plasma chemical. Hydrogenation CO_2 is one of the broadly research areas to produce methanol. The conventional CO_2 hydrogenation requires high H_2 pressure and high temperature, but the extensively developed nonthermal plasma (NTP) is utilized for CO_2 hydrogenation to methanol. The plasma-based techniques not only have outstanding advantages, such as ambient temperature and atmospheric H_2 pressure but also carries terrific potential to be power by electricity in a flexible manner due to its easy operation (just switching on/off) [312]. For example, a pioneering work done by Wang et al. [313], on the utilization of CuO/Al_2O_3 in plasma for methanol synthesis. 21.2% CO_2 conversion with 53.7% selectivity to CH_3OH (11.3% yield) in atmospheric pressure and room temperature using an NTP reactor has been reported. In other experiments, Cu/g-Al_2O_3 catalyst at 4 wt% Cu loading and CO_2/H_2 plasma led to the success of 10% CO_2 conversion with ~ 50% CH_3OH selectivity [314]. Upon H_2O addition the selectivity increases to 65% (for H_2O/CO_2 ratio = 1). The density functional theory reveals that the interfacial sites of Cu cluster and g-Al_2O_3 establish a bifunctional effect: activate CO_2 molecules and strongly adsorb the key intermediates to support hydrogenation. In this case H_2O promotes CH_3OH desorption by competitive adsorption over Cu/g-Al_2O_3 surface. Similarly, plasma-driven CO_2 hydrogenation at near-ambient temperature and pressure by adding MgO, γ-Al_2O_3, and a series of Co_xO_y/MgO catalysts separately has been investigated to enhance CO_2 conversion and products selectivity. Co_xO_y/MgO exhibited excellent results, converting up to 35% of CO_2 with highest methanol yield (10%) [315]. The CO_2 hydrogenation to methanol has also been studied in a DBD with and without a catalyst ($CuO/ZnO/Al_2O_3$ catalyst in pellets containing copper content of about 440 kg/m^3) system, at high pressure (up to 8 bar) and at temperature (50°C–250°C) [316]. It is noteworthy to include that the plasma discharge effectively lowered the optimum catalyst performance temperature. Similarly, a series of binary mixed metal oxides, such as, NiO, Fe_2O_3, 5% NiO–Fe_2O_3 (5NF), 10% NiO–Fe_2O_3 (10NF), and 15% NiO–Fe_2O_3 (15NF) catalysts are explored for CO_2 conversion to CH_3OH. These binary mixed metal oxides are highly active as compared to their pure metal oxides forms. Moreover, increasing NiO mixings lead to the agglomeration of NiO particles. At 200°C, around 1.5%, 2%, and 3.2% CO_2 conversion is achieved for 5NF, 10NF, and 15NF combination respectively. Excitingly, with cold plasma ignition at 200°C, around 5.4%, 6.2%, and 10.2% CO_2 conversion is obtained for 5NF, 10NF and 15NF respectively. The 15NF catalysts exhibit the maximum CO_2 conversion and produce only CH_4. Plasma coupling with the catalyst led to high CH_3OH yield, and around 5.8 times enhancement is reached with 10NF at 200°C as compared to thermal catalysis. It revealed that the combination of plasma and thermal heating makes a significant change to the catalyst morphology (creation of a mixture of spinel compounds (NiO–Fe_2O_3, $NiFe_2O_4$, and Fe_3O_4)), which in turn leads to a substantial increase in the catalytic activity [317,318].

3.2.5. Methane. Methane (CH_4), the simplest one carbon atom containing hydrocarbon, is a powerful greenhouse gas available in small quantities in the atmosphere. The natural sources of CH_4 include emissions from oceans and wetlands (emission from marshy land hence known as marsh gas), and from the digestive processes of termites. Being the main constituent in natural gas, CH_4 fuels industrial plants and powers homes among its other major applications. High concentration of CH_4 can reduce the amount of oxygen breathed from air resulting in slurred speech, memory loss, vision problems, nausea, facial flushing, and headache. Severely, there is possibility of changes in heart and breathing rate, balance problems, and numbness. In 2019, 360 million tons (~ 60%) of CH_4 released worldwide was through anthropogenic activities, whereas the natural sources contributed around 230 million tons of CH_4 [319]. Reducing its emission by capturing and utilizing leads to environmental and economic benefits.

Sabatier reaction, a known reaction produces CH_4 and H_2O from H_2 and CO_2 at elevated temperatures (300°C–400°C) and ~ 3 MPa pressures in presence of nickel catalyst. CO_2 hydrogenation to both CH_3OH and CH_4 is the most valuable process to convert the renewable energy to carbon-based fuels along with liquid product [320]. However, the utilization of this reaction for CO_2 methanation is already in use on the International Space Station to reuse atomic oxygen, and the propulsion systems utilizing cryogenic liquid CH_4. Ni nano-catalyst has shown excellent activity and high stability for CO_2 reduction to CH_4 in presence of water, where water acts both as hydrogen source and reaction medium [321]. The earth's abundant metals such as Fe or Zn are used as re-generable reducing agents. An exceptional yield (98%) of CH_4 from either CO_2 or HCO_3^- has been reported at 300°C where the in situ generated Ni nanoparticle catalyst demonstrates not only the exceptional catalytic activity but also its high stability. Mechanistic studies recommend that the CH_4 formation from HCO_3^- or CO_2 follows $HCO_3^- \rightarrow CO_2 \rightarrow HCOOH \rightarrow CH_4$ pathway.

3.2.5.1. Electrochemical. Electrochemical reduction of CO_2 into beneficial compounds is a major challenge in helping the closed carbon cycle. An approach aiming for CO_2 electrochemical reduction empowered by electricity from renewable sources, but photochemical methods driven by solar light are also doable. The great challenge in these approaches is for the development of catalysts based on low-cost Earth-abundant elements instead of costly precious metals. Few of these catalysts are stable and selective for CO_2 reduction and generate CO or HCOOH, and quite a few catalysts can be able to produce low yields of hydrocarbons [322]. The trimethylammonio groups functionalized iron tetraphenylporphyrin complex has been proved as an efficient and

selective electrocatalyst for CO_2 reduction to CO and also catalyzes CO_2 for eight-electron reduction to yield CH_4 with visible light irradiation under ambient conditions [322–324]. The nanostructured copper cathodes are efficient and selective catalysts for producing multicarbon (> C_1) compounds during CO_2 reduction electrochemically in which the produced copper nanocube catalyst favors ethylene (C_2H_4) over CH_4 production [325].

The Cu-based conductive metal-organic framework is used for CO_2 electrochemical reduction to CH_4 with high FE 80%, where the Cu-based conductive metal-organic framework oxygen-coordinated Cu sites exhibit higher selectivity [326]. In another research the introduction of Au in Cu polytetrafluoroethylene (PTFE) nanofibers has demonstrated high selectivity towards hydrogenation by suppressing C–C coupling leading to methane formation with ~ 56% FE in CO_2-reduction [327]. Furthermore, the recently designed glutathione-modified copper electrode exhibited superior CO_2 electrochemical reduction to CH_4 (61.7% FE with 153.7 mA · cm^{-2} current density) and the yield reported is 35-fold higher than that observed in neat copper electrode [328].

Cobalt protoporphyrin restrained on a pyrolytic graphite electrode reduces CO_2 in acidic aqueous solution at 0.5 V overpotential. CO is the main reduction product along with CH_4 as by-product. The pH-dependent studies insight into the reaction mechanism in which CO_2 is activated by cobalt protoporphyrin via the stabilization of an intermediate, which performs as Brønsted base. The basic nature of the intermediate in CO_2 reduction bypasses a rigorous proton–electron transfer mechanism, in contrary to H_2 evolution [329]. In this case the initially generated CO_2^- (with high negative potential value) is shifted to less negative potential upon coordination with the catalyst (carboxylation), which later generates CO. The CO formation reaction dominated more at higher pH and later reduced to CH_4 via HCHO. The reduction of catalytically inactive Co^{2+} to Co^+ is expected to trigger both H_2 evolution and CO_2 reduction pathways. Similarly, the electrochemical reduction of CO_2 with Cu electrode has been studied in methanol-based electrolyte containing lithium salts such as LiBr, LiI, LiCl, $LiClO_4$, etc. At low temperature (−30°C). CO, CH_4, C_2H_4, and HCOOH are reported as major products from CO_2 with maximum FE 71.8% for CH_4 production at −3.0 V vs. SCE in $LiClO_4$ electrolyte system [330].

3.2.5.2. Photochemical. The novel photocatalysts containing porphyrin and graphene have been designed for CO_2 reduction to hydrocarbons (CH_4, etc.) utilizing visible light. These catalysts reduce CO_2 to hydrocarbons (mainly C_2H_2) effectively and control selectively over the transfer of photogenerated electrons from graphene to CO_2 instead of H_2O [331].

The Pt-sensitized graphene-wrapped defect-induced blue titania photocatalyst generates ethane (C_2H_6) and CH_4 during photocatalytic reduction of CO_2 [332]. The blue titania, a reduced TiO_2 (TiO_{2-x}) has oxygen vacancies (VO–Ti^{3+}) but possesses high photocatalytic activity at 425 nm than P25 and rutile. It contains 85% rutile and 15% anatase along with multitude defect surface sites [333]. Furthermore, the transient absorption spectroscopy study reveals that the photogenerated holes move into graphene while the electrons pile up on Ti^{3+} sites develop the multielectron transfer processes and generate $^{\bullet}CH_3$. This leads to ~ 259 μmol·g^{-1} CH_4 (H addition) and 77 μmol·g^{-1} C_2H_6 (through dimerization) production under one Sun (AM 1.5G) radiance [332].

The ternary photocatalysts CdS/(Cu-TNTs) (sodium trititanate nanotubes (TNTs; $Na_xH_{2-x}Ti_3O_7$)) can catalyze to CO_2 and water conversion into C_1–C_3 hydrocarbons such as CH_4, C_2H_4, C_2H_6, C_3H_6, and C_3H_8 during visible light irradiation in absence of any sacrificial electron donors. In this system CO_2 bound composite surface serves as electron accepter whereas water serves the principal photoexcited-state electron donor. The binding of CO_2 with composite material plays an important role in this conversion [334]. Interestingly, the Cu addition to SiO_2 supported in-house synthesized TiO_2 samples using $Ti(OC_4H_9)_4$ increased the photocatalytic reactivity of CO_2 with and without water and led to CH_4 formation [138].

The adsorbed 5 nm average sized Cu_2O nanoparticles (1.74 wt% loading) onto defective graphene (Cu_2O/G) formerly synthesized using alginic acid sodium salt have been used in photocatalytic reduction of CO_2 to CH_4 in the presence of dimethylaniline (sacrificial agents). The CH_4 formation rate achieved maximum (326 μmol CH_4 $g^{-1}\cdot h^{-1}$) in UV–Vis irradiation conditions. The spectral response of Cu_2O reveals that the light absorption with low Cu_2O loading Cu_2O/G happens mainly due to the graphene part [335]. Furthermore, the efficiency of monolith photoreactor for CH_4 production during CO_2 reduction fetches 6 folds higher than TiO_2 dispersed reactor system [217]. Under combined CO_2 capture and methanation (CCCM), the different reactor configurations have been suggested with different formulations such as dual functional materials, adsorbent, methanation catalysts, etc. [336]. The adsorbent developing materials for example basic zeolites, carbon-based materials, basic clays, amine-functionalized materials, alkali metal oxides, etc. are used whereas methanation catalysts based on Ru or Ni or other noble metals helps in hydrogenation.

The coal-based luminescent carbon dots (CDots) have been synthesized by H_2O_2 oxidation of inexpensive coal samples and then coated composite nanoparticle Ag/CDots are fabricated to attach CDots in situ to Ag surface following the simple silver mirror reaction method. Its performance on photocatalytic reduction of CO_2 to hydrocarbons (CH_4, etc.) has been investigated. The composite surface contains many oxygen groups, which exhibit good adsorption of CO_2 and also enhances photocatalytic activity as compared to individual Ag and CDots for organic fuels (hydrocarbon) generation [337].

The ambient such as N_2, Air, O_2, CO_2 are significant for CO_2 reduction in suspended TiO_2 aqueous systems containing 2-propanol as hole scavenger in which CO_2 has been generated *in-situ* (except in the CO_2 systems) through 2-propanol photo mineralization [134,135]. The deviation of CH_4 yields, in N_2, aerated, O_2 and CO_2 systems insight an interesting chemistry of the *in-situ* generated CO_2. CH_4 formation yields trend as reported is: CH_4 yield in CO_2-purged = aerated > oxygenated > N_2-purged systems. It is noteworthy to mention that the presence of O_2 in aerated and oxygenated systems does not support the Photo Kolbe reaction [135] to generate methane through $^{\bullet}CH_3$ formation. In this study $C^{\bullet}$ and $^{\bullet}CH_2$ species are recommended as enroute reaction intermediates to yield CH_4.

3.2.5.3. Plasma chemical. As explained above in methanol section, the *plasma discharge* with a series of binary mixed metal oxides catalysts, such as, NiO, Fe_2O_3, 5% NiO–Fe_2O_3 (5NF), 10% NiO–Fe_2O_3 (10NF), and 15% NiO–Fe_2O_3 (15NF) convert CO_2 to CH_3OH and CH_4. The 15NF catalysts exhibit the highest CO_2 conversion and produce only CH_4 [316,317].

As discussed above the products on chemical reduction of CO_2 using electro-, photo- and plasma chemical methods depend on many factors such as catalysts materials, CO_2 concentration (or its pressure), reaction conditions, input energy/applied potential, presence of additional chemicals (hole scavengers/ionic salt), etc. Moreover, all these techniques lead to free radical based reactions following two different pathways to produce methane as final product under C_1 chemical category as shown in Scheme 1.

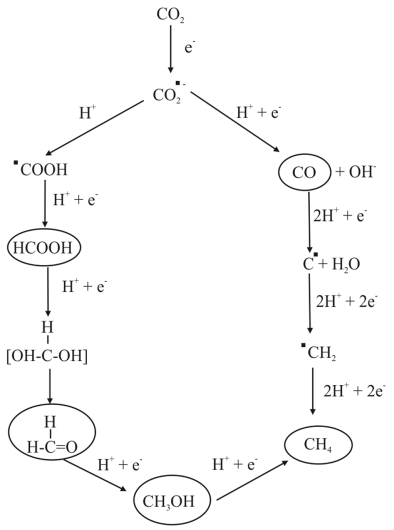

Scheme 1. The mechanistic formation of C_1 products.

3.3. C_2 compounds

CO_2 is the most abundant and manageable carbon source on the Earth, its utilization as beneficial chemicals produced through the creation of C—C bond(s) is an important strategy. Various compounds containing > C_1 atoms are mostly generated through radical based reactions. Moreover, the carboxylic acids and its derivatives found by carboxylation of carbon nucleophiles with the reaction of CO_2 have extensive applications in pharmaceuticals and in material sciences [338]. The CO_2 conversion to liquid fuels and multi-carbon (> C_1 atoms) products is of technological significance with respect to the negative CO_2 emissions approach. The formations of a few important C_2 compounds are considered in the following section.

3.3.1. Electrochemical

Cu is an important transient metal, which catalyzes CO_2 reduction reaction (CO_2RR) to produce C_2 and/or higher carbon containing hydrocarbons. Wei et al. [339], have reported a simplistic way to enhance ≥ C_2 products selectivity using polycrystalline Cu toward CO_2RR. By coating Cu surface with a 50 nm thick polyaniline (PANI) film, the FE of C_2H_4 (C_2+ hydrocarbons) has been enhanced to 60% from 15% at −1.1 V_{RHE} in $KHCO_3$ electrolyte solution. High performance of Cu/PANI is explained with the electronic properties of Cu substrate. This leads to the interaction of initially generated CO intermediate and facilities in CO—CO coupling, which finally ended with C_2 or higher hydrocarbon formation. In another research, a simple and effective benzimidazole (BMZ)-modified Cu foil catalyst has been developed to improve CO_2

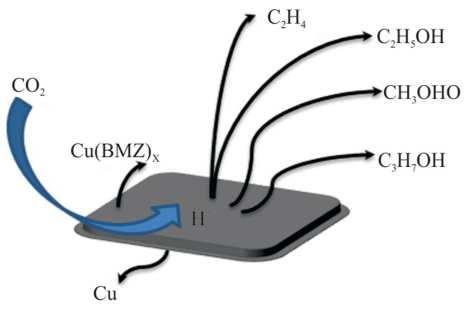

Scheme 2. Cu benzimidazole generates C_2 products from CO_2.

conversion to selective C_2/C_3 products. In this case FE reaches 92.1% for CO_2 reduction by lowering the HER to 7% FE at −1.07 V_{RHE} [340]. In this process low to high yields of ethylene (C_2H_4), ethanol (C_2H_5OH), acetaldehyde (CH_3CHO), 1 propanol (C_3H_7OH) along with propionaldehyde (C_2H_5CHO) are generated (see Scheme 2).

C_2H_6 and C_2H_4 generations using Cu-based catalysts have been reported with a photovoltaic (PV) cell and electrochemical cell (EC) coupling system in CO_2 reduction with 21% energy efficiency [341]. In such a coupling system, a PV cell normally provides photogenerated electrons and holes to an EC for CO_2 reduction as well as water oxidation respectively at cathode and anode [342,343]. Furthermore, the electrochemical conversion of CO_2 to C_2H_6 is very rare because the higher selectivity normally goes towards CH_4, C_2H_4, and C_2H_5OH formations. The iodide-derived copper (ID-Cu) and oxide-derived copper (OD-Cu) systems are employed to get in-depth knowledge of the mechanism of CO_2 conversion to C_2H_6. With traces of iodine species on the surface and positively charged Cu species observations, the generation of C_2H_6 is preferred more on ID-Cu than OD-Cu. C_2H_6 formation follows the similar pathway as C_2H_4 and C_2H_5OH formations perform [344].

The single-crystal electrodes of Cu such as Cu(111), Cu(100), Cu(S)-[n(100) × (111)], and Cu(S)-[n(100) × (110)] produced C_2 compounds on electrochemical reduction of CO_2 at a constant current density (5 $mA \cdot cm^{-2}$) in 0.1 M $KHCO_3$ aqueous electrolyte [74]. Copper single crystals are prepared using 99.999% pure copper metal in graphite crucibles following Bridgeman method [345]. Cu(111) electrode generates mostly CH_4 from CO_2, while Cu(100) favorably produces C_2H_4 showing the importance of crystal orientations. Introduction of (111) steps to Cu(100) basal plane directs to Cu(S)-[n(100) × (111)] orientations, which promotes C_2H_4 formation by suppressing CH_4 generation. Furthermore, the electrochemical reduction of CO_2 to C ≥ 2 hydrocarbons on a polycrystalline Cu electrode in bicarbonate aqueous electrolyte has been investigated using N-substituted pyridinium additives. High (70%—80%) selectivity for C_2 and C_3 compounds with significant C ≥ 2/CH_4 products ratio (> 100) have been observed [346]. Importantly, the product selectivity has been altered from C ≥ 2 species to H_2 (~ 90%) with certain N-heterocyclic additives.

Various forms of oxidized Cu materials utilized as electrocatalysts require large overpotentials. Moreover, a densely packed Cu nanoparticles (NPs) ensemble has been utilized for selective C_2—C_3 products formation. During electrolysis, Cu NP ensembles undergo structural change into remarkable electrocatalytically active cube-like particles combined with smaller nanoparticles. C_2H_4, C_2H_5OH and n-propanol (n-C_3H_7OH) are found as main C_2—C_3 products with low onset potential (−0.53 V vs. RHE). The C_2—C_3 attains 50% FE at only −0.75 V showing the performances of catalyst at considerably lower overpotentials for selective product. This approach indicates a new opportunity to realize multicarbon products formation from CO_2 [347,348]. The hydrocarbon formation mechanism follows dual pathways: one (C_1) pathway leading to CH_4 and the other (C_2) pathway leading to C_2H_4. In C_1 pathway, CHOads, the main intermediate produced through the breaking of C—O linkage, which generates CH_4. Whereas in C_2 pathway, the first step is CO dimer formation, followed by the formation of a surface-bound enediol or enediolate, or oxametallacycle formation. The enediol(ate) and oxametallacycle intermediates control the selectivity of C_2 to C_2H_4 formation [349].

The reduction of CO_2 to C_2 products such as acetic acid (CH_3COOH) and ethanol (C_2H_5OH) over a 3D dendritic copper-cuprous oxide composite has been investigated. In KCl aqueous electrolyte, 0.53 V and 0.48 V overpotentials are required respectively for CH_3COOH and C_2H_5OH formations [350]. The conversion of CO_2 to selective C_2+ compounds endure from a high

overpotential, low selectivity with a low reaction rate, and the process is very sensitive to catalyst structure and the electrolyte [351]. The electrochemical CO_2 reduction at an extremely low temperature (− 30°C) has also been investigated (discussed above) using Cu electrode in methanol electrolyte. C_2H_4 along with CH_4 and CO are reported as reduction products. Because of C based compound formation, the FE of H_2 formation is depressed to < 8% due to CO_2 competitive reaction [200].

The oxalate ion ($C_2O_4^{2-}$) production as a Zn salt through electrolytic reduction of CO_2 in electrochemical cell containing CrNi-steel cathode and zinc anode with acetonitrile mixed 0.2 M tetrabutylammonium perchlorate electrolyte has been obtained [352]. The reactions taking place are given below:

$$CO_2 + e^- \rightarrow CO_2^{\bullet-} \quad (66)$$

$$CO_2^{\bullet-} + CO_2 \rightarrow C_2O_4^{\bullet-} \quad (67)$$

$$C_2O_4^{\bullet-} + CO_2^{\bullet-} \rightarrow C_2O_4^{2-} + CO_2 \quad (68)$$

$$CO_2^{\bullet-} + CO_2^{\bullet-} \rightarrow C_2O_4^{2-} \quad (69)$$

$$Zn + C_2O_4^{2-} \rightarrow ZnC_2O_4 \quad (70)$$

$C_2O_4^{2-}$ thus precipitates as ZnC_2O_4 and recovers later by simple filtration.

3.3.2. Photochemical

The production of solar fuels brings a feasible way for decreasing CO_2 concentration in atmosphere, which is an important step for societal application. An efficient stable Pt-sensitized graphene-wrapped defect-induced blue-coloured titania synthesized photocatalyst has been developed, which produces high yield of C_2H_6 along with CH_4 (discussed above) during CO_2-reduction [333].

On increase in CO_2 pressure, CH_3COOH and C_2H_6 are generated in TiO_2 photo-catalytic systems. More recently, to counteract the CO_2 balance in the atmosphere, CH_3OH or C_2H_5OH are produced using graphene oxide (GO) and TiO_2 composite materials in photocatalytic CO_2 reduction in water under UV/vis light irradiation [353]. pH is a potential variable towards the product (CH_3OH and C_2H_5OH) selectivity. For example: GO-TiO_2 exhibited excellent photocatalytic activity for C_2H_5OH formation at pH 11.0, whereas CH_3OH production takes place at pH 4.0. With pH variation the solubility of CO_2 changes (discussed above) along with various CO_2 species, for example, H_2CO_3 dominates at acidic pH (4.0), HCO_3^- at pH 7.0 ($pK_a = 6.4$) and CO_3^{2-} at alkaline pH 11.0 ($pK_a = 10.3$). The low pH favors higher proton concentrations which reduce the theoretical reduction potential of CO_2 by assisting electron transfer to CO_2 followed by protonation of the negative species, whereas at higher pH the carbonates and bicarbonates act as hole scavengers and are easily oxidized, reversing the overall process and lead to more C_2H_5OH formation. Similarly, Li et al. [354] have also demonstrated CH_3OH and C_2H_5OH generation during CO_2 photo catalytically reduction in suspended CuO-loaded titania powders in water in the presence of Na_2SO_3, a hole scavenger. The yields of alcohols increase with CuO loading up to 3.0 wt%, beyond which the yields decrease because of the masking effect of CuO on TiO_2. The enhancement of methanol and ethanol yields with more CuO loading is due to formation of more active sites. Copper serves in this case as an electron trapper and prohibits the recombination of charge carriers, increasing photo efficiency significantly. These investigations highlight that the modification of photocatalytic materials and the reaction conditions are important for product selectivity. Oxalic acid ($H_2C_2O_4$), another useful product has been obtained in photocatalytic CO_2 reduction on TiO_2 [355] and its

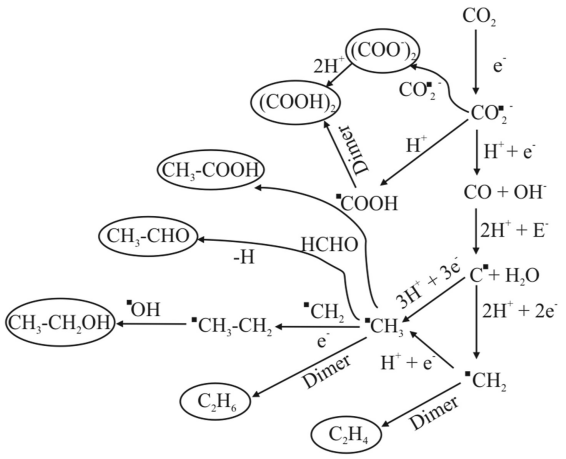

Scheme 3. The mechanistic formation of a few selective C2 products.

generation has been proposed with $2CO_2^{\bullet-} + 2H^+ \rightarrow HOOC{-}COOH$ reaction. The overall mechanisms for above-mentioned C_2 product formation in photochemical reduction of CO_2 are summarized in Scheme 3.

As the investigation for efficient catalysts for photoreduction of CO_2 progresses, the nanostructured perovskite oxides have emerged as a new group of high-performing photocatalytic materials. Perovskite is a semiconductor material that has a similar crystal structure like calcium titanium oxide and used to transport the electric charge whenever the light hits the material [356]. The perovskite oxide materials for CO_2 photoreduction are mostly nanostructured forms of titanates, tantalates, cobaltates and niobates, which are much preferred owing to their better chemical stability, bandgaps, nontoxic nature, tunable crystal structures and surface energies. These materials display an extended optical-absorption edge, favorable band-alignment and longer charge carrier lifetimes relating to reduction potential of activated CO_2 as compared to conventional semiconductors and nanomaterial catalysts and yielded C_1 and C_2 species as CO_2 reduction products [357]. Furthermore, the CO_2 reduction requires significant energy because of its remarkable thermodynamic stability. Using sunlight along with co-catalysts to reduce CO_2 and simultaneous to overcome these shortcomings leads to a great achievement in the fields of photocatalysis. Several approaches have been applied to improve the photocatalytic

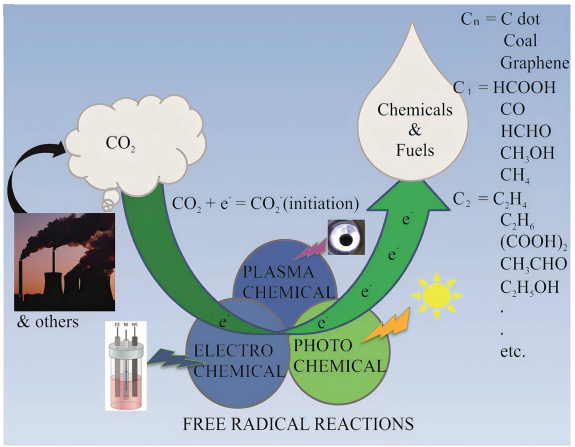

Scheme 4. The schematic presentation of CO_2 mitigation through electro-, photo- and plasma-chemical reactions to various products.

efficiency of CO_2 reduction in the most effective TiO_2 based photocatalytic systems [358,359] for oxalic acid, formic acid and other C_1–C_2 products.

As discussed in CH_4 section, the CdS/(Cu-TNTs) ternary photocatalyst has been employed to convert CO_2 and water into C_1–C_3 hydrocarbons such as CH_4, C_2H_6, C_3H_8, C_2H_4, C_3H_6 using visible light irradiation without any sacrificial electron donor. Free H_2 was not observed over 5 h of photo-irradiation although the proton reduction is thermodynamically favored over CO_2 reduction in aqueous system. The stoichiometric fraction of Na^+ in TNTs is an important factor affecting hydrocarbon formation. The coordination of CO_2 on the ternary catalyst leads to surface-bound CO_2 and related carbonate species formation. As proposed the bidentate binding of CO_2 at particular reactive sites reduces the reaction energy barrier. The copper on TNTs plays a key role in the transient trapping of $^{\bullet}CH_3$ (confirmed with ESR), and finally dimerized to C_2H_6 [334].

TiO_2 and different Cu wt% loaded TiO_2 (TC(0.5–5.0)), 10 wt% TC(2.0) supported on molecular sieve 5A (10 wt% TC(2.0)/MS) have been employed for CO_2 reduction in alkaline aqueous solution in a batch reactor. $H_2C_2O_4$ yield increased remarkably in Cu–TiO_2 supported molecular sieve catalyst system. This catalyst stimulates charge separation, which enhances the selective formation of $H_2C_2O_4$ along with CH_3OH, and CH_3COOH. The product formation depends on the extent of CO_2 adsorption by the composite photocatalyst. The adsorption and desorption mechanism of CO_2 on a catalyst has been suggested for the reason of products selectivity. The maximum yield of $H_2C_2O_4$ reported is 65.6 $\mu g \cdot h^{-1} \cdot g^{-1}$ per cat in 0.2 N NaOH containing solution over 10 wt% TC(2.0)/MS photocatalyst. The formation of CH_3OH (0.4 $\mu g \cdot h^{-1} \cdot g^{-1}$ per cat) and

Table 1
The list of the electrochemical reduction products of CO_2 along with their faradaic efficiency.

Products	Electrode/electrocatalyst used	Stability	FE (%)	Ref	Remarks
Carbon flakes	Ce–Ga/dimethyl formamide	Not gumming up		[158]	Worked at −310 mV
Graphene	Stainless steel/$CaCl_2$–NaCl–CuO			[166]	At controlled reaction kinetics
	Molten carbonate			[167]	Economical
CO	Carbon/Acidic Bi^{3+}		95	[175]	Economical
	Ni-single atom dispersed into graphene nanosheet	High		[176]	97% CO selectivity
	Iron porphyrin-based graphene		96.2	[182]	Worked at low over potential (280 mV)
	Ni-nitrogen doped porous carbon		85	[183]	At alkaline conditions
	Ni–Fe ($KHCO_3$)		> 97	[185]	Considered oxygen evolution reaction (OER)
	Polycrystalline Sn		70	[186]	Theoretically supported intermediate
	Cu in methanol		42	[200]	At −30°C
HCOOH	Multiwalled carbon nanotube SnO_2		64	[242]	Importance of Particle morphology
	SnO_2 quantum wires		80	[247]	Importance of Surface area
	Si decorated Sn porous nano wire		60	[248]	Worked at −0.4 V
	Sn–Si doped Ga_2O_3		80	[249]	Importance of adsorbed CO_2
	BiO_2CO_3 coated nanofibre	High	69	[252]	High selectivity
HCHO	Boron doped diamond	high	74	[284]	CO_2 reduction in sea water
	Multi layered Cu/rGO/PVP/Nafion			[285]	Photoelectrochemical
CH_3OH	p-GaP with pyridinium ion		100	[293]	Photoelectrochemical
	Cu_2O–ZnO	> 20 h	54.8	[296]	Filter press electrochemical cell
CH_4	Cu-metal-organic framework		80	[320]	High CH_4 selectivity
	Au in Cu polytetrafluoroethylene		56	[321]	Suppressing C–C coupling
	Glutathione-modified Cu		61.7	[322]	Importance of COOH and NH_2 groups of glutathione
	Co protoporphyrin			[323]	In acidic conditions
	Cu		71.8	[324]	At −30°C
C_2H_4	Cu-polyaniline		60	[333]	Favors CO–CO coupling
C_2H_4, ethanol etc.	Cu-benimidazole		92.1	[334]	
C_2H_4, ethanol etc.	Cu-nanoparticle		50	[342]	CHO_{ads} intermediate
CH_3COOH, ethanol	3D dendritic Cu–Cu_2O		80	[344]	Different overpotential for different products
$H_2C_2O_4$	Cr–Ni steel Zn salt		90	[346]	No unwanted by-products

Table 2
The list of the photochemical reduction products of CO_2.

Products	Photocatalyst	Light	Ref	Remarks
CO	Cu(II)quaterpyridine complex	Visible	[218]	97% selectivity and turnover no. > 12,400
	Rhenium(I) trinuclear complex	436 nm	[219]	Quantum efficiency 0.45
	N,S doped NH_2CNPs	Visible	[222]	76.6% conversion efficiency
	TiO_2- carbon/silica	350–400 nm	[223]	~ 100% selectivity
	$CsPbBr_3$/CoAl	Visible	[224]	Boost electron–hole separation
HCOOH	AlGaN/GaN	300 nm	[259]	28% quantum efficiency
	ZnS–CdS	–	[264]	32.5% quantum efficiency
HCHO	Cu-loaded SiO_2	UV	[138]	%age of Cu control product yields
	MgO, Al_2O_3, SiO_2 system		[287]	> 6 h stability of catalysts
CH_3OH	CdS/Bi_2S_3	Visible	[303]	Heterojunction photocatalyst
	CdSe–Pt decorated TiO_2 nanofibre	290–320 nm	[262]	~ 90 $ppmg^{-1} \cdot h^{-1}$methanol
CH_4	Porphyrin graphene	Visible	[325]	Selectively control of photogenerated electrons
	Pt-sensitized graphene blue TiO_2	425 nm	[327]	~ 259 $\mu mol \cdot g^{-1}$ CH_4 through H addition to $^{\bullet}CH_3$
	CdS/Cu-Trititanate nanotube	Visible	[328]	No sacrificial electron donor
	Cu_2O/G	UV–Vis	[329]	Maximum 326 $\mu mol \cdot g^{-1}$ CH_4
	TiO_2	UV	[49,134]	High yields in aerated systems containing hole scavenger
C_2H_5OH	GO-TiO_2	UV–Vis	[348]	Crucial role of pH
$H_2C_2O_4$	Cu TiO_2 molecular sieve		[354]	High yields of oxalic acid due to high adsorption of CO_2

CH_3COOH (15 $\mu g \cdot h^{-1} \cdot g^{-1}$ per cat) is quite low [360]. Interestingly, a substantial amount of CH_3COOH has been produced when photocatalysts such as Rh–TiO_2, Cu–TiO_2, and Ru–TiO_2 [361] are used in CO_2 reduction, and in Cu–TiO_2 and Rh–TiO_2 systems the yields are maximum (4.1–5 $\times$ 10^{-8} mol).

In electrochemical studies, various intermediates play crucial role in product formation where Cu and/or Cu-based material exhibit superior contribution in free radical based CO_2 reduction. Copper is the only metal that has shown high selectivity over CO_2RR to multi-carbon products under these three selective fields. Moreover, the selectivity of different C_1–C_2 products along with carbon species introduced in detail have limited energy efficiency, uncontrolled selectivity, low stability, and unknown mechanisms. Hence, there are yet many tough challenges, which should be addressed in the near future.

Furthermore, various forms of semiconductors such as anchored, highly dispersed, and finely powdered varieties lead to CH_4, CH_3OH, HCHO, HCOOH and CO formation. The formation efficiencies of photolytic products depend on catalyst, reaction temperature and CO_2 to H_2O ratio. The increase in CO_2 to H_2O ratio and the temperature enhance the catalytic activity, but the presence of excess H_2O decreases the reaction rate. At high pressure CO_2, (~ 2.5 MPa pressure) HCOOH, CH_3OH in radical-based liquid phase and CH_4 are major products in gas phase in TiO_2 containing systems, and CH_4 yield enhances upon addition of NaOH/Na_2SO_4. The low CH_4 yields obtained in HCOOH and $HCOO^-$ reduction systems support two different routes for CH_4 formation in CO_2 photolysis in presence of TiO_2 namely. $CO_2 \rightarrow$ HCOOH $\rightarrow$ HCHO $\rightarrow$ CH_3OH $\rightarrow$ CH_4 and $CO_2 \rightarrow CO \rightarrow C^{\bullet} \rightarrow {}^{\bullet}CH_2 \rightarrow CH_4$.

In plasma chemical reaction, the plasma carrier, gas-gap, frequency, applied fields, and the electrode material along with packing material are important in product yields and their selectivity. Many reports are available for C_1 products. The free radical based reactions in these three systems are summarized in Scheme 4 and a few selective products along with their quantitative values are listed in Tables 1 and 2.

4. Conclusion and future prospects

In this review we have tried to demonstrate the interest developed so far on CO_2 reduction by electrochemical, photocatalytic and plasma chemical means for seeking alternatives to the depletion of fossil resources utilizing CO_2 as carbon source. Topics covered include techniques, details in brief and the outcome of CO_2RR along with interpretation of mechanistic details of product specifications. Moreover, this review is still far from the optimal method in these fields for CO_2 reduction which can be applied commercially. Since the free radical based production derived from CO_2 is the primary objective of this article, it is apparent that further work in these fields independently and/or together will possibly bring interesting insight to improve artificial photosynthesis to utilize CO_2. In this context, as of today, the use of Cu and Cu-based materials have shown better controls over the product selectivity with excellent efficiency in all three areas. Utilization of theoretical calculations and in situ spectroscopic techniques at advanced level will certainly help to improve the understanding of the real and hidden mechanisms. The *in-situ* supervising the surface reaction intermediates, the adsorption and desorption dynamics of these species with temperature-programmed studies and the investigation of the rate limiting step will boost the knowledge of free radical based CO_2 reduction reaction, which finally provide direction for new materials developments. It is essential to increase the CO_2 conversion efficiency to a higher order of magnitude for actual in-field application. We hope the content of this article will provide substantial information to those who are interested in these multi-process research topics.

Declaration of competing interest

There are no conflicts to declare.

Acknowledgements

This research was carried out under plan project no: RBA4013. Author thanks Bhabha Atomic Research Centre, for funding and all the members of Radiation and Photochemistry Division, BARC and all his collaborators for their supports. He also thanks his wife, Mrs. Chaitali Dey, for her help during the article preparation.

References

[1] K. de Kleijne, S.V. Hanssen, L. van Dinteren, M.A.J. Huijbregts, R. van Zelm, H. de Coninck, Limits to Paris compatibility of CO_2 capture and utilization, One Earth 5 (2022) 168–185, https://doi.org/10.1016/j.oneear.2022.01.006. J. Rogelj, M. den Elzen, N. Höhne, T. Fransen, H. Fekete, H. Winkler et al., Paris agreement climate proposals need a boost to keep warming well below 2°C, Nature 534 (2016) 631-639. https://doi.org/10.1038/nature18307.
[2] K. Permentier, S. Vercammen, S. Soetaert, C. Schellemans, Carbon dioxide poisoning: a literature review of an often forgotten cause of intoxication in the emergency department, Int. J. Emerg. Med. 10 (2017), https://doi.org/10.1186/s12245-017-0142-y article 14.
[3] M.A. Scibioh, B. Viswanathan, in: S. Kaneco (Ed.), Photo/Electrochemistry & Photobiology in Environment, Energy and Fuel, Research Signpost, Trivandrum, Kerala, India, 2002, p. 1.
[4] G. Herzberg, Molecular Spectra & Molecular Structure, III Electronic Spectra and Electronic Structure of Polyatomic Molecules, D. Van Nostrand Com.Inc., New York, 1966, p. 500.
[5] E.C.Y. Inn, K. Watanabe, M. Zelikoff, Absorption coefficient of gases in the vacuum ultraviolet. Part III, CO_2, J. Chem. Phys. 21 (1953) 1648, https://doi.org/10.1063/1.1698637.
[6] M. Orchin, H.H. Jaffe, Symmetry, Orbitals and Spectra, Wiley, New York, 1971, p. 242.
[7] G. Chatwal, S. Anand, in: M. Arora, S. Puri (Eds.), Spectroscopy (Atomic and Molecular), Himalaya Publishing House, Bombay, India, 1985, p. 110.
[8] http://www.eng.buffalo.edu/&ajs42/pchem/co2/co2.html accessed on 1 August 2020.
[9] Daily CO_2. https://www.co2.earth/. (Accessed 8 May 2020).
[10] Carbon dioxide. https://en.wikipedia.org/wiki/Carbon_dioxide_(data_page. (Accessed 1 July 2019).
[11] R. Wiebe, V.L. Gaddy, The solubility of carbon dioxide in water at various temperatures from 12 to 40° and at pressures to 500 atmospheres. Critical phenomena, J. Am. Chem. Soc. 62 (1940) 815–817, https://doi.org/10.1021/ja01861a033.
[12] R. Wiebe, V.L. Gaddy, The solubility in water of carbon dioxide at 50, 75 and 100°, at pressures to 700 atmospheres, J. Am. Chem. Soc. 61 (1939) 315–318, https://doi.org/10.1021/ja01871a025.
[13] https://srdata.nist.gov/solubility/IUPAC/SDS-50/SDS-50.pdf accessed on 15 September 2020.
[14] M.B. Miller, D.-L. Chen, D.R. Luebke, J.K. Johnson, R.M. Enick, Critical assessment of CO_2 solubility in volatile solvents at 298.15 K, J. Chem. Eng. Data 56 (2011) 1565–1572, https://doi.org/10.1021/je101161d.
[15] R.C. Weast, CRC Handbook of Chemistry and Physics, Boca Rotan, (1979-80) B-85; D-121.
[16] F.A. Cotton, G. Wilkinson, Advanced Inorganic Chemistry a Comprehensive Test, third ed., Wiley Eastern Limited, New Delhi, 1984, p. 296.
[17] http://scifun.chem.wisc.edu/chemweek/CO2/CO2.html. (Accessed 18 March 2021).
[18] U. Siegenthaler, J.L. Sarmiento, Atmospheric carbon dioxide and the ocean, Nature 365 (1993) 119–125, https://doi.org/10.1038/365119a0.
[19] P. Matthews, Advanced Chemistry, Cambridge University Press, Cambridge, GB, 1996.
[20] G.R. Dey, in: G. Centi, S. Perathoner (Eds.), Green Carbon Dioxide: Advances in CO_2 Utilization, John Wiley, USA, 2014, pp. 25–50, https://doi.org/10.1002/9781118831922.ch2.
[21] J.E. Hansen, A.A. Lacis, Sun and dust versus greenhouse gases: an assessment of their relative roles in global climate change, Nature 346 (1990) 713–719, https://doi.org/10.1038/346713a0.
[22] R.A. Bermer, A model for atmospheric CO_2 over Phanerozoic time, Am. J. Sci. 291 (1991) 339–376, https://doi.org/10.2475/ajs.291.4.339.
[23] G.R. Dey, K. Kishore, in: S. Kaneco (Ed.), Carbon Dioxide Reduction: A Brief Review *in* Photo/Electrochemistry & Photobiology in the Environment, Energy and Fuel (PE&PB in EEF), Research Signpost, Kerala, India, 2005, p. 357.

[24] http://www.doc.mmk.ac.uk/aric/eae/global-waming/older/carbo-dioxide.html.

[25] S. Chu, Y. Cui, N. Liu, The path towards sustainable energy, Nat. Mater. 16 (2017) 16–22, https://doi.org/10.1038/nmat4834; BP Statistical Review of World Energy, 2015, http://large.stanford.edu/courses/2015/ph240/zerkalov2/docs/bp2015.pdf.

[26] B.I. McNeil, R.J. Matear, R.M. Key, J.L. Bullister, J.L. Sarmiento, Anthropogenic CO_2 uptake by the ocean based on the global chlorofluorocarbon data set, Science 299 (2003) 235–239, https://doi.org/10.1126/science.1077429.

[27] T. Coffey, D.R. Hardy, G.E. Besenbruch, K.R. Schultz, L.C. Brown, J.P. Dahlburg, Hydrogen as a fuel for DOD, Defense Horizons 36 (2003) 1–11. https://ndupress.ndu.edu/Portals/68/Documents/defensehorizon/DH-036.pdf?ver=2016-11-15-092814-620.

[28] R.W. Dorner, D.R. Hardy, F.W. Williams, H.D. Willauer, Heterogeneous catalytic CO_2 conversion to value-added hydrocarbons, Energy Environ. Sci. 3 (2010) 884–890, https://doi.org/10.1039/C001514H.

[29] https://www.climate.gov/news-features/understanding-climate/climate-change-atmospheric-carbon-dioxide downloaded on 1 July 2019.

[30] https://www.chemistryworld.com/news/can-catalysis-save-us-from-our-co2-problem/3010555.article accessed on June 4, 2020.

[31] https://en.wikipedia.org/wiki/Greenhouse_gas downloadedon 18 May 2020.

[32] R.A. Bermer, The rise of plants and their effect on weathering and atmospheric CO_2, Science 276 (1997) 544–546. https://www.science.org/doi/full/10.1126/science.276.5312.544.

[33] Earth System Research Laboratory, 2011. Available from: http://www.esrl.noaa.gov/gmd/ccgg/trends/global.html.

[34] C. Kuo, C.R. Lindberg, D.J. Thornson, Coherence established between atmospheric carbon dioxide and global temperature, Nature 343 (1990) 709–714, https://doi.org/10.1038/343709a0.

[35] S.H. Schneider, What is 'dangerous' climate change? Nature 411 (2001) 17–19, https://doi.org/10.1038/35075167.

[36] S.H. Schneider, Can we estimate the likelihood of climatic changes at 2100? Climatic Change 52 (2002) 441–451, https://doi.org/10.1023/A:1014276210717.

[37] S.H. Schneider, R.S. Chen, Carbon dioxide warming and coastline flooding: physical factors and climatic impact, Annu. Rev. Energy 5 (1980) 107–140, https://doi.org/10.1146/annurev.eg.05.110180.000543.

[38] H. Friedli, H. Lotscher, H. Oeschger, U. Siegenthhaler, B. Stauffer, Ice core record of the $^{13}C/^{12}C$ ratio of atmospheric CO_2 in the past two centuries, Nature 324 (1986) 237–238, https://doi.org/10.1038/324237a0.

[39] R. Snoeckx, A. Bogaerts, Plasma technology – a novel solution for CO_2 conversion? Chem. Soc. Rev. 46 (2017) 5805–5863, https://doi.org/10.1039/C6CS00066E.

[40] F.M. Mota, D.H. Kim, From CO_2 methanation to ambitious long-chain hydrocarbons: alternative fuels paving the path to sustainability, Chem. Soc. Rev. 48 (2019) 205–259, https://doi.org/10.1039/C8CS00527C.

[41] L. Liu, Y. Li, Understanding the reaction mechanism of photocatalytic reduction of CO_2 with H_2O on TiO_2-based photocatalysts: a review, Aerosol Air Qual. Res. 14 (2014) 453–469, https://doi.org/10.4209/aaqr.2013.06.0186.

[42] B. Hu, C. Guild, S.L. Suib, Thermal, electrochemical, and photochemical conversion of CO_2 to fuels and value-added products, J. CO_2 Util. 1 (2013) 18–27, https://doi.org/10.1016/j.jcou.2013.03.004.

[43] E.C. Hann, S. Overa, M. Harland-Dunaway, A.F. Narvaez, D.N. Le, M.L. Orozco, F. Jiao, R.E. Jinkerso, A hybrid inorganic-biological artificial photosynthesis system for energy-efficient food production, Nature Food 3 (2022) 461–471, https://doi.org/10.1038/s43016-022-00530-x.

[44] S.R. Lingampalli, M.M. Ayyub, C.N.R. Rao, Recent progress in the photocatalytic reduction of carbon dioxide, ACS Omega 2 (2017) 2740–2748, https://doi.org/10.1021/acsomega.7b00721.

[45] T. Inoue, A. Fujishima, S. Konishi, K. Honda, Photoelectrocatalytic reduction of carbon dioxide in aqueous suspensions of semiconductor powders, Nature 277 (1979) 637–638, https://doi.org/10.1038/277637a0.

[46] T. Mizuno, K. Adhachi, K. Ohta, A. Saji, Effect of CO_2 pressure on photocatalytic reduction of CO_2 using TiO_2 in aqueous solutions, J. Photochem. Photobiol., A: Chem 98 (1996) 87–90, https://doi.org/10.1016/1010-6030(96)04334-1.

[47] S. Kaneco, Y. Shimizu, K. Ohta, T. Mizuno, Photocatalytic reduction of high pressure carbon dioxide using TiO_2 powders with a positive hole scavenger, J. Photochem. Photobiol., A: Chem 115 (1998) 223–226, https://doi.org/10.1016/S1010-6030(98)00274-3.

[48] S. Kaneco, H. Kurimoto, K. Ohta, T. Mizuno, A. Saji, Photocatalytic reduction of CO_2 using TiO_2 powders in liquid CO_2 medium, J. Photochem. Photobiol., A: Chem 109 (1997) 59–63, https://doi.org/10.1016/S1010-6030(97)00107-X.

[49] G.R. Dey, A.D. Belapurkar, K. Kishore, Photo-catalytic reduction of carbon dioxide to methane using TiO_2 as suspension in water, J. Photochem. Photobiol., A: Chem 163 (2004) 503–508, https://doi.org/10.1016/j.jphotochem.2004.01.022.

[50] P. Usubharatana, D. McMartin, A. Veawab, P. Tontiwachwuthikul, Photocatalytic process for CO_2 emission reduction from industrial flue gas streams, Ind. Eng. Chem. Res. 45 (2006) 2558–2568, https://doi.org/10.1021/ie0505763.

[51] G.R. Dey, K.N.R. Nair, K.K. Pushpa, Photolysis studies on HCOOH and $HCOO^-$ in presence of TiO_2 photocatalyst as suspension in aqueous medium, J. Nat. Gas Chem. 18 (2009) 50–54, https://doi.org/10.1016/S1003-9953(08)60075-4.

[52] G.R. Dey, Chemical reduction of CO_2 to different products during photo catalytic reaction on TiO_2 under diverse conditions: an overview, J. Nat. Gas Chem. 16 (2007) 217–226, https://doi.org/10.1016/S1003-9953(07)60052-8.

[53] C. Wang, Z. Sun, Y. Zheng, Y.H. Hu, Recent progress in visible light photocatalytic conversion of carbon dioxide, J. Mater. Chem. 7 (2019) 865–887, https://doi.org/10.1039/C8TA09865D.

[54] S. Nahar, M.F.M. Zain, A.A.H. Kadhum, H.A. Hasan, Md R. Hasan, Advances in photocatalytic CO_2 reduction with water: a review, Materials 10 (2017) 629, https://doi.org/10.3390/ma10060629.

[55] K. Abhinima, G.R. Dey, The effect of non-thermal argon plasma treatment on material properties and photo-catalytic behavior of TiO_2 nanoparticles, AIP Conf. Proc. 2265 (2020) 030047, https://doi.org/10.1063/5.0017270.

[56] M.R. Hoffmann, J.A. Moss, M.M. Baum, Artificial photosynthesis: semiconductor photocatalytic fixation of CO_2 to afford higher organic compounds, Dalton Trans. 40 (2011) 5151, https://doi.org/10.1039/C0DT01777A.

[57] N. Getoff, Control of greenhouse gases emission by radiation-induced formation of useful products. Utilization of CO_2, Radiat. Phys. Chem. 75 (2006) 514–523, https://doi.org/10.1016/j.radphyschem.2005.09.014.

[58] N. Getoff, Possibilities on the radiation-induced incorporation of CO_2 and CO into organic compounds Internat, J. Hydro. Ener. 19 (1994) 667–672, https://doi.org/10.1016/0360-3199(94)90151-1.

[59] V.V. Fjodorov, N. Getoff, Radiation induced carboxylation of methanol under elevated CO_2-pressure, Radiat. Phys. Chem. 22 (1983) 841–848, https://doi.org/10.1016/0146-5724(83)90103-6.

[60] N. Getoff, Reduction of carbon dioxide in aqueous solution under the influence of uv-light, Int. J. Appl. Radiat. Isot. 13 (1962) 205.

[61] N. Fujita, C. Matsuura, Radiation induced reduction of CO_2 in iron containing solution Radiat, Phys. Chem. 43 (1994) 205–213, https://doi.org/10.1016/0969-806X(94)90180-5.

[62] R.J. Woods, A.K. Pikaev, Applied Radiation Chemistry, Wiley, New York, 1994.

[63] S. Wang, G.R. Lu, A comprehensive study on carbon dioxide reforming of methane over $Ni/\gamma\text{-}Al_2O_3$ catalysts, Ind. Eng. Chem. Res. 38 (1999) 2615–2625, https://doi.org/10.1021/ie980489t.

[64] N. Fujita, C. Matsuura, K. Ishigure, The effect of silica on hydrogen evolution and corrosion of iron in high-temperature water, Corrosion 46 (1990) 804–812, https://doi.org/10.5006/1.3585038.

[65] K.W. Frese Jr., S. Leach, Electrochemical reduction of carbon dioxide to methane, methanol, and CO on Ru electrodes, J. Electrochem. Soc. 132 (1985) 259, https://doi.org/10.1149/1.2113780.

[66] Y. Hori, S. Suzuki, Electrolytic reduction of carbon dioxide at mercury electrode in aqueous solution, Bull. Chem. Soc. Jpn. 55 (1982) 660–665, https://doi.org/10.1246/bcsj.55.660.

[67] Y. Hori, A. Murata, R. Takahashi, S. Suzuki, Electroreduction of carbon monoxide to methane and ethylene at a copper electrode in aqueous solutions at ambient temperature and pressure, J. Am. Chem. Soc. 109 (1987) 5022–5023, https://doi.org/10.1021/ja00250a044.

[68] S. Ikeda, T. Takagi, K. Ito, Selective formation of formic acid, oxalic acid, and carbon monoxide by electrochemical reduction of carbon dioxide, Bull. Chem. Soc. Jpn. 60 (1987) 2517–2522, https://doi.org/10.1246/bcsj.60.2517.

[69] S. Ikeda, A. Hattori, M. Maeda, K. Ito, H. Noda, Electrochemical reduction behavior of carbon dioxide on sintered zinc oxide electrode in aqueous solution, Electrochemistry 68 (2000) 257–261, https://doi.org/10.5796/electrochemistry.68.257.

[70] M. Jitaru, Electrochemical carbon dioxide reduction - fundamental and applied topics (review), J. Uni. Chem. Tech. Metal. 42 (2007) 333–344. https://dl.uctm.edu/journal/node/j2007-4/1_Jitaru_333-344.pdf.

[71] H. Noda, S. Ikeda, Y. Oda, K. Imai, M. Maeda, K. Ito, Electrochemical reduction of carbon dioxide at various metal electrodes in aqueous potassium hydrogen carbonate solution, Bull. Chem. Soc. Jpn. 63 (1990) 2459–2462, https://doi.org/10.1246/bcsj.63.2459.

[72] M.A. Scibioh, B. Viswanathan, Electrochemical reduction of carbon dioxide: a status report, Proc. Indian. Nat. Sci. Acad. 70 (2004) 407–762.

[73] M. Le, M. Ren, Z.P. Zhang, T. Sprunger, R.L. Kurtz, J.C. Flake, Electrochemical reduction of CO_2 to CH_3OH at copper oxide surfaces, J. Electrochem. Soc. 158 (2011) E45, https://doi.org/10.1149/1.3561636.

[74] Y. Hori, I. Takahashi, O. Koga, N. Hoshi, Selective formation of C_2 compounds from electrochemical reduction of CO_2 at a series of copper single crystal electrodes, J. Phys. Chem. B 106 (2002) 15–17, https://doi.org/10.1021/jp013478d.

[75] R. Francke, B. Schille, M. Roemelt, Homogeneously catalyzed electroreduction of carbon dioxide-methods, mechanisms, and catalysts, Chem. Rev. 118 (2018) 4631–4701, https://doi.org/10.1021/acs.chemrev.7b00459.

[76] X. Lu, D.Y.C. Leung, H. Wang, M.K.H. Leung, J. Xuan, Electrochemical reduction of carbon dioxide to formic acid, CH_3OH generation, Chemelectrochem 1 (2014) 836–849, https://doi.org/10.1002/celc.201300206.

[77] M. Ramdin, A.R.T. Morrison, M. de Groen, R. van Haperen, R. de Kler, L.J.P. van den Broeke, J.P.M. Trusler, W. de Jong, T.J.H. Vlugt, High pressure electrochemical reduction of CO_2 to formic acid/formate: a comparison between bipolar membranes and cation exchange membranes, Ind. Eng. Chem. Res. 58 (2019) 1834–1847, https://doi.org/10.1021/acs.iecr.8b04944.

[78] H. Harada, Sonochemical reduction of carbon dioxide, Ultrason. Sonochem. 5 (1998) 73–77, https://doi.org/10.1016/S1350-4177(98)00015-7.
[79] A. Henglein, Sonolysis of carbon dioxide, nitrous oxide and methane in aqueous solution, Z. Naturforsch. 40b (1985) 100–107. https://www.degruyter.com/document/doi/10.1515/znb-1985-0119/pdf.
[80] D. Mei, X. Zhu, Y.L. He, J.D. Yan, X. Tu, Plasma-assisted conversion of CO_2 in a dielectric barrier discharge reactor: understanding the effect of packing materials, Plasma Sources Sci. Technol. 24 (2015) 015011, https://doi.org/10.1088/0963-0252/24/1/015011.
[81] T. Wang, H. Liu, X. Xiong, X. Feng, Conversion of carbon dioxide to carbon monoxide by pulse dielectric barrier discharge plasma, IOP Conf. Ser. Earth Environ. Sci. 52 (2017) 012100, https://doi.org/10.1088/1742-6596/52/1/012100.
[82] Y. Liu, F. Rehman, W.B. Zimmerman, Reaction engineering of carbon monoxide generation by treatment with atmospheric pressure, low power O_2 DBD plasma, Fuel 209 (2017) 117–126, https://doi.org/10.1016/j.fuel.2017.07.097.
[83] A.M. Banerjee, J. Billinger, K.J. Nordheden, F.J.J. Peeters, Conversion of CO_2 in a packed-bed dielectric barrier discharge reactor, J. Vac. Sci. Technol. A 36 (2018) 04F403, https://doi.org/10.1116/1.5024400.
[84] B. Eliasson, F.G. Simon, W. Egli, P. Brunner, Hydrogenation of CO_2 in a silent discharge, Helv. Phys. Acta 65 (1992) 129–130. https://www.e-periodica.ch/digbib/view?pid=hpa-0011992653#111.
[85] W. Egli, B. Eliasson, Numerical calculation of breakdown channel formation of silent discharge in CO_2, Helv. Phys. Acta 65 (1992) 127–128. https://www.e-periodica.ch/digbib/view?pid=hpa-0011992653#111.
[86] R. Aerts, T. Martens, A. Bogaerts, Influence of vibrational states on CO_2 splitting by dielectric barrier discharges, J. Phys. Chem. C 116 (2012) 23257–23273, https://doi.org/10.1021/jp307525t.
[87] H. Machrafi, S. Cavadias, J. Amouroux, CO_2 valorization by means of dielectric barrier discharge, J. Phys.: Conf. Series 275 (2011) 012016, https://doi.org/10.1088/1742-6596/275/1/012016.
[88] B. Eliasson, W. Egli, U. Kogelschatz, Modelling of dielectric barrier discharge chemistry, Pure Appl. Chem. 66 (1994) 1275–1286, https://doi.org/10.1351/pac199466061275.
[89] G.R. Dey, T.N. Das, Gas-phase and on-surface chemical reduction of CO_2 to HCHO and CO under dielectric barrier discharge, Plasma Chem. Plasma Process. 26 (2006) 495–505, https://doi.org/10.1007/s11090-006-9031-5.
[90] G.R. Dey, B.N. Singh, S.D. Kumar, T.N. Das, Dielectric barrier discharge initiated gas-phase decomposition of CO_2 to CO and C_6-C_9 alkanes to C_1-C_3 hydrocarbons on glass, molecular sieve 10X and TiO_2/ZnO surfaces, Plasma Chem. Plasma Process. 27 (2007) 669–678, https://doi.org/10.1007/s11090-007-9096-9.
[91] G.R. Dey, S. Kamble, Effects of electrode material and frequency on carbon monoxide formation in carbon dioxide dielectric barrier discharge, J. CO_2 Util. 40 (2020) 101207, https://doi.org/10.1016/j.jcou.2020.101207.
[92] G. Dey, Easing of frequency gaps in carbon monoxide formation with argon diluents in carbon dioxide dielectric barrier discharge, Chem. Eng. J. Adv. 6 (2021) 100099, https://doi.org/10.1016/j.ceja.2021.100099.
[93] L. Wang, Y. Yi, C. Wu, H. Guo, X. Tu, One-step reforming of CO_2 and CH_4 into high-value liquid chemicals and fuels at room temperature by plasma-driven catalysis, Angew. Chem. 129 (2017) 13867–13871, https://doi.org/10.1002/ange.201707131.
[94] A. George, B. Shen, M. Craven, Y. Wang, D. Kang, C. Wu, X. Tu, A review of non-thermal plasma technology: a novel solution for CO_2 conversion and utilization, Renew. Sustain. Energy Rev. (2021) 135 109702, https://doi.org/10.1016/j.rser.2020.109702.
[95] https://www.sciencedirect.com/topics/engineering/boudouard-reaction accessed on June 2, 2020.
[96] P. Lahijani, Z.A. Zainal, M. Mohammadi, A.R. Mohamed, Conversion of the greenhouse gas CO_2 to the fuel gas CO via the Boudouard reaction: a review, Renew. Sustain. Energy Rev. 41 (2015) 615–632, https://doi.org/10.1016/j.rser.2014.08.034.
[97] M. Rauch, Z. Strater, G. Parkin, Selective conversion of carbon dioxide to formaldehyde via a bis(silyl)acetal: incorporation of isotopically labeled C_1 moieties derived from carbon dioxide into organic molecules, J. Am. Chem. Soc. 141 (2019) 17754–17762, https://doi.org/10.1021/jacs.9b08342.
[98] W. Sattler, G. Parkin, Zinc Catalysts for on-demand hydrogen generation and carbon dioxide functionalization, J. Am. Chem. Soc. 134 (2012) 17462–17465, dx.doi.org/10.1021/ja308500s.
[99] M. Siebert, M. Seibicke, A.F. Siegle, S. Kräh, O. Trapp, Selective ruthenium-catalyzed transformation of carbon dioxide: an alternative approach toward formaldehyde, J. Am. Chem. Soc. 141 (2019) 334–341, https://doi.org/10.1021/jacs.8b10233.
[100] F.L. Chan, G. Altinkaya, N. Fung, A. Tanksale, Low temperature hydrogenation of carbon dioxide into formaldehyde in liquid media, Catal. Today 309 (2018) 242–247, https://doi.org/10.1016/j.cattod.2017.06.012.
[101] D.K. Lee, D.S. Kim, S.W. Kim, Selective formation of formaldehyde from carbon dioxide and hydrogen over PtCu/SiO_2, Appl. Organomet. Chem. 15 (2001) 148–150, https://doi.org/10.1002/1099-0739(200102)15:2<148::AID-AOC104>3.0.CO;2-N.
[102] G. Meńard, D.W. Stephan, Room temperature reduction of CO_2 to methanol by Al-based frustrated Lewis pairs and ammonia borane CH_4 generation, J. Am. Chem. Soc. 132 (2010) 1796–1797, https://doi.org/10.1021/ja9104792.
[103] N.M. Rezayee, C.A. Huff, M.S. Sanford, Tandem amine and ruthenium-catalyzed hydrogenation of CO_2 to methanol, J. Am. Chem. Soc. 137 (2015) 1028–1031, https://doi.org/10.1021/ja511329m.
[104] S. Glasstone, Textbook of Physical Chemistry, M.I. Press, Madras, India, 1981, p. 112.
[105] R.N. Compton, P.W. Reinhardt, C.D. Cooper, Collisional ionization of Na, K, and Cs by CO_2, COS, and CS_2: molecular electron affinities, J. Chem. Phys. 63 (1975) 3821, https://doi.org/10.1063/1.431875.
[106] K. Tennakone, A.H. Jayatissa, S. Punchihewa, Selective photoreduction of carbon dioxide to methanol with hydrous cuprous oxide, J. Photochem. Photobiol., A: Chem 49 (1989) 369–375, https://doi.org/10.1016/1010-6030(89)87134-5.
[107] K. Hara, A. Kudo, T. Sakata, Electrochemical reduction of carbon dioxide under high pressure on various electrodes in an aqueous electrolyte, J. Electroanal. Chem. 391 (1995) 141–147, https://doi.org/10.1016/0022-0728(95)03935-A.
[108] C.W. Tobias, Advances in Electrochemistry and Electrochemical Engineering, vol. 2, Interscience Pub. John Wiley & Sons, New York, 1961, p. 262.
[109] R.G. Russell, N. Kovac, S. Srinivasan, M. Steinberg, The electrochemical reduction of carbon dioxide, formic acid, and formaldehyde, J. Electrochem. Soc. 124 (1977) 1329–1337, https://doi.org/10.1149/1.2133624.
[110] E. Lamy, L. Ladjo, J.M. Saveant, J. Electroanal. Chem. 78 (1977) 403. A.J. Bard, Encyclopedia of electrochemistry of elements, Dekker, New York, 7 (1976).
[111] J.P. Collin, J.P. Sauvage, Electrochemical reduction of carbon dioxide mediated by molecular catalysts, Coord. Chem. Rev. 93 (1989) 245–268, https://doi.org/10.1016/0010-8545(89)80018-9.
[112] R. Memming, Photo electrochemical solar energy conversion, Top. Curr. Chem. 143 (1988) 79–112, https://doi.org/10.1007/BFb0018072.
[113] M.R. Hoffmann, S.T. Martin, W. Choi, D.W. Bahnemann, Chem. Rev. 95 (1995) 69–96, https://doi.org/10.1021/cr00033a004.
[114] D.W. Bahnemann, in: E. Pelizzetti, M. Schiavello (Eds.), Photochemical Conversion and Storage of Solar Energy, Kluwer Academic Publishers, Dordrecht, 1991, p. 251.
[115] G. Mills, M.R. Hoffmann, Photocatalytic degradation of pentachlorophenol on titanium dioxide particles: identification of intermediates and mechanism of reaction, Environ. Sci. Technol. 27 (1993) 1681–1689, https://doi.org/10.1021/es00045a027.
[116] M. Anpo, Photocatalysis on small particle TiO_2 catalysts. reaction intermediates and reaction mechanisms, Res. Chem. Intermed. 11 (1989) 67, https://doi.org/10.1007/BF03051818.
[117] A. Fujishima, T.N. Rao, D.A. Tryk, Titanium dioxide photocatalysis, J. Photochem. Phtobiol. C: Photochem. Rev. 1 (2000) 1–21, https://doi.org/10.1016/S1389-5567(00)00002-2.
[118] A. Mills, S. Le Hunte, An overview of semiconductor photocatalysis, J. Photochem. Photobiol., A: Chem 108 (1997) 1–35, https://doi.org/10.1016/S1010-6030(97)00118-4.
[119] U. Diebold, The surface science of titanium dioxide, Surf. Sci. Rep. 48 (2003) 53–229, https://doi.org/10.1016/S0167-5729(02)00100-0.
[120] J. Rabani, M.S. Metheson, Pulse radiolytic determination of p*K* for hydroxyl ionic dissociation in water, J. Am. Chem. Soc. 80 (1964) 3175–3176, https://doi.org/10.1021/ja01069a058.
[121] Y. Tabata, in: Pulse Radiolysis, CRC Press, Boca Raton, 1991, p. 399. Ann Arbar-Botson.
[122] B.H.J. Bieski, D.E. Cabelli, R.L. Arudi, A.B. Ross, Reactivity of HO_2/O_2^- radicals in aqueous solution, J. Phys. Chem. Ref. Data 14 (1985) 1041, https://doi.org/10.1063/1.555739.
[123] P.V. Kamat, Photochemistry on nonreactive and reactive (semiconductor) surfaces, Chem. Rev. 93 (1993) 267–300, https://doi.org/10.1021/cr00017a013.
[124] G.R. Dey, Significant roles of oxygen and unbound •OH radical in phenol formation during photo-catalytic degradation of benzene on TiO_2 suspension in aqueous system, Res. Chem. Intermed. 35 (2009) 573–587, https://doi.org/10.1007/s11164-009-0066-0.
[125] J.R. Harbour, M.L. Hair, Radical intermediates in the photosynthetic generation of hydrogen peroxide with aqueous zinc oxide dispersions, J. Phys. Chem. 83 (1979) 652–656, https://doi.org/10.1021/j100469a003.
[126] C.D. Jaeger, A.J. Bard, Spin trapping and electron spin resonance detection of radical intermediates in the photodecomposition of water at titanium dioxide particulate systems, J. Phys. Chem. 83 (1979) 3146–3152, https://doi.org/10.1021/j100487a017.
[127] V.C. Anitha, A.N. Banerjee, S.W. Joo, Recent developments in TiO_2 as n- and p-type transparent semiconductors: synthesis, modification, properties, and energy-related applications, J. Mater. Sci. 50 (2015) 7495–7536, https://doi.org/10.1007/s10853-015-9303-7.
[128] J. Cao, Y. Zhang, L. Liu, J. Ye, A p-type Cr-doped TiO_2 photo-electrode for photo-reduction, Chem. Commun. 49 (2013) 3440–3442, https://doi.org/10.1039/C3CC40394G.
[129] G. Thomas, Invisible circuits, Nature 389 (1997) 907–908, https://doi.org/10.1038/39999.
[130] D. Bahnemann, A. Henglein, J. Lilie, L. Spanhel, Flash photolysis observation of the absorption spectra of trapped positive holes and electrons in colloidal titanium dioxide, J. Phys. Chem. 88 (1984) 709–711, https://doi.org/10.1021/j150648a018.

[131] Z. Zang, C.-C. Wang, R. Zakaria, J.Y. Ying, Role of particle size in nanocrystalline TiO_2-based photocatalysts, J. Phys. Chem. B 102 (1998) 10871–10878, https://doi.org/10.1021/jp982948+.
[132] I.-H. Tseng, W.-C. Cheng, J.C.S. Wu, Photoreduction of CO_2 using sol–gel derived titania and titania-supported copper catalysts, Appl. Catal. B Environ. 37 (2002) 37–48, https://doi.org/10.1016/S0926-3373(01)00322-8.
[133] M. Anpo, H. Yamashita, Y. Ichihashi, S. Ehara, Photocatalytic reduction of CO_2 with H_2O on various titanium oxide catalysts, J. Electroanal. Chem. 396 (1995) 21–26, https://doi.org/10.1016/0022-0728(95)04141-A.
[134] G.R. Dey, K.K. Pushpa, Methane generated during photocatalytic redox reaction of alcohols on TiO_2 suspension in aqueous solutions, Res. Chem. Intermed. 32 (2006) 725–736, https://doi.org/10.1163/156856706778606462.
[135] G.R. Dey, K.K. Pushpa, Formation of different products during photo-catalytic reaction on TiO_2 suspension in water with and without 2-propanol under diverse ambient conditions, Res. Chem. Intermed. 33 (2007) 631–644, https://doi.org/10.1163/156856707781749883.
[136] S. Kuwabata, H. Uchida, A. Ogawa, S. Hirao, H. Yoneyama, Selective photoreduction of carbon dioxide to methanol on titanium dioxide photocatalysts in propylene carbonate solution, J. Chem. Soc. Chem. Commun. (1995) 829–830, https://doi.org/10.1039/C39950000829.
[137] K.R. Thampi, J. Kiwi, M. Gratzel, Methanation and photo-methanation of carbon dioxide at room temperature and atmospheric pressure, Nature 327 (1987) 506–508, https://doi.org/10.1038/327506a0.
[138] M. Bellardita, A.D. Paola, E. García-López, V. Loddo, G. Marcì, L. Palmisano, Photocatalytic CO_2 reduction in gas-solid regime in the presence of bare, SiO_2 supported or Cu-loaded TiO_2 samples, Curr. Org. Chem. 17 (2013) 2440–2448. https://core.ac.uk/download/pdf/53291549.pdf.
[139] M. Keidar, I. Beilis, Plasma Engineering Applications from Aerospace to Bio and Nanotechnology, second ed., Academic Press, 2018 eBook ISBN: 9780128137031.
[140] R.N. Franklin, N. St, J. Braithwaite, Electron plasma waves and plasma resonances, Plasma Sources Sci. Technol. 18 (2008) 1–4, https://doi.org/10.1088/0963-0252/18/1/014019.
[141] R.C. Davidson, Physics of Non-neutral Plasmas, Published by Addison-Wesley, University of California, 2001.
[142] T.N. Das, G.R. Dey, Cold Plasma: Simple Tool for Convenient Utilitarian Chemistry in Homogeneous and Heterogeneous Environments, 2015. BARC Report, BARC/2015/E/007, https://inis.iaea.org/search/search.aspx?orig_q=RN:46076132.
[143] S. Starostine, E. Aldea, H. de Vries, M. Creatore, M.C.M. Van de Sanden, Atmospheric pressure barrier discharge deposition of silica-like films on polymeric substrates, Plasma Process. Polym. 4 (2007) S440–S444, https://doi.org/10.1002/ppap.200731203.
[144] T. Andrews, P.G. Tait, Phil.Trans. VII. On the volumetric relations of ozone, and the action of the electrical discharge on oxygen and other gases, Royal Soc. Lond. 150 (1860) 113–131, https://doi.org/10.1098/rstl.1860.0008.
[145] U. Kogelschatz, Dielectric-barrier discharges: their history, discharge Physics, and industrial applications, Plasma Chem. Plasma Process. 23 (2003) 1–46, https://doi.org/10.1023/A:1022470901385.
[146] J.J. Coogan, A.D. Sappey, Distribution of OH within silent discharge plasma reactors, IEEE Trans. Plasma Sci. 24 (1996) 91–92. https://ieeexplore.ieee.org/document/491706.
[147] U. Kogelschatz, B. Eliasson, Micro-discharge properties in dielectric-barrier discharges, in: Proc. Symp. High Pressure Low-Temp. Plasma Chem. (Hakone, Japan), 1987, pp. 1–8.
[148] B. Eliasson, U. Kogelschatz, Modeling and applications of silent discharge plasmas, IEEE Trans. Plasma Sci. 19 (1991) 309–323. https://ieeexplore.ieee.org/document/106829.
[149] K. Pochner, W. Neff, R. Leber, Atmospheric pressure gas discharges for surface treatment, Surf. Coat. Technol. 74/75 (1995) 394–398, https://doi.org/10.1016/0257-8972(95)08325-1.
[150] X. Bonnin, J. Brandelero, N. Videau, H. Piquet, T. Meynard, A high voltage high frequency resonant inverter for supplying DBD devices with short discharge current pulses, IEEE Trans. Power Electron. 29 (2014) 4261–4269, https://doi.org/10.1109/TPEL.2013.2295525.
[151] K. Zhang, G. Zhang, X. Liu, A.N. Phan, K. Luo, A study on CO_2 decomposition to CO and O_2 by the combination of catalysis and dielectric-barrier discharges at low temperatures and ambient pressure, Ind. Eng. Chem. Res. 56 (2017) 3204–3216, https://doi.org/10.1021/acs.iecr.6b04570.
[152] W. Luc, M. Jouny, J. Rosen, F. Jiao, Carbon dioxide splitting using an electrothermochemical hybrid looping strategy, Energy Environ. Sci. 11 (2018) 2928–2934, https://doi.org/10.1039/C8EE00532J.
[153] Y. Tamaura, K. Nishizawa, CO_2 decomposition into C and conversion into CH_4 using the H_2-reduced magnetite, Energy Convers. Manag. 33 (1992) 573–577, https://doi.org/10.1016/0196-8904(92)90058-5.
[154] W.C. Chueh, C. Falter, M. Abbott, D. Scipio, P. Furler, S.M. Haile, A. Steinfeld, High-flux solar-driven thermochemical dissociation of CO_2 and H_2O using nonstoichiometric ceria, Science 330 (2010) 1797–1801, https://doi.org/10.1126/science.1197834.
[155] S. Ackermann, L. Sauvin, R. Castiglioni, J.L.M. Rupp, J.R. Scheffe, A. Steinfeld, Kinetics of CO_2 reduction over nonstoichiometric ceria, J. Phys. Chem. C 119 (2015) 16452–16461, https://doi.org/10.1021/acs.jpcc.5b03464.
[156] N. Taccardi, M. Grabau, J. Debuschewitz, M. Distaso, M. Brandl, R. Hock, F. Maier, C. Papp, J. Erhard, C. Neiss, W. Peukert, A. Görling, H.-P. Steinrück, P. Wasserscheid, Gallium-rich Pd–Ga phases as supported liquid metal catalysts, Nat. Chem. 9 (2017) 862–867, https://doi.org/10.1038/nchem.2822.
[157] D. Esrafilzadeh, A. Zavabeti, R. Jalili, P. Atkin, J. Choi, Benjamin J. Carey, Robert Brkljača, Anthony P. O'Mullane, Michael D. Dickey, David L. Officer, Douglas R. MacFarlane, Torben Daeneke, Kourosh Kalantar-Zadeh, Room temperature CO_2 reduction to solid carbon species on liquid metals featuring atomically thin ceria interfaces, Nat. Commun. 10 (2019) 865, https://doi.org/10.1038/s41467-019-08824-8.
[158] https://www.sciencemag.org/news/2019/02/liquid-metal-catalyst-turns-carbon-dioxide-coal accessed on June 14, 2020.
[159] https://www.designnews.com/batteryenergy-storage/co2-converted-solid-carbon/206299923860346 accessed on 14 June 2020 under CO_2 Converted to Solid Carbon.
[160] https://www.sustainability-times.com/low-carbon-energy/scientists-can-now-turning-atmospheric-co2-back-into-coal/accessed on 14 June 2020.
[161] L.D. Burke, An interfacial mediator interpretation of noble metal electrocatalysis, Platin. Met. Rev. 38 (1994) 166–173.
[162] Graphene, https://en.wikipedia.org/wiki/Graphene accessed on 3 March 2022.
[163] C. Molina-Jirjn, M.R. Chellali, C.N. Shyam Kumar, C. Kebel, L. Velasco, H. Hahn, E. Moreno-Pineda, M. Ruben, Direct conversion of CO_2 to multi-layer graphene using Cu–Pd alloys, ChemSusChem 12 (2019) 3509–3514, https://doi.org/10.1002/cssc.201901404.
[164] S. Xu, L. Zhang, B. Wang, R.S. Ruoff, Chemical vapor deposition of graphene on thin-metal films, Cell Reports Phys. Sci. 2 (2021) 100372, https://doi.org/10.1016/j.xcrp.2021.100372.
[165] M. Hajian, M. Zareie, D. Hashemian, M. Bahrami, Room-temperature synthesis of graphene-like carbon sheets from C_2H_2, CO_2 and CO on copper foil, https://arxiv.org/ftp/arxiv/papers/1608/1608.03791.pdf.
[166] L. Hu, Y. Song, S. Jiao, Y. Liu, J. Ge, H. Jiao, J. Zhu, J. Wang, H. Zhu, D.J. Fray, Direct conversion of greenhouse gas CO_2 into graphene via molten salts electrolysis, ChemSusChem 9 (2016) 588–594, https://doi.org/10.1002/cssc.201501591.
[167] X. Liu, X. Wang, G. Licht, S. Licht, Transformation of the greenhouse gas carbon dioxide to graphene, J. CO_2 Util. 36 (2020) 288–294, https://doi.org/10.1016/j.jcou.2019.11.019.
[168] G. Allaedini, S.M. Tasirin, P. Aminayi, Synthesis of graphene through direct decomposition of CO_2 with the aid of Ni–Ce–Fe trimetallic catalyst, Bull. Mater. Sci. 39 (2016) 235–240, https://doi.org/10.1007/s12034-015-1125-3.
[169] W. Wei, K. Sun, Y.H. Hu, Direct conversion of CO_2 to 3D graphene and its excellent performance for dye-sensitized solar cells with 10% efficiency, J. Mater. Chem. 4 (2016) 12054–12057, https://doi.org/10.1039/C6TA04008J.
[170] A. Chakrabarti, J. Lu, J.C. Skrabutenas, T. Xu, Z. Xiao, J.A. Maguire, N.S. Hosmane, Conversion of carbon dioxide to few-layer graphene, J. Mater. Chem. 21 (2011) 9491–9493, https://doi.org/10.1039/C1JM11227A.
[171] Gaphene, https://patents.google.com/patent/CN106335896A/en, accessed on 3 March 2022.
[172] M.Y. Svavil'nyi, V.Y. Panarin, A.A. Shkola, A.S. Nikolenko, V.V. Strelchuk, Plasma enhanced chemical vapor deposition synthesis of graphene-like structures from plasma state of CO_2 gas, Carbon 167 (2020) 132–139, https://doi.org/10.1016/j.carbon.2020.05.057.
[173] V. Kumaravel, J. Bartlett, S.C. Pillai, Photoelectrochemical conversion of carbon dioxide into fuels and value-added products, ACS Energy Lett. 5 (2020) 486–519, https://doi.org/10.1021/acsenergylett.9b02585.
[174] Carbon monoxide. https://www.linde-gas.com/en/products_and_supply/packaged_chemicals/product_range/carbon_monoxide.html. (Accessed 22 November 2019).
[175] J.L. DiMeglio, J. Rosenthal, Selective conversion of CO_2 to CO with high efficiency using an inexpensive bismuth-based electrocatalyst, J. Am. Chem. Soc. 135 (2013) 8798–8801, https://doi.org/10.1021/ja4033549.
[176] K. Jiang, S. Siahrostami, T. Zheng, Y. Hu, S. Hwang, E. Stavitski, Y. Peng, J. Dynes, M. Gangisetty, D. Su, K. Attenkofer, H. Wang, Isolated Ni single atoms in graphene nanosheets for high-performance CO_2 reduction, Energy Environ. Sci. (2018), https://doi.org/10.1039/C7EE03245E.
[177] J. O'm. Bockris, E.C. Potter, The mechanism of the cathodic hydrogen evolution reaction, J. Electrochem. Soc. 99 (1952) 169–186, https://doi.org/10.1149/1.2779692.
[178] A. Lasia, Hydrogen evolution reaction, in: W. Vielstich, A. Lamm, H.A. Gasteiger (Eds.), Handbook of Fuel Cells – Fundamentals, Technology and Applications, vol. 2, John Wiley & Sons, Ltd, Chichester, 2003, pp. 416–440.
[179] X. Liu, J. Xiao, H. Peng, X. Hong, K. Chan, J.K. Nørskov, Understanding trends in electrochemical carbon dioxide reduction rates, Nat. Commun. 8 (2017) 15438, https://doi.org/10.1038/ncomms15438.
[180] H. Ooka, M.C. Figueiredo, M.T.M. Koper, Competition between hydrogen evolution and carbon dioxide reduction on copper electrodes in mildly acidic media, Langmuir 33 (2017) 9307–9313, https://doi.org/10.1021/acs.langmuir.7b00696.
[181] Y.-J. Zhang, V. Sethuraman, R. Michalsky, A.A. Peterson, Competition between CO_2 reduction and H_2 evolution on transition-metal electrocatalysts, ACS Catal. 4 (2014) 3742–3748, https://doi.org/10.1021/cs5012298.

[182] J. Choi, J. Kim, P. Wagner, S. Gambhir, R. Jalili, S. Byun, S. Sayyar, Y.M. Lee, D.R. MacFarlane, G.G. Wallace, D.L. Officer, Energy efficient electrochemical reduction of CO_2 to CO using a three-dimensional porphyrin/graphene hydrogel, Energy Environ. Sci. 12 (2019) 747–755, https://doi.org/10.1039/C8EE03403F.

[183] Precious metals catalyst: understanding the technology (ERTC). https://www.digitalrefining.com/article/1001449/precious-metals-catalyst-understanding-the-technology-ert#.YtWZ-HZBxnI. (Accessed 18 July 2022).

[184] T. Möller, W. Ju, A. Bagger, X. Wang, F. Luo, T.N. Thanh, A.S. Varela, J. Rossmeisl, P. Strasser, Efficient CO_2 to CO electrolysis on solid Ni–N–C catalysts at industrial current densities, Energy Environ. Sci. 12 (2019) 640–647, https://doi.org/10.1039/C8EE02662A.

[185] Y. Meng, X. Zhang, W.-H. Hung, J. Hee, Y.-S. Tsai, Y. Kuang, M.J. Kenney, J.-J. Shyue, Y. Liu, K.H. Stone, X. Zheng, S.L. Suib, M.-C. Lin, Y. Liang, H. Dai, Highly active oxygen evolution integrated with efficient CO_2 to CO electroreduction, Proc. Natl. Acad. Sci. USA 116 (2019) 23915–23922, https://doi.org/10.1073/pnas.191531911.

[186] J.T. Feaster, C. Shi, E.R. Cave, T. Hatsukade, D.N. Abram, K.P. Kuhl, C. Hahn, J.K. Nørskov, T.F. Jaramillo, Understanding selectivity for the electrochemical reduction of carbon dioxide to formic acid and carbon onoxide on metal electrodes, ACS Catal. 7 (2017) 4822–4827, https://doi.org/10.1021/acscatal.7b00687.

[187] T. Zheng, K. Jiang, H. Wang, Recent advances in electrochemical CO_2 -to- CO conversion on heterogeneous catalysts, Adv. Mater. (Weinheim, Ger.) 30 (2018) e1802066, https://doi.org/10.1002/adma.201802066.

[188] water-gas shift reaction. https://en.wikipedia.org/wiki/Water-gas_shift_reaction. (Accessed 5 June 2020).

[189] K. Zhao, Q. Bkour, X. Hou, S.W. Kang, J.C. Park, M.G. Norton, J.-I. Yang, S. Ha, Reverse water gas shift reaction over $CuFe/Al_2O_3$ catalyst in solid oxide electrolysis cell, Chem. Eng. J. 336 (2018) 20–27, https://doi.org/10.1016/j.cej.2017.11.028.

[190] A. Trovarelli, C. Mustazza, G. Dolcetti, J. Kaspar, M. Graziani, Carbon dioxide hydrogenation on rhodium supported on transition metal oxides: effect of reduction temperature on product distribution, Appl. Catal. 65 (1990) 129–142, https://doi.org/10.1016/S0166-9834(00)81593-6.

[191] C.-K. Kuei, M.-D. Lee, Hydrogenation of carbon dioxide by hybrid catalysts, direct synthesis of aromatics from carbon dioxide and hydrogen, Can. J. Chem. Eng. 69 (1991) 347–354, https://doi.org/10.1002/cjce.5450690142.

[192] M.J.L. Ginés, A.J. Marchi, C.R. Apesteguía, Kinetic study of the reverse water-gas shift reaction over $CuO/ZnO/Al_2O_3$ catalysts, Appl. Catal. Gen. 154 (1997) 155–171, https://doi.org/10.1016/S0926-860X(96)00369-9.

[193] Y.A. Daza, J.N. Kuhn, CO_2 conversion by reverse water gas shift catalysis: comparison of catalysts, mechanisms and their consequences for CO_2 conversion to liquid fuels, RSC Adv. 6 (2016) 49675–49691, https://doi.org/10.1039/C6RA05414E.

[194] L. Pastor-Pérez, F. Baibars, E. Le Sache, H. Arellano-García, S. Gu, T.R. Reina, CO_2 valorisation via reverse water-gas shift reaction using advanced Cs doped $Fe-Cu/Al_2O_3$ catalysts, J. CO_2 Util. 21 (2017) 423–428, https://doi.org/10.1016/j.jcou.2017.08.009.

[195] C.-S. Chen, W.-H. Cheng, S.-S. Lin, Mechanism of CO formation in reverse water–gas shift reaction over Cu/Al_2O_3 catalyst, Catal. Lett. 68 (2000) 45–48, https://doi.org/10.1023/A:1019071117449.

[196] L. Pastor-Pérez, M. Shah, E. le Saché, T.R. Reina, Improving Fe/Al_2O_3 catalysts for the reverse water-gas shift reaction: on the effect of Cs as activity/selectivity promoter, Catalysts 8 (2018) 608, https://doi.org/10.3390/catal8120608.

[197] B. Dai, S. Cao, H. Xie, G. Zhou, S. Chen, Reduction of CO_2 to CO via reverse water-gas shift reaction over CeO_2 catalyst, Kor. J. Chem. Eng. 35 (2018) 421–427, https://doi.org/10.1007/s11814-017-0267-y.

[198] E. Schwab, A. Milanov, S.A. Schunk, A. Behrens, N. Schödel, Dry reforming and reverse water gas shift: alternatives for syngas production? Chem. Ing. Tech. 87 (2015) 347–353, https://doi.org/10.1002/cite.201400111.

[199] A. de Klerk, Fischer–Tropsch Process, Kirk-Othmer Encyclopedia of Chemical Technology, Wiley-VCH, Weinheim, 2013, https://doi.org/10.1002/0471238961.fiscdekl.a01. (Accessed 26 July 2021).

[200] T. Mizuno, A. Naitoh, K. Ohta, Electrochemical reduction of CO_2 in methanol at −30°C, J. Electroanal. Chem. 391 (1995) 199–201, https://doi.org/10.1016/0022-0728(95)03936-B.

[201] Q. Lin, X.Y. Liu, Y. Jiang, Y. Wang, Y. Huang, T. Zhang, Crystal phase effects on the structure and performance of ruthenium nanoparticles for CO_2 hydrogenation, Catal. Sci. Technol. 4 (2014) 2058–2063, https://doi.org/10.1039/C4CY00030G.

[202] A. Kim, C. Sanchez, G. Patriarche, O. Ersen, S. Moldovan, A. Wisnet, C. Sassoye, D.P. Debecker, Selective CO_2 methanation on Ru/TiO_2 catalysts: unravelling the decisive role of the TiO_2 support crystal structure, Catal. Sci. Technol. 6 (2016) 8117–8128, https://doi.org/10.1039/C6CY01677D.

[203] Z. Chen, J.J. Concepcion, M.K. Brennaman, P. Kang, M.R. Norris, P.G. Hoertz, T.J. Meyer, Splitting CO_2 into CO and O_2 by a single catalyst, Proc. Natl. Acad. Sci. USA 109 (2012) 15606–15611, https://doi.org/10.1073/pnas.12031221.

[204] H. Takeda, O. Ishitani, Development of efficient photocatalytic systems for CO_2 reduction using mononuclear and multinuclear metal complexes based on mechanistic studies, Coord. Chem. Rev. 254 (2010) 346–354, https://doi.org/10.1016/j.ccr.2009.09.030.

[205] M.R. Dubois, D.L. Dubois, Development of molecular electrocatalysts for CO_2 reduction and H_2 production/oxidation, Acc. Chem. Res. 42 (2009) 1974–1982, https://doi.org/10.1021/ar900110c.

[206] A.J. Morris, G.J. Meyer, E. Fujita, Molecular approaches to the photocatalytic reduction of carbon dioxide for solar fuels, Acc. Chem. Res. 42 (2009) 1983–1994, https://doi.org/10.1021/ar9001679.

[207] E.E. Benson, C.P. Kubiak, A.J. Sathrum, J.M. Smieja, Electrocatalytic and homogeneous approaches to conversion of CO_2 to liquid fuels, Chem. Soc. Rev. 38 (2009) 89–99, https://doi.org/10.1039/B804323J.

[208] H. Nagao, T. Mizukawa, K. Tanaka, Carbon–carbon bond formation in the electrochemical reduction of carbon dioxide catalyzed by a ruthenium complex, Inorg. Chem. 33 (1994) 3415–3420, https://doi.org/10.1021/ic00093a033.

[209] J.M. Smieja, C.P. Kubiak, Reðbipy-tBuþðCOþ3Cl-improved catalytic activity for reduction of carbon dioxide: IR-spectroelectrochemical and mechanistic studies, Inorg. Chem. 49 (2010) 9283–9289, https://doi.org/10.1021/ic1008363.

[210] A.T. Radosevich, J.G. Melnick, S.A. Stoian, D. Bacciu, C.-H. Chen, B.M. Foxman, O.V. Ozerov, D.G. Nocera, Ligand reactivity in diarylamido/bis(phosphine) PNP complexes of $Mn(CO)_3$ and $Re(CO)_3$, Inorg, Chem 48 (2009) 9214–9221, https://doi.org/10.1021/ic9010218.

[211] J.R. Pugh, M.R.M. Bruce, B.P. Sullivan, T.J. Meyer, Formation of a metal-hydride bond and the insertion of carbon dioxide: key steps in the electrocatalytic reduction of carbon dioxide to formate anion, Inorg. Chem. 30 (1991) 86–91, https://doi.org/10.1021/ic00001a016.

[212] M.R.M. Bruce, E. Megehee, B.P. Sullivan, H.H. Thorp, T.R. O'Toole, A. Downard, J.R. Pugh, T.J. Meyer, Electrocatalytic reduction of carbon dioxide based on 2,2′-bipyridyl complexes of osmium, Inorg. Chem. 31 (1992) 4864–4873, https://doi.org/10.1021/ic00049a027.

[213] C.M. Bolinger, N. Story, B.P. Sullivan, T.J. Meyer, Electrocatalytic reduction of carbon dioxide by 2,2′-bipyridine complexes of rhodium and iridium, Inorg. Chem. 27 (1988) 4582–4587, https://doi.org/10.1021/ic00298a016.

[214] Z.F. Chen, D.R. Weinberg, P. Kang, J.J. Cocepcion, D.P. Harrison, S. Brookhart, T.J. Meyer, Electrocatalytic reduction of CO_2 to CO by polypyridyl ruthenium complexes, Chem. Commun. 47 (2011) 12607–12609, https://doi.org/10.1039/C1CC15071E.

[215] M.R. Prairie, A. Renken, J.G. Highfield, K.R. Thampi, M. Grätzel, A fourier transform infrared spectroscopic study of CO_2 methanation on supported ruthenium, J. Catal. 129 (1991) 130–144, https://doi.org/10.1016/0021-9517(91)90017-X.

[216] S. Protti, A. Albini, N. Serpone, Photocatalytic generation of solar fuels from the reduction of H_2O and CO_2: a look at the patent literature, Phys. Chem. Chem. Phys. 16 (2014) 19790–19827, https://doi.org/10.1039/C4CP02828G.

[217] B. Tahir, M. Tahir, N.S. Amin, Performance analysis of monolith photoreactor for CO_2 reduction with H_2, Energy Convers. Manag. 90 (2015) 272–281, https://doi.org/10.1016/j.enconman.2014.11.018.

[218] Z. Guo, F. Yu, Y. Yang, C.F. Leung, S.M. Ng, C.C. Ko, C. Cometto, T.C. Lau, M. Robert, Photocatalytic conversion of CO_2 to CO by a copper(II) quaterpyridine complex, ChemSusChem 10 (2017) 4009–4013, https://doi.org/10.1002/cssc.201701354.

[219] G. Sahara, O. Ishitani, Efficient photocatalysts for CO_2 reduction, Inorg. Chem. 54 (2015) 5096–5104, https://doi.org/10.1021/ic502675a.

[220] B.-J. Ng, L.K. Putri, X.Y. Kong, Y.W. Teh, P. Pasbakhsh, S.-P. Chai, Z-Scheme photocatalytic systems for solar water splitting, Adv. Sci. 7 (2020) 1903171, https://doi.org/10.1002/advs.201903171.

[221] G. Zhang, Z. Wang, J. Wu, Construction of a Z-scheme heterojunction for high-efficiency visible-light-driven photocatalytic CO_2 reduction, Nanoscale 13 (2021) 4359–4389, https://doi.org/10.1039/D0NR08442E.

[222] H. Maimaiti, A. Awati, D. Zhang, G. Yisilamu, B. Xu, Synthesis and photocatalytic CO_2 reduction performance of aminated coal-based carbon nanoparticles, RSC Adv. 8 (2018) 35989–35997, https://doi.org/10.1039/C8RA06062B.

[223] A.W. Morawski, K. Cmielewska, K. Witkowski, E. Kusiak-Nejman, I. Pełech, P. Staciwa, E. Ekiert, D. Sibera, A. Wanag, M. Gano, U. Narkiewicz, CO_2 reduction to valuable chemicals on TiO_2-carbon photocatalysts deposited on silica cloth, Catalysts 12 (2022) 31, https://doi.org/10.3390/catal12010031.

[224] D. Li, J. Zhou, Z. Zhang, Y. Jiang, Z. Dong, J. Xu, C. Yao, Enhanced photocatalytic activity for CO_2 reduction over a $CsPbBr_3$/CoAl-LDH composite: insight into the S-scheme charge transfer mechanism, ACS Appl. Energy Mater. 5 (2022) 6238–6247, https://doi.org/10.1021/acsaem.2c00612.

[225] P.G. Reyes, E.F. Mendez, D. Osorio-Gonzalez, F. Castillo, H. Martínez, Optical emission spectroscopy of CO_2 glow discharge at low pressure, Phys. Status Solidi 5 (2008) 907–910, https://doi.org/10.1002/pssc.200778306.

[226] N. Lu, C. Zhang, K. Shang, N. Jiang, J. Li, Y. Wu, Dielectric barrier discharge plasma assisted CO_2 conversion: understanding the effects of reactor design and operating parameters, J. Phys. D Appl. Phys. 52 (2019) 224003, https://doi.org/10.1088/1361-6463/ab2171.

[227] A. Bogaerts, G. Centi, Plasma Technology for CO_2 Conversion: a personal perspective on prospects and gaps, Front. Energy Res. (2020), https://doi.org/10.3389/fenrg.2020.00111.

[228] S. Xu, H. Chen, C. Hardacre, X. Fan, Non-thermal plasma catalysis for CO_2 conversion and catalyst design for the process, J. Phys. D Appl. Phys. 54 (2021) 233001, https://doi.org/10.1088/1361-6463/abe9e1.

[229] A. Lebouvier, S.A. Iwarere, P. d'Argenlieu, D. Ramjugernath, L. Fulcheri, Assessment of carbon dioxide dissociation as a new route for syngas production: a comparative review and potential of plasma-based technologies, Energy Fuels 27 (2013) 2712–2722, https://doi.org/10.1021/ef301991d.
[230] J. Li, C. Ma, S. Zhu, F. Yu, B. Dai, D. Yang, A review of recent advances of dielectric barrier discharge plasma in catalysis, Nanomaterials 9 (2019) 1428, https://doi.org/10.3390/nano9101428.
[231] R. Aerts, W. Somers, A. Bogaerts, Carbon dioxide splitting in a dielectric barrier discharge plasma: a combined experimental and computational study, ChemSusChem 8 (2015) 702–716, https://doi.org/10.1002/cssc.201402818.
[232] D. Ray, R. Saha, C. Subrahmanyam, DBD plasma assisted CO_2 decomposition: influence of diluent gases, Catalysts 7 (2017) 244, https://doi.org/10.3390/catal7090244.
[233] M. Ramakers, I. Michielsen, R. Aerts, V. Meynen, A. Bogaerts, Effect of argon or helium on the CO_2 conversion in a dielectric barrier discharge, Plasma Process. Polym. 12 (2015) 755–763, https://doi.org/10.1002/ppap.201400213.
[234] S.L. Brock, M. Marquez, S.L. Suib, Y. Hayashi, H. Matsumoto, Plasma decomposition of CO_2 in the presence of metal catalysts, J. Catal. 180 (1998) 225–233, https://doi.org/10.1006/jcat.1998.2258.
[235] Y. Zeng, X. Tu, Plasma-catalytic hydrogenation of CO_2 for the cogeneration of CO and CH_4 in a dielectric barrier discharge reactor: effect of argon addition, J. Phys. D Appl. Phys. 50 (2017) 184004. https://iopscience.iop.org/article/10.1088/1361-6463/aa64bb/pdf.
[236] S. Li, M. Ongis, G. Manzolini, F. Gallucci, Non-thermal plasma-assisted capture and conversion of CO_2, Chem. Eng. J. 410 (2021) 128335, https://doi.org/10.1016/j.cej.2020.128335.
[237] R. Li, Q. Tang, S. Yin, Y. Yaaguchi, T. Sato, Decomposition of carbon dioxide by the dielectric barrier discharge (DBD) plasma using $Ca_{0.7}Sr_{0.3}TiO_3$ Barrier, Chem. Lett. 33 (2004) 412–413, https://doi.org/10.1246/cl.2004.412.
[238] J. Li, X. Zhai, C. Ma, S. Zhu, F. Yu, B. Dai, G. Ge, D. Yang, DBD plasma combined with different foam metal electrodes for CO_2 decomposition: experimental results and DFT validations, Nanomaterials 9 (2019) 1595, https://doi.org/10.3390/nano9111595.
[239] K. Zhang, A.P. Harvey, CO_2 decomposition to CO in the presence of up to 50% O_2 using a non-thermal plasma at atmospheric temperature and pressure, Chem. Eng. J. 405 (2021) 126625, https://doi.org/10.1016/j.cej.2020.126625.
[240] M. Grasemann, G. Laurenczy, Formic acid as a hydrogen source recent developments and future trends, Energy Environ. Sci. 5 (2012) 8171–8181, https://doi.org/10.1039/C2EE21928J.
[241] M. Rumayor, A. Dominguez-Ramos, A. Irabien, Formic acid manufacture: carbon dioxide utilization alternatives, Appl. Sci. 8 (2018) 914, https://doi.org/10.3390/app8060914.
[242] C. Zhao, J. Wang, J.B. Goodenough, Comparison of electrocatalytic reduction of CO_2 to HCOOH with different tin oxides on carbon nanotubes, Electrochem. Commun. 65 (2016) 9–13, https://doi.org/10.1016/j.elecom.2016.01.019.
[243] H. Strathmann, A. Grabowski, G. Eigenberger, Ion-Exchange membranes in the chemical process industry, Ind. Eng. Chem. Res. 52 (2013) 10364–10379, https://doi.org/10.1021/ie4002102.
[244] X. Tongwen, Electrodialysis processes with bipolar membranes (EDBM) in environmental protection-A Review, Resour. Conserv. Recycl. 37 (2002) 1–22, https://doi.org/10.1016/S0921-3449(02)00032-0.
[245] C. Huang, T. Xu, Electrodialysis with bipolar membranes for sustainable development, Environ. Sci. Technol. 40 (2006) 5233–5243, https://doi.org/10.1021/es060039p.
[246] T. Luo, S. Abdu, M. Wessling, Selectivity of ion exchange membranes: a Review, J. Membr. Sci. 555 (2018) 429–454, https://doi.org/10.1016/j.memsci.2018.03.051.
[247] S. Liu, J. Xiao, X.F. Lu, J. Wang, X. Wang, X. Wen, Efficient electrochemical reduction of CO_2 to HCOOH over sub-2nm SnO_2 quantum wires with exposed grain boundaries, Angew. Chem. Int. Ed. 58 (2019) 8499–8503, https://doi.org/10.1002/anie.201903613.
[248] K.R. Rao, S. Pishgar, J. Strain, B. Kumar, V. Atla, S. Kumari, J.M. Spurgeon, Photoelectrochemical reduction of CO_2 to HCOOH on silicon photocathodes with reduced SnO_2 porous nanowire catalysts, J. Mater. Chem. 6 (2018) 1736–1742, https://doi.org/10.1039/C7TA09672K.
[249] T. Sekimoto, M. Deguchi, S. Yotsuhashi, Y. Yamada, T. Masui, A. Kuramata, S. Yamakoshi, Highly selective electrochemical reduction of CO_2 to HCOOH on a gallium oxide cathode, Electrochem. Commun. 43 (2014) 95–97, https://doi.org/10.1016/j.elecom.2014.03.023.
[250] H. Tsuneoka, K. Teramura, T. Shishido, T. Tanaka, Adsorbed species of CO_2 and H_2 on Ga_2O_3 for the photocatalytic reduction of CO_2, J. Phys. Chem. C 114 (2010) 8892–8898, https://doi.org/10.1021/jp910835k.
[251] H. Yang, J.J. Kaczur, S.D. Sajjad, R.I. Masel, Electrochemical conversion of CO_2 to formic acid utilizing SustainionTM membranes, J. CO_2 Util. 20 (2017) 208–217, https://doi.org/10.1016/j.jcou.2017.04.011.
[252] L.G. Puppin, M. Khalid, G.T.T. da Silva, C. Ribeiro, H. Varela, O.F. Lopes, Electrochemical reduction of CO_2 to formic acid on $Bi_2O_2CO_3$/carbon fiber electrodes, J. Mater. Res. 35 (2020) 272–280, https://doi.org/10.1557/jmr.2020.16.
[253] H. Wu, J. Song, C. Xie, Y. Hua, B. Han, Highly efficient electrochemical reduction of CO_2 into formic acid over lead dioxide in an ionic liquid–catholyte mixture, Green Chem. 20 (2018) 1765–1769, https://doi.org/10.1039/C8GC00471D.
[254] S. Gao, Z. Sun, W. Liu, X. Jiao, X. Zu, Q. Hu, Y. Sun, T. Yao, W. Zhang, S. Wei, Y. Xie, Atomic layer confined vacancies for atomic-level insights into carbon dioxide electroreduction, Nat. Commun. 8 (2017) 14503, https://doi.org/10.1038/ncomms14503.
[255] S. Ohya, S. Kaneco, H. Katsumata, T. Suzuki, K. Ohta, Electrochemical reduction of CO_2 in methanol with aid of CuO and Cu_2O, Catal. Today 148 (2009) 329–334, https://doi.org/10.1016/j.cattod.2009.07.077.
[256] B. Zhou, J. Song, C. Xie, C. Chen, Q. Qian, B. Han, Mo–Bi–Cd ternary metal chalcogenides: highly efficient photocatalyst for CO_2 reduction to formic acid under visible light, ACS Sustain. Chem. Eng. 6 (2018) 5754–5759, https://doi.org/10.1021/acssuschemeng.8b00956.
[257] G. Mele, C. Annese, L. D'Accolti, A. De Riccardis, C. Fusco, Photoreduction of carbon dioxide to formic acid in aqueous suspension: a comparison between phthalocyanine/TiO_2 and porphyrin/TiO_2 catalysed processes, Molecules 20 (2015) 396–415, https://doi.org/10.3390/molecules20010396.
[258] U. Fegade, G. Jethave, Conversion of carbon dioxide into formic acid, in: A.A. Inamuddin, E. Lichtfouse (Eds.), Conversion of Carbon Dioxide into Hydrocarbons Volume 2 Technology. Environmental Chemistry for a Sustainable World, vol. 41, Springer, Cham, 2020.
[259] S. Yotsuhashi, H. Hashiba, M. Deguchi, Y. Zenitani, R. Hinogami, Y. Yamada, M. Deura, K. Ohkawa, Highly efficient photochemical HCOOH production from CO_2 and water using an inorganic system, AIP Adv. 2 (2012) 042160, https://doi.org/10.1063/1.4769356.
[260] T.M. Suzuki, T. Takayama, S. Sato, A. Iwase, A. Kudo, T. Morikawa, Enhancement of CO_2 reduction activity under visible light irradiation over Zn-based metal sulfides by combination with Ru-complex catalysts, Appl. Catal. B Environ. 224 (2018) 572–578, https://doi.org/10.1016/j.apcatb.2017.10.053.
[261] H. Reymond, J.J. Corral-Pérez, A. Urakawa, P.R. von Rohr, Towards a continuous formic acid synthesis: a two-step carbon dioxide hydrogenation in flow, React. Chem. Eng 3 (2018) 912–919, https://doi.org/10.1039/C8RE00142A.
[262] A. Sarkar, E. Gracia-Espino, T. Wågberg, A. Shchukarev, M. Mohl, A.-R. Rautio, O. Pitkänen, T. Sharifi, K. Kordas, J.-P. Mikkola, Photocatalytic reduction of CO_2 with H_2O over modified TiO_2 nanofibers: understanding the reduction pathway, Nano Res. 9 (2016) 1956–1968, https://doi.org/10.1007/s12274-016-1087-9.
[263] O. Teruhisa, M. Naoya, K. Takahiro, Y. Yin, Photocatalytic reduction of CO_2 over a hybridphotocatalyst composed of WO_3 and graphitic carbon nitride ($g\text{-}C_3N_4$) under visible light, J. CO_2 Util. 6 (2014) 17–25, https://doi.org/10.1016/j.jcou.2014.02.002.
[264] H. Inoue, H. Moriwaki, K. Maeda, H. Yoneyama, Photoreduction of carbon dioxide using chalcogenide semiconductor microcrystals, J. Photochem. Photobiol., A: Chem 86 (1995) 191–196, https://doi.org/10.1016/1010-6030(94)03936-O.
[265] S.T. Meek, J.A. Greathouse, M.D. Allendorf, Metal-organic frameworks: a rapidly growing class of versatile nanoporous materials, Adv. Mater. 23 (2011) 249–267, https://doi.org/10.1002/adma.201002854.
[266] J.-R. Li, R.J. Kuppler, H.-C. Zhou, Selective gas adsorption and separation in metal–organic frameworks, Chem. Soc. Rev. 38 (2009) 1477–1504, https://doi.org/10.1039/B802426J.
[267] B. Chen, S. Xiang, G. Qian, Metal–organic frameworks with functional pores for recognition of small molecules, Acc. Chem. Res. 43 (2010) 1115–1124, https://doi.org/10.1021/ar100023y.
[268] S. Qiu, G. Zhu, Molecular engineering for synthesizing novel structures of metal–organic frameworks with multifunctional properties, Coord. Chem. Rev. 253 (2009) 2891–2911, https://doi.org/10.1016/j.ccr.2009.07.020.
[269] A.U. Czaja, N. Trukhan, U. Müller, Industrial applications of metal–organic frameworks, Chem. Soc. Rev. 38 (2009) 1284–1293, https://doi.org/10.1039/B804680H.
[270] S. Keskin, S. Kızılel, Biomedical applications of metal organic frameworks, Ind. Eng. Chem. Res. 50 (2011) 1799–1812, https://doi.org/10.1021/ie101312k.
[271] J. Lee, O.K. Farha, J. Roberts, K.A. Scheidt, S.T. Nguyen, J.T. Hupp, Metal–organic framework materials as catalysts, Chem. Soc. Rev. 38 (2009) 1450–1459, https://doi.org/10.1039/B807080F.
[272] Y. Fu, D. Sun, Y. Chen, R. Huang, Dr Z. Ding, X. Fu, Z. Li, An amine-functionalized titanium metal–organic framework photocatalyst with visible-light-induced activity for CO_2 reduction, Angew. Chem. Int. Ed. 51 (2012) 3364–3367, https://doi.org/10.1002/anie.201108357.
[273] S. Li, K. Ji, M. Zhang, C. He, J. Wang, Z. Li, Boosting the photocatalytic CO_2 reduction of metal–organic frameworks by encapsulating carbon dots, Nanoscale 12 (2020) 9533–9540, https://doi.org/10.1039/D0NR01696A.
[274] B.-J. Liu, T. Torimoto, H. Matsumoto, H. Yoneyama, Effect of solvents on photocatalytic reduction of carbon dioxide using TiO_2 nanocrystal photocatalyst embedded in SiO_2 matrices, J. Photochem. Photobiol. Chem. 108 (1997) 187–192, https://doi.org/10.1016/S1010-6030(97)00082-8.
[275] X. Li, J. Wen, J. Low, et al., Design and fabrication of semiconductor photocatalyst for photocatalytic reduction of CO_2 to solar fuel, Sci. Chin. Mater. 57 (2014) 70–100, https://doi.org/10.1007/s40843-014-0003-1.
[276] K. Li, X. An, K.H. Park, et al., A critical review of CO_2 photoconversion: catalysts and reactors, Catal. Today 224 (2014) 3–12, https://doi.org/10.1016/j.cattod.2013.12.006.

[277] K. Iizuka, T. Wato, Y. Miseki, et al., Photocatalytic reduction of carbon dioxide over Ag cocatalyst-loaded $ALa_4Ti_4O_{15}$ (A = Ca, Sr, and Ba) using water as a reducing reagent, J. Am. Chem. Soc. 133 (2011) 20863–20868, https://doi.org/10.1021/ja207586e.
[278] E. Bahadori, A. Tripodi, A. Villa, C. Pirola, L. Prati, G. Ramis, I. Rossetti, High pressure photoreduction of CO_2: effect of catalyst formulation, hole scavenger addition and operating conditions, Catalysts 8 (2018) 430, https://doi.org/10.3390/catal8100430.
[279] H. Pan, M.D. Heagy, Photons to Formate: a review on photocatalytic reduction of CO_2 to formic acid, Nanomaterials 10 (2020) 2422, https://doi.org/10.3390/nano10122422.
[280] D.P. Leonard, H. Pan, M.D. Heagy, Photocatalyzed reduction of bicarbonate to formate: effect of ZnS crystal structure and positive hole scavenger, ACS Appl. Mater. Interfaces 7 (2015) 24543–24549, https://doi.org/10.1021/acsami.5b06054.
[281] H. Pan, S. Chowdhury, D. Premachandra, S. Olguin, M.D. Heagy, Semiconductor photocatalysis of bicarbonate to solar fuels: formate production from copper (I) oxide, ACS Sustain. Chem. Eng. 6 (2018) 1872–1880, https://doi.org/10.1021/acssuschemeng.7b03244.
[282] H. Pan, K.R. Martindale, M.D. Heagy, Iron oxide nanostructures for the reduction of bicarbonate to solar fuels, Top. Catal. 61 (2018) 601–609, https://doi.org/10.1007/s11244-018-0959-5.
[283] H. Pan, D. Premachandra, M.D. Heagy, Artificial foliage with remarkable quantum conversion efficiency in bicarbonate to formate Sustainable, Energy Fuels 6 (2022) 267–270, https://doi.org/10.1039/D1SE01307F.
[284] P. Yang, Liquid sunlight: the evolution of photosynthetic biohybrids, Nano Lett. 21 (2021) 5453–5456, https://doi.org/10.1021/acs.nanolett.1c02172.
[285] P. Rumbach, R. Xu, D.B. Go, Electrochemical production of oxalate and formate from CO_2 by solvated electrons produced using an atmospheric-pressure plasma, J. Electrochem. Soc. 163 (2016) F1157–F1161, https://doi.org/10.1149/2.0521610jes.
[286] Formaldehyde https://en.wikipedia.org/wiki/Formaldehyde Accessed on 28 January 2022.
[287] A. Andersson, J. Holmberg, R. Häggblad, Process improvements in methanol oxidation to formaldehyde: application and catalyst development, Top. Catal. 59 (2016) 1589–1599, https://doi.org/10.1007/s11244-016-0680-1.
[288] T.D. Nguyen, T.V. Tran, S. Singh, P.T.T. Phuong, L.G. Bach, S. Nanda, D.-V.N. Vo, Conversion of carbon dioxide into formaldehyde, in: A.A. Inamuddin, E. Lichtfouse (Eds.), Conversion of Carbon Dioxide into Hydrocarbons Volume 2 Technology. Environmental Chemistry for a Sustainable World, vol. 41, Springer, Cham, 2020, pp. 159–183.
[289] L.E. Heim, H. Konnerth, M.H.G. Prechtl, Future perspectives for formaldehyde: pathways for reductive synthesis and energy storage, Green Chem. 19 (2017) 2347–2355, https://doi.org/10.1039/C6GC03093A.
[290] K. Nakata, T. Ozaki, C. Terashima, A. Fujishima, Y. Einaga, High-yield electrochemical production of formaldehyde from CO_2 and seawater, Angew. Chem. Int. Ed. 53 (2013) 871–874, https://doi.org/10.1002/anie.201308657.
[291] A.U. Pawar, U. Pal, J.Y. Zheng, C.W. Kim, Y.S. Kang, Thermodynamically controlled photo-electrochemical CO_2 reduction at Cu/rGO/PVP/Nafion multi-layered dark cathode for selective production of formaldehyde and acetaldehyde, Appl. Catal. B Environ. 303 (2022) 120921, https://doi.org/10.1016/j.apcatb.2021.120921.
[292] G. Qin, Y. Zhang, X. Ke, et al., Photocatalytic reduction of carbon dioxide to formic acid, formaldehyde, and methanol using dye-sensitized TiO_2 film, Appl. Catal. B Environ. 129 (2013) 59–605, https://doi.org/10.1016/j.apcatb.2012.10.012.
[293] M. Subrahmanyam, S. Kaneco, N. Alonso-Vante, A screening for the photo reduction of carbon dioxide supported on metal oxide catalysts for C_1-C_3 selectivity, Appl. Catal. B Environ. 23 (1999) 169–174, https://doi.org/10.1016/S0926-3373(99)00079-X.
[294] C.C. Yang, J. Vernimmen, V. Meynen, et al., Mechanistic study of hydrocarbon formation in photocatalytic CO_2 reduction over Ti-SBA-15, J. Catal. 284 (2011) 1–8, https://doi.org/10.1016/j.jcat.2011.08.005.
[295] Q. Zhai, S. Xie, W. Fan, et al., Photocatalytic conversion of carbon dioxide with water into methane: platinum and copper(I) oxide co-catalysts with a core-shell structure, Angew. Chem. Int. Ed. 52 (2013) 5776–5779, https://doi.org/10.1002/anie.201301473.
[296] Methanol, https://en.wikipedia.org/wiki/Methanol. (Accessed 8 February 2022).
[297] G. Hochgesand, Rectisol, Purisol, Efficient acid gas removal for high-pressure hydrogen and syngas production, Ind. Eng. Chem. 62 (1970) 37–43, https://doi.org/10.1021/ie50727a007.
[298] D.S. Marlin, E. Sarron, Ó. Sigurbjörnsson, Process advantages of direct CO_2 to methanol synthesis, Front. Chem. 6 (2018) 446, https://doi.org/10.3389/fchem.2018.00446.
[299] E.E. Barton, D.M. Rampulla, A.B. Bocarsly, Selective solar-driven reduction of CO_2 to methanol using a catalyzed p-GaP based photoelectrochemical cell, J. Am. Chem. Soc. 130 (2008) 6342–6344, https://doi.org/10.1021/ja0776327.
[300] E.B. Cole, P.S. Lakkaraju, D.M. Rampulla, A.J. Morris, E. Abelev, A.B. Bocarsly, Using a one-electron shuttle for the multielectron reduction of CO_2 to methanol: kinetic, mechanistic, and structural insights, J. Am. Chem. Soc. 132 (2010) 11539–11551, https://doi.org/10.1021/ja1023496.
[301] C.-H. Lim, A.M. Holder, J.T. Hynes, C.B. Musgrave, Reduction of CO_2 to methanol catalyzed by a biomimetic organohydride produced from pyridine, J. Am. Chem. Soc. 136 (2014) 16081–16095, https://doi.org/10.1021/ja510131a.
[302] J. Albo, A. Irabien, Cu_2O-loaded gas diffusion electrodes for the continuous electrochemical reduction of CO_2 to methanol, J. Catal. 343 (2016) 232–239, https://doi.org/10.1016/j.jcat.2015.11.014.
[303] K.P. Kuhl, T. Hatsukade, E.R. Cave, et al., Electrocatalytic conversion of carbon dioxide to methane and methanol on transition metal surfaces, J. Am. Chem. Soc. 136 (2014) 14107–14113, https://doi.org/10.1021/ja505791r.
[304] M. Anpo, H. Yamashita, K. Ikeue, et al., Photocatalytic reduction of CO_2 with H_2O on Ti-MCM-41 and Ti-MCM-48 mesoporous zeolite catalysts, Catal. Today 44 (1998) 327–332, https://doi.org/10.1016/S0920-5861(98)00206-5.
[305] J.C.S. Wu, H.-M. Lin, C.-L. Lai, Photo reduction of CO_2 to methanol using optical-fiber photoreactor, Appl. Catal. Gen. 296 (2005) 194–200, https://doi.org/10.1016/j.apcata.2005.08.021.
[306] R. Gusain, P. Kumar, O.P. Sharma, S.L. Jain, O.P. Khatri, Reduced graphene oxide–CuO nanocomposites for photocatalytic conversion of CO_2 into methanol under visible light irradiation, Appl. Catal. B Environ. 181 (2016) 352–362, https://doi.org/10.1016/j.apcatb.2015.08.012.
[307] J. Liu, Y. Niu, X. He, J. Qi, X. Li, Photocatalytic reduction of CO_2 using TiO_2-graphene nanocomposites, J. Nanomater. (2016), https://doi.org/10.1155/2016/6012896. Article ID 6012896.
[308] Q. Sun, Y. Jiang, Z. Jiang, L. Zhang, X. Sun, J. Li, Green and efficient conversion of CO_2 to methanol by biomimetic coimmobilization of three dehydrogenases in protamine-templated titania, Ind. Eng. Chem. Res. 48 (2009) 4210–4215, https://doi.org/10.1021/ie801931j.
[309] X. Li, J. Chen, H. Li, J. Li, Y. Xu, Y. Liu, J. Zhou, Photoreduction of CO_2 to methanol over Bi_2S_3/CdS photocatalyst under visible light irradiation, J. Nat. Gas Chem. 20 (2011) 413–417, https://doi.org/10.1016/S1003-9953(10)60212-5.
[310] D. Chen, X. Zhang, A.F. Lee, Synthetic strategies to nanostructured photocatalysts for CO_2 reduction to solar fuels and chemicals, J. Mater. Chem. 3 (2015) 14487–14516, https://doi.org/10.1039/C5TA01592H.
[311] A. Sharma, B.-K. Lee, Photocatalytic reduction of carbon dioxide to methanol using nickel-loaded TiO_2 supported on activated carbon fiber, Catal. Today 298 (2017) 158–167, https://doi.org/10.1016/j.cattod.2017.05.003.
[312] M.D. Farahani, Y. Zeng, Y. Zheng, The application of nonthermal plasma in methanolsynthesis via CO_2 hydrogenation, Energy Sci. Eng. 10 (2022) 1572–1583, https://doi.org/10.1002/ese3.1107.
[313] L. Wang, Y.H. Yi, H.C. Guo, X. Tu, Atmospheric pressure and room temperature synthesis of methanol through plasma-catalytic hydrogenation of CO_2, ACS Catal. 8 (2018) 90–100, https://doi.org/10.1021/acscatal.7b02733.
[314] Z. Cui, S. Meng, Y. Yi, A. Jafarzadeh, S. Li, E.C. Neyts, Y. Hao, L. Li, X. Zhang, X. Wang, A. Bogaerts, Plasma-catalytic methanol synthesis from CO2 hydrogenation over a supported Cu cluster catalyst: insights into the reaction mechanism, ACS Catal. 12 (2022) 1326–1337, https://doi.org/10.1021/acscatal.1c04678.
[315] M. Ronda-Lloret, Y. Wang, P. Oulego, G. Rothenberg, X. Tu, N.R. Shiju, CO_2 hydrogenation at atmospheric pressure and low temperature using plasma-enhanced catalysis over supported cobalt oxide catalysts, ACS Sustain. Chem. Eng. 8 (2020) 17397–17407, https://doi.org/10.1021/acssuschemeng.0c05565.
[316] B. Eliasson, U. Kogelschatz, B. Xue, L.-M. Zhou, Hydrogenation of carbon dioxide to methanol with a discharge-activated catalyst, Ind. Eng. Chem. Res. 37 (1998) 3350–3357, https://doi.org/10.1021/ie9709401.
[317] N. Joshi, L. Sivachandiran, Exploring the feasibility of liquid fuelsynthesis from CO_2 under cold plasma discharge: role of plasma discharge in binary metal oxide surface modification, RSC Adv. 11 (2021) 27757–27766, https://doi.org/10.1039/D1RA04852J.
[318] M.Q. Feliz, I. Polaert, A. Ledoux, C. Fernandez, F. Azzolina-Jury, Influence of ionic conductivity and dielectric constant of the catalyst on DBD plasma-assisted CO_2 hydrogenation into methanol, J. Phys. D Appl. Phys. 54 (2021) 334003, https://doi.org/10.1088/1361-6463/abfddd.
[319] Methane. https://www.britannica.com/science/methane. (Accessed 26 April 2022). https://en.wikipedia.org/wiki/Methane.
[320] E. Moioli, R. Mutschler, A. Züttel, Renewable energy storage via CO_2 and H_2 conversion to methane and methanol: assessment for small scale applications, Renew. Sustain. Energy Rev. 107 (2019) 497–506, https://doi.org/10.1016/j.rser.2019.03.022.
[321] H. Zhong, G. Yao, X. Cui, P. Yan, X. Wang, F. Jin, Selective conversion of carbon dioxide into methane with a 98% yield on an *in situ* formed Ni nanoparticle catalyst in water, Chem. Eng. J. 357 (2019) 421–427, https://doi.org/10.1016/j.cej.2018.09.155.
[322] H. Rao, L.C. Schmidt, J. Bonin, M. Robert, Visible-light-driven methane formation from CO_2 with a molecular iron catalyst, Nature 548 (2017) 74–77, https://doi.org/10.1038/nature23016.
[323] C. Costentin, M. Robert, J.-M. Savéant, A. Tatin, Efficient and selective molecular catalyst for the CO_2-to-CO electrochemical conversion in water, Proc. Natl. Acad. Sci. USA 112 (2015) 6882–6886, https://doi.org/10.1073/pnas.150706311.
[324] J. Bonin, A. Maurin, M. Robert, Molecular catalysis of the electrochemical and photochemical reduction of CO_2 with Fe and Co metal based complexes,

Recent advances. Coord. Chem. Rev. 334 (2017) 184–198, https://doi.org/10.1016/j.ccr.2016.09.005.
[325] A. Eilert, F.S. Roberts, D. Friebel, A. Nilsson, Formation of copper catalysts for CO_2 reduction with high ethylene/methane product ratio investigated with in situ X-ray absorption spectroscopy, J. Phys. Chem. Lett. 7 (8) (2016) 1466–1470, https://doi.org/10.1021/acs.jpclett.6b00367.
[326] Y. Zhang, L.-Z. Dong, S. Li, X. Huang, J.-N. Chang, J.-H. Wang, J. Zhou, S.-L. Li, Y.-Q. Lan, Coordination environment dependent selectivity of single-site-Cu enriched crystalline porous catalysts in CO_2 reduction to CH_4, Nat. Commun. 12 (2021), https://doi.org/10.1038/s41467-021-26724-8. Article number: 6390.
[327] X. Wang, P. Ou, J. Wicks, Y. Xie, Y. Wang, J. Li, J. Tam, D. Ren, J.Y. Howe, Z. Wang, A. Ozden, Y.Z. Finfrock, Y. Xu, Y. Li, A.S. Rasouli, K. Bertens, A.H. Ip, M. Graetzel, D. Sinton, E.H. Sargent, Gold-in-copper at low *CO coverage enables efficient electromethanation of CO_2, Nat. Commun. 12 (2021), https://doi.org/10.1038/s41467-021-23699-4. Article number: 3387.
[328] Y. Shi, K. Sun, J. Shan, H. Li, J. Gao, Z. Chen, C. Sun, Y. Shuai, Z. Wang, Selective CO_2 electromethanation on surface-modified Cu catalyst by local microenvironment modulation, ACS Catal. 12 (2022) 8252–8258, https://doi.org/10.1021/acscatal.2c01544.
[329] J. Shen, R. Kortlever, R. Kas, Y.Y. Birdja, O. Diaz-Morales, Y. Kwon, I. Ledezma-Yanez, K.J.P. Schouten, G. Mul, M.T.M. Koper, Electrocatalytic reduction of carbon dioxide to carbon monoxide and methane at an immobilized cobalt protoporphyrin, Nat. Commun. 6 (2015) 8177, https://doi.org/10.1038/ncomms9177.
[330] S. Kaneco, K. Iiba, M. Yabuuchi, N. Nishio, H. Ohnishi, H. Katsumata, T. Suzuki, K. Ohta, High efficiency electrochemical CO_2-to-methane conversion method using methanol with lithium supporting electrolytes, Ind. Eng. Chem. Res. 41 (2002) 5165–5170, https://doi.org/10.1021/ie0200454.
[331] T. Wu, L. Zou, D. Han, F. Li, Q. Zhang, L. Niu, A carbon-based photocatalyst efficiently converts CO_2 to CH_4 and C_2H_2 under visible light, Green Chem. 16 (2014) 2142–2146, https://doi.org/10.1039/C3GC42454E.
[332] S. Sorcar, J. Thompson, Y. Hwang, Y.H. Park, T. Majima, C.A. Grimes, J.R. Durrant, S.-I. In, High-rate solar-light photoconversion of CO_2 to fuel: controllable transformation from C_1 to C_2 products, Energy Environ. Sci. 11 (2018) 3183–3193, https://doi.org/10.1039/C8EE00983J.
[333] M.S. Hamdy, R. Amrollahi, G. Mul, Surface Ti_3+-containing (blue) titania: a unique photocatalyst with high activity and selectivity in visible light-stimulated selective oxidation, ACS Catal. 2 (2012) 2641–2647, https://doi.org/10.1021/cs300593d.
[334] H. Park, H.-H. Ou, A.J. Colussi, M.R. Hoffmann, Artificial photosynthesis of C_1–C_3 hydrocarbons from water and CO_2 on titanate nanotubes decorated with nanoparticle elemental copper and CdS quantum dots, J. Phys. Chem. A 119 (2015) 4658–4666, https://doi.org/10.1021/jp511329d.
[335] D. Mateo, A.M. Asiri, J. Albero, H. Garcíav, The mechanism of photocatalytic CO_2 reduction by graphene-supported Cu_2O probed by sacrificial electron donors, Photochem. Photobiol. Sci. 17 (2018) 829–834, https://doi.org/10.1039/C7PP00442G.
[336] P.M. Bravo, D.P. Debecker, Combining CO_2 capture and catalytic conversion to methane, Waste Dispos. Sustain. Energy 1 (2019) 53–65, https://doi.org/10.1007/s42768-019-00004-0.
[337] F. Sun, H. Maimaiti, Y. Liu, A. Awati, Preparation and photocatalytic CO_2 reduction performance of silver nanoparticles coated with coal-based carbon dots, Int. J. Energy Res. 42 (2018) 4458–4469, https://doi.org/10.1002/er.4191.
[338] J. Luo, I. Larrosa, C-H carboxylation of aromatic compounds through CO_2 fixation, ChemSusChem 10 (2017) 3317–3332, https://doi.org/10.1002/cssc.201701058.
[339] X. Wei, Z. Yin, K. Lyu, Z. Li, J. Gong, G. Wang, L. Xiao, J. Lu, L. Zhuang, Highly selective reduction of CO_2 to C_2+ hydrocarbons at copper/polyaniline interfaces, ACS Catal. 10 (2020) 4103–4111, https://doi.org/10.1021/acscatal.0c00049.
[340] S. Zhong, X. Yang, Z. Cao, X. Dong, S.M. Kozlov, L. Falivene, J.-K. Huang, X. Zhou, M.N. Hedhili, Z. Lai, K.-W. Huang, Y. Han, L. Cavallo, L.-J. Li, Efficient electrochemical transformation of CO_2 to C_2/C_3 chemicals on benzimidazole-functionalized copper surfaces, Chem. Commun. 54 (2018) 11324–11327, https://doi.org/10.1039/C8CC04735A.
[341] T.N. Huan, D.A.D. Corte, S. Lamaison, D. Karapinar, L. Lutz, N. Menguy, M. Foldyna, S.-H. Turren-Cruz, A. Hagfeldt, F. Bella, M. Fontecave, V. Mougel, Low-cost high-efficiency system for solar-driven conversion of CO_2 to hydrocarbons, Proc. Natl. Acad. Sci. USA 116 (2019) 9735–9740, https://doi.org/10.1073/pnas.18154121.
[342] M. Schreier, et al., Efficient photosynthesis of carbon monoxide from CO_2 using perovskite photovoltaics, Nat. Commun. 6 (2015) 7326, https://doi.org/10.1038/ncomms8326.
[343] J.L. White, J.T. Herb, J.J. Kaczur, P.W. Majsztrik, A.B. Bocarsly, Photons to formate: efficient electrochemical solar energy conversion via reduction of carbon dioxide, J. CO_2 Util. 7 (2014) 1–5, https://doi.org/10.1016/j.jcou.2014.05.002.
[344] A. Vasileff, Y. Zhu, X. Zhi, Y. Zhao, L. Ge, H.M. Chen, Y. Zheng, S.Z. Qiao, Electrochemical reduction of CO_2 to ethane through stabilization of an ethoxy intermediate, Angew. Chem. Int. Ed. 59 (2020) 1–6, https://doi.org/10.1002/anie.202004846.
[345] P.W. Bridgman, Certain physical properties of single crystals of tungsten, antimony, bismuth, tellurium, cadmium, zinc, and tin, Proc. Am. Acad. Arts Sci. 60 (1925) 305–383. https://www.jstor.org/stable/25130058.
[346] Z. Han, R. Kortlever, H.-Y. Chen, J.C. Peters, T. Agapie, CO_2 reduction selective for C≥2 products on polycrystalline copper with N-substituted pyridinium additives, ACS Cent. Sci. 3 (2017) 853–859, https://doi.org/10.1021/acscentsci.7b00180.
[347] D. Kim, C.S. Kley, Y. Li, P. Yang, Copper nanoparticle ensembles for selective electroreduction of CO_2 to C_2–C_3 products, Proc. Natl. Acad. Sci. USA 114 (2017) 10560–10565, https://doi.org/10.1073/pnas.171149311.
[348] E. Alper, O.Y. Orhan, CO_2 utilization: developments in conversion processes, Petroleum 3 (2017) 109–126, https://doi.org/10.1016/j.petlm.2016.11.003.
[349] K.J.P. Schouten, Y. Kwon, C.J.M. van der Ham, Z. Qin, M.T.M. Koper, A new mechanism for the selectivity to C_1 and C_2 species in the electrochemical reduction of carbon dioxide on copper electrodes, Chem. Sci. 2 (2011) 1902–1909, https://doi.org/10.1039/C1SC00277E.
[350] Q. Zhu, X. Sun, D. Yang, J. Ma, X. Kang, L. Zheng, J. Zhang, Z. Wu, B. Han, Carbon dioxide electroreduction to C_2 products over copper-cuprous oxide derived from electrosynthesized copper complex, Nat. Commun. 10 (2019) 3851, https://doi.org/10.1038/s41467-019-11599-7.
[351] D. Gao, R.M. Arán-Ais, H.S. Jeon, R.C. Beatriz, Rational catalyst and electrolyte design for CO_2 electroreduction towards multicarbon products, Nat. Catal. 2 (2019) 198–210, https://doi.org/10.1038/s41929-019-0235-5.
[352] J. Fischer, T. Lehmann, E. Heitz, The production of oxalic acid from CO_2 and H_2O, J. Appl. Electrochem. 11 (1981) 743–750, https://doi.org/10.1007/BF00615179.
[353] L.M. Pastrana-Martínez, A.M.T. Silva, N.N.C. Fonseca, J.,R. Vaz, J.L. Figueiredo, J.L. Faria, Photocatalytic reduction of CO_2 with water into methanol and ethanol using graphene derivative–TiO_2 composites: effect of pH and copper(I) oxide, Top. Catal. 59 (2016) 1279–1291, https://doi.org/10.1007/s11244-016-0655-2.
[354] H. Li, C. Li, L. Han, C. Li, S. Zhang, Photocatalytic reduction of CO_2 with H_2O on CuO/TiO_2 catalysts, Energy Sources, Part A Recovery, Util. Environ. Eff. 38 (2016), https://doi.org/10.1080/15567036.2011.598910.
[355] A. Pougin, M. Dilla, J. Strunk, Identification and exclusion of intermediates of photocatalytic CO_2 reduction on TiO_2 under conditions of highest purity, Phys. Chem. Chem. Phys. 18 (2016) 10809–10817, https://doi.org/10.1039/C5CP07148H.
[356] Perovskite. https://encyclopedia.pub/entry/228. (Accessed 28 April 2022).
[357] S. Zeng, P. Kar, U.K. Thakur, K. Shankar, A review on photocatalytic CO_2 reduction using perovskite oxide nanomaterials, Nanotech 29 (2018) 052001, https://doi.org/10.1088/1361-6528/aa9fb1.
[358] Ș. Neațu, J.A. Maciá-Agulló, H. Garcia, Solar light photocatalytic CO_2 reduction: general considerations and selected bench-mark photocatalysts, Int. J. Mol. Sci. 15 (2014) 5246–5262, https://doi.org/10.3390/ijms15045246.
[359] V. Jeyalakshmi, R. Mahalakshmya, K.R. Krishnamurthy, B. Viswanathan, Titania based catalysts for photoreduction of carbon dioxide: role of modifiers, Indian J. Chem. 51A (2012) 1263–1283.
[360] B. Srinivas, B. Shubhamangala, K. Lalitha, P.A.K. Reddy, V. Durga Kumari, M. Subrahmanyam, B.R. De, Photocatalytic reduction of CO_2 over Cu-TiO_2/molecular sieve 5A composite, Photochem. Photobiol. 87 (2011) 995–1001, https://doi.org/10.1111/j.1751-1097.2011.00946.x.
[361] O. Ishitani, C. Inoue, Y. Suzuki, T. Ibusuki, Photocatalytic reduction of carbon dioxide to methane and acetic acid by an aqueous suspension of metal-deposited TiO_2, J. Photochem. Photobiol. A: Chem 72 (1993) 269–271, https://doi.org/10.1016/1010-6030(93)80023-3.